DOCTORAL DISSERTATION

SYNTHESIS AND CHARACTERIZATION OF BLOCK COPOLYMERS BASED ON POLYTHIOPHENE FOR PHOTOVOLTAIC DEVICE

A DISSERTATION SUBMITTED IN POLYMER
PHOTOVOLTAIC DEVICE FOR DEGREE
OF
DOCTOR OF ENGINEERING

February, 2011

Presented by Zhijie Gu

Directed by Professor Kenji Ogino

Graduate School of Bio-Applications and Systems Engineering

Tokyo University of Agriculture and Technology

Preface

The conversion efficiency of organic solar cells, which consist of *p*-type semiconducting polymer and *n*-type fullerene derivative, strongly depends on the morphology of the composites. In addition to post treatments such as thermal or solvent annealing, the author proposes the novel strategy for the control of the morphology, i.e., the utilization of block consisting of regioregular poly(3-hexylthiophene) (P3HT) and electrically inert polymer, such as polystyrene (PS) and poly(ethylene glycol) (PEO) for active layers in organic solar cells.

At first above mentioned two types of block copolymers were successfully synthesized utilizing Suzuki coupling reaction between bromo terminated P3HT and PS or PEO containing bronic acid ester moiety. ^{1}H-NMR analysis elucidated no contamination with homo-P3HT. Microphase separation in both block copolymers thin films was confirmed by DSC, UV-vis, and AFM experiments.

The film morphology of the composites of block copolymers with [6,6]-phenyl-C_{61}-butyric acid methyl ester (PCBM) was strongly dependent on the nature of inert block. P3HT-*b*-PS composite showed distinct and larger domain compared with P3HT/PCBM. On the other hand, P3HT-*b*-PEO showed smaller size of regular phase separated structure. In some cases (e.g. solvent annealed films), each lamellar domain aligned perpendicular to the substrate. Photovoltaic devices based on block copolymers were fabricated. Conversion efficiency was almost comparable to that of homo-P3HT based device.

Content

Chapter 1 . Introduction

1.1 Photovoltaic device

1.1.1 Solar energy

The Earth receives 174 petawatts (PW) of incoming solar radiation (insolation) at the upper atmosphere [1]. The spectrum of solar light at the Earth's surface is mostly spread across the visible and near-infrared ranges with a small part in the near-ultraviolet (Figure 1-1),, and then the materials for efficient solar cells must have characteristics matched to the spectrum of available light.

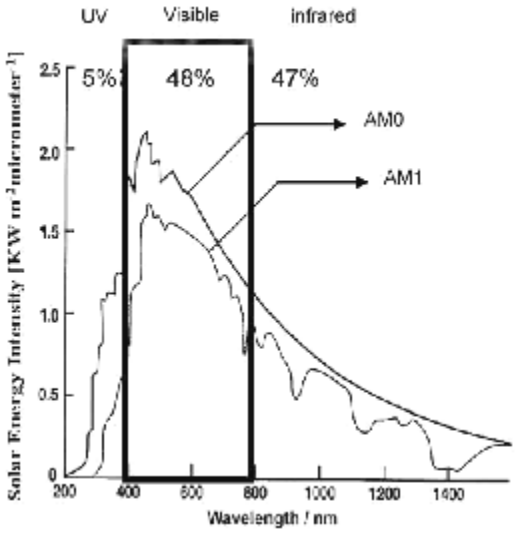

Figure 1-1. Spectrum of sunlight.

(AM0: the out side Earth’s atmosphere; AM1: when the sun is directly overhead at sea level).

1.1.2 Photovoltaic device (solar cell)

Current-voltage characteristic of the solar cell using an ideal diode under the light irradiation shows an actual *J-V* curve (b) resulting from parallel displacement of an ideal diode curve (a) (Figure 1-2) [1]. In the other words, the parameter of z in an ideal diode curve formula of

$J = z + j_0 [\exp (eV'/kT) - 1]$

was changed into $|J_{sc}|$ for a solar cell curve formula as follows.

$J = J_{sc} + j_0 [\exp (eV'/kT) - 1]$

However, because of the existence of leakage current j_p (resistance R_p) due to series resistance R_s and internal short current, as shown in Figure 1-2(b) the *J-V* curve formula in an actual solar cell should be expressed as

$J=J'_{sc}+j_0 [\exp (e (V-jR_s)/\gamma kT)-1] + (V-jR_s)/R_p$.

The electrical equivalent circuit corresponding to this *J-V* curve is shown in Figure. 1-3. The enlargement of R_p and the reduction of R_s increase the short circuit current and improve a fill factor, which are important characteristics in organic thin-film solar cells.

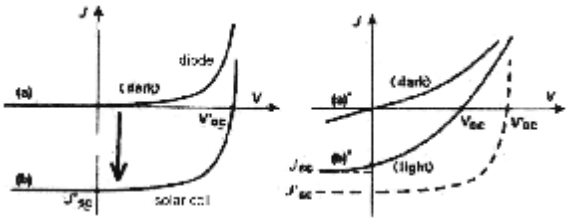

(a) ideal *J-V* curve; (b) actual *J-V* curve.

Figure 1-2. Current-voltage characteristic of the solar cell.

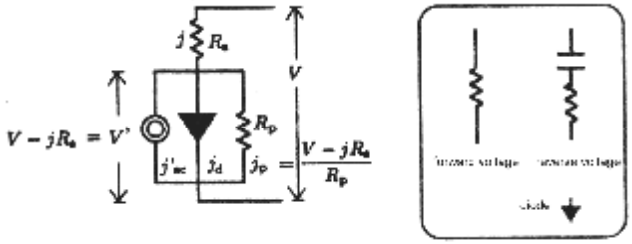

Figure 1-3. Electrical equivalent circuit.

1.1.3 Photovoltaic conversion efficiency

Due to the difficulty measuring these parameters (R_s, R_p, J_{sc} and J_o) directly, other parameters are measured instead: thermodynamic efficiency, quantum efficiency, V_{oc} ratio, and fill factor. The efficiency

of a solar cell may be broken down into reflectance efficiency, thermodynamic efficiency, charge carrier separation efficiency and conductive efficiency. The overall efficiency is the product of these individual efficiencies.

Reflectance losses are a portion of the quantum efficiency under "external quantum efficiency" [2]. Recombination losses make up a portion of the quantum efficiency, V_{oc} ratio, and fill factor. Resistive losses predominantly govern fill factor and also make up minor portions of the quantum efficiency, V_{oc} ratio.

On the current-voltage (*I*-*V*) curve as shown in Figure 1-4, P_{max} can be obtained with the maximum |*IV*| dissipation on the solid line, and can be expressed by I_{max} and V_{max}

$P_{max}=I_{max}V_{max}$

When the incident light energy is assumed to be P_{in}, the efficiency of converting light into electricity (photo-electric conversion efficiency: η) can be shown as follows

$\eta=P_{max}/P_{in}\times100$ (%)

Moreover, since fill factor (FF) is defined as

$FF=P_{in}/I_{sc}V_{oc}$ ι$=I_{max}V_{max}/I_{sc}V_{oc}$

and the conversion efficiency could be defined as follows.

$\eta=I_{sc}V_{oc}FF/P_{in}\times100$ (%)

.

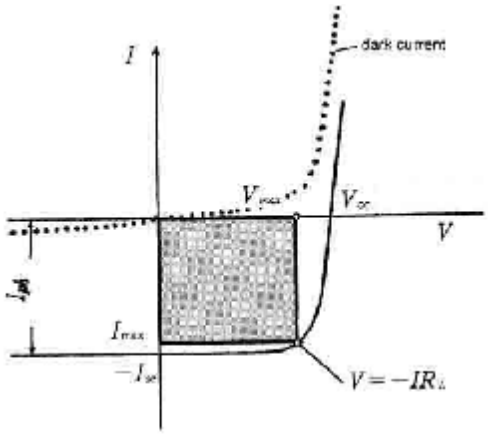

Figure 1-4. Current-voltage (*I*-*V*) curve.

1.1.4 Photo-voltaic materials

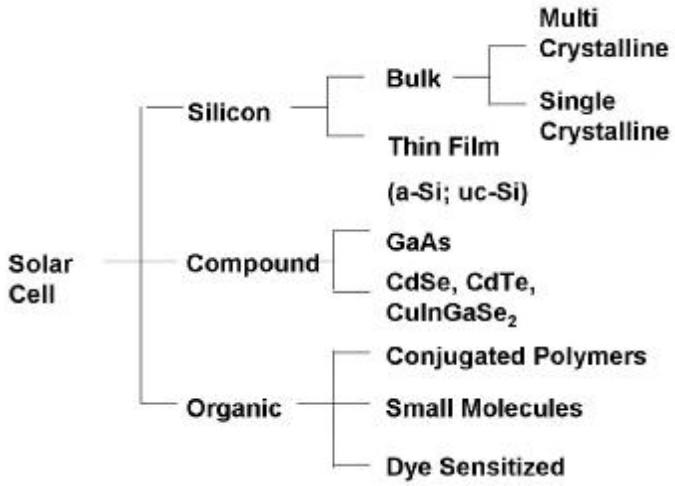

Figure 1-5. Materials of solar cell.

Solar cells consist usually of crystalline silicon and generate direct current when light reaches the cell. Crystalline silicon devices are now approaching the theoretical limiting efficiency of 29% [2]. However, the further development was baffled by the high cost of silicon materials. Inorganic materials (silicon and compound) which have been attempted for photovoltaic solar cells include monocrystalline silicon, polycrystalline silicon, amorphous silicon, cadmium telluride, and copper indium selenide/sulfide. On the same time, the organic materials represented by *n*-type conjugated polymers doped with *p*-type molecules have been also utilized mostly.

1.2 Conjugated polymers and their application to photovoltaic device

Converting solar energy into electricity provides a desirable solution to the energy crisis the world is facing today. Organic solar cells have many advantages such as low cost, light weight, high flexbility and so on [1-3]. Furthermore, polymer-based photovoltaic systems can be subject to wet-processes, e.g. spin-coating and ink-jetting for facile large-area production. Compared with commonly used inorganic photovoltaic solar cells showing the efficiency of around 20%, the solar cells based on the organic materials are still in a narrow field because of its low efficiency approximately 5% [4]. Therefore, the significant efforts are underway to improve their efficiency to the level of practical applications.

1.2.1 Basic theory of photo-voltaic conversion in conjugated polymer device

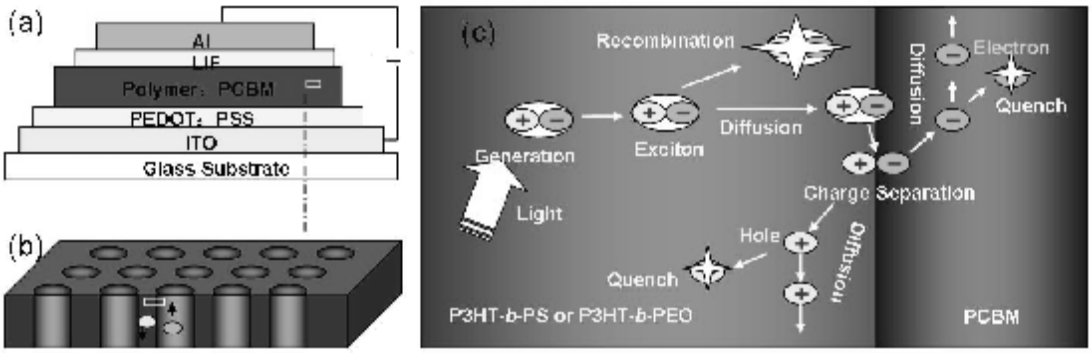

Figure 1-6. Structure of device: ITO / PEDOT: PSS (30 nm) / active layer / LiF (0.5 nm) / Al (100 nm); b) bulk heterojunction micro-phase separated structure of active layer; c) mechanism of electron transportation in active layer: i) excitation via light illumination at donor polymer; ii) electron and hole pair diffusing into the interface of donor and acceptor polymer; iii) electron and hole separating in the interface; iv) electron and hole transporting into the opponent electrodes respectively.

Organic solar cells are known as excitonic solar cells, which are characterized by strongly bound electron–hole pairs (excitons) that are formed after excitation with light. Strongly bound excitons exist in these materials as a consequence of the low dielectric constants in the organic components, which are insufficient to affect direct electron–hole dissociation, as is found in their high dielectric inorganic counterparts. As shown in Figure 1-6, in excitonic solar cells, exciton dissociation occurs almost exclusively at the interface between two materials of different electron affinities (and/or ionization potentials): the electron donor (or simply donor) and the electron acceptor (or simply acceptor). To generate an effective photocurrent in these organic solar cells, an appropriate donor–acceptor pair and device architecture must be selected. Since it is found that the length of exciton diffusion is within around 10 nanometer, the domain sizes of semiconductors significantly influence the external quantum efficiency.

1.2.2 Bulk heterojunction conjugated polymers (BHJ)

Two main approaches have been explored in the effort to develop practicable devices: the donor–acceptor bilayer, commonly achieved by vacuum deposition of molecular components, and the so-called bulk heterojunction (BHJ). The latter is represented as a bi-continuous composite of donor and acceptor phases in the ideal case, thereby maximizing the interfacial area between the donors and acceptors. A BHJ system formed from two different conjugated polymers : poly[2-methoxy-5-(2-ethylhexyloxy)-1,4-phenylene vinylene] (MEHPPV) as the donor and cyano-modifed poly (phenylene vinylene) (CNPPV) as the acceptor was reported [5,6].

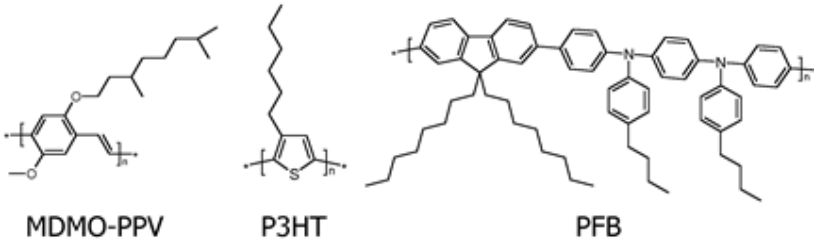

p-type hole-conduction donor polymers

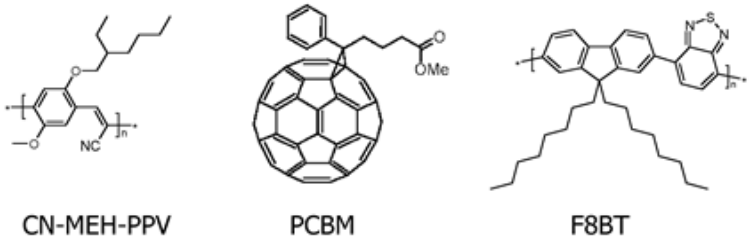

n-type electron-conduction acceptor polymers

Figure 1-7. Bulk heterojunction materials.

Some commonly used conjugated polymers are shown in Figure 1-7. Three important representatives of hole-transporting donor type polymers are MDMO-PPV (poly[2-methoxy-5-(3,7-dimethyl octyloxy)]-1,4-phenylenevinylene), P3HT (poly(3-hexylthio- phene-2,5-diyl) and PFB (poly(9,9'-dioctylfluorene-co-bis-*N*,*N*'-(4-butylphenyl)-bis-*N*,*N*'-phenyl- 1,4-phenylenediamine). They are shown together with electron-transporting acceptor polymers like CN-MEH-PPV-(poly-[2-methoxy-5-(2'-ethylhexyloxy)-1,4-(1-cyanovinylene)-phenylene) and F8TB (poly(9,9'-dioctylfluoreneco-benzothiadiazole) and a soluble derivative of C_{60}, namely PCBM (1-(3-methoxycarbonyl)propyl-1-phenyl[6,6]C_{61}). All of these materials are solution processable due to their side-chain solubilization, and the polymers show photo- and electroluminescence. For the construction of donor–acceptor solar cells, the donor polymers can be either combined with an acceptor polymer or with fullerenes either in planar or diffuse bilayer structures or in blends [7-9].

1.3 Polythiophene

1.3.1 Characteristics of Polythiophene and Poly(3-hexylthiophene) (P3HT)

Polythiophenes (PTs) result from the polymerization of thiophenes, a sulfur heterocycle, which can become conducting when electrons are added or removed from the conjugated π-orbitals via doping.

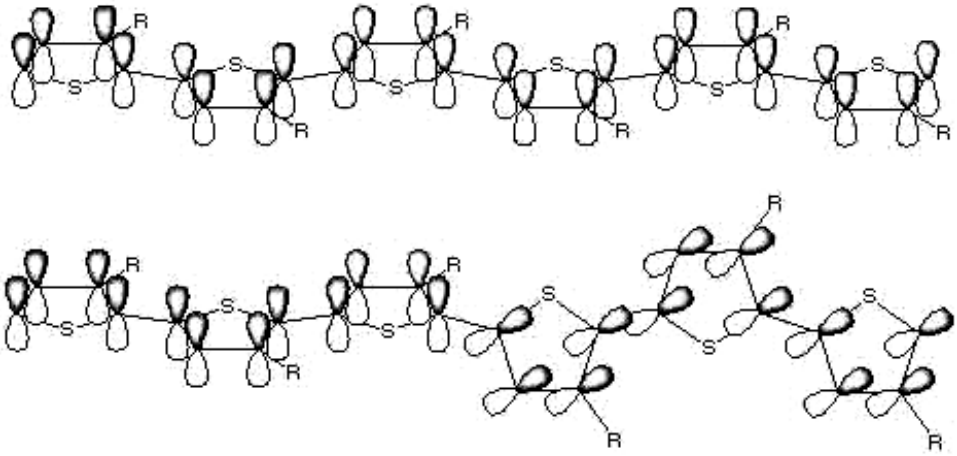

Figure 1-8. Conjugated π-orbits of a coplanar and a twisted substituted of PT.

The studies of PTs have been actively conducted over the last three decades. The maturation of the field of conducting polymers was confirmed by the awarding of the 2000 Nobel Prize in Chemistry.

PTs are one of the most studied and important classes of linear conjugated polymers [10]. Versatile synthetic approaches to PTs, including chemical and electrochemical methods [11], easy functionalization and unique electric properties, which can be widely tuned, focus a tremendous interest on this class of polymers.

Early preparations of PTs have been conducted via both electrochemical and chemical methods. The first chemical preparation of PT was a metal-catalyzed polycondensation polymerization of 2,5-dibromothiophene, reported in 1980 by two groups [12,13]. However, the solubility of these unsubstituted PTs are poor, and they are not soluble even in hot chloroform when the molecular weight greater than 3000 [14].

The introduction of flexible alkyl side-chains transversely attached to the rigid backbone renders the conjugated polymers more readily soluble in organic solvents. The solubility of the polymers allowed the structural characterization and the polymer processing using spin or drop cast methods. In the mid 1980s, Elsenbaumer and co-workers reported the groundbreaking synthesis of soluble and processable PTs by attaching an alkyl side chain on PT (Figure 1-9) [15-17]. Alkyl chains longer than butyl render poly(3-alkylthiophene)s (PATs) soluble in common organic solvents at room temperature [18-20].

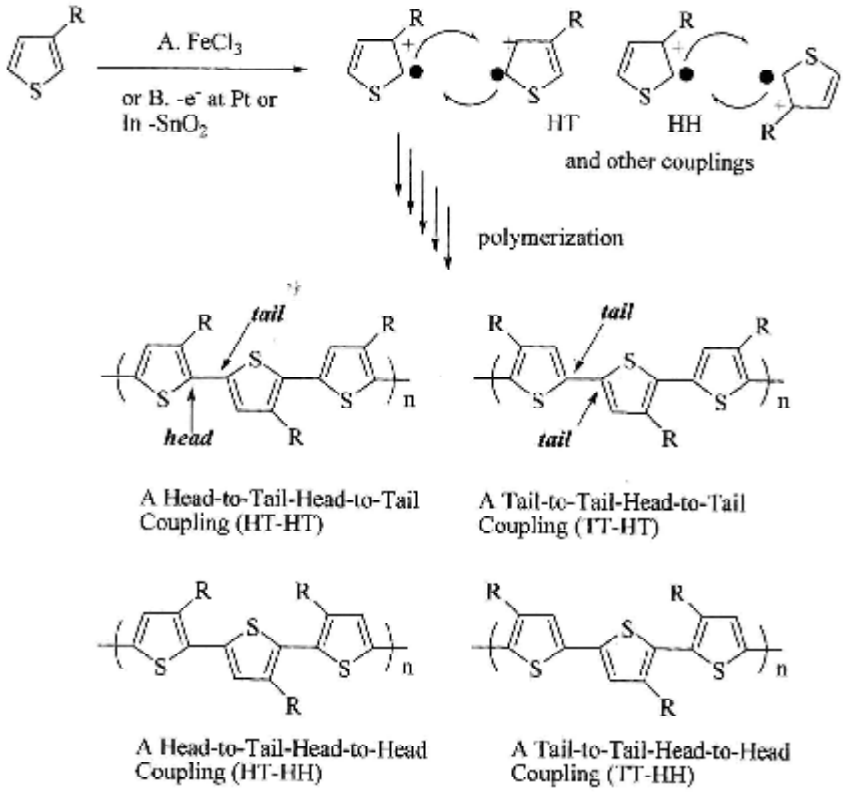

Figure 1-9. Possible regiochemical couplings for PATs.

Schopf and Kobmehl reported a comprehensive review of the literatures in 1990 [21] and 1994 [22]. A general review of conjugated polymers from the 1990s was conducted by Reddinger and Reynolds in 1999 [23]. Finally, Swager *et al.* examined conjugated-polymer-based chemical sensors in 2000. These reviews are excellent guides to the highlights of the primary PT literature from the last two decades. Electrons are delocalized along the conjugated backbones of conducting polymers, usually through overlap of π-orbit, resulting in an extended π-system with a filled valence band. By removing electrons from the π-system (*p*-doping), or adding electrons into the π-system (*n*-doping), a charged unit called a

bipolaron is formed.

The monomer, 3-alkylthiophene, is dissolved in chloroform and oxidatively polymerized with $FeCl_3$, $MoCl_5$ or $RuCl_3$ [24,25]. Generally the "$FeCl_3$ method" has been used to prepare PATs [24-31]. Materials prepared by the $FeCl_3$ method produce PATs with molecular weight ranging from M_n = 30000, to 300000. The $FeCl_3$ method is now well-established as the most widely used and straightforward method to prepare PT and its derivatives [32-43].

1.3.2 Regioregularity of polythiophene

Since 3-alkylthiophene is not a symmetrical molecule, there are three relative orientations available when two thiophene rings are coupling between the 2- and 5- positions. The first of these is 2,5' or head-to-tail coupling (referred to HT hereafter), the second is 2,2' or head-to-head coupling (HH) and the third is 5,5' or tail-to-tail coupling (TT). All of the above methods afford products with three possible regiochemical couplings: HH, TT and HT)s (Figure 1-9). This leads to a mixture of four chemically distinct triad regioisomers when 3-substituted (asymmetric) thiophene monomers are employed [44,45]. The structurally irregular polymers (regiorandom) have a shorter conjugation length due to the twist of adjacent thiophene rings with unfavorable HH couplings.

Regioregular HT poly(3-alkylthiophene)s have a longer conjugation length and a more planar backbone than regiorandom ones, which give a lower band gap, a lower oxidation potential and a higher electrical conductivity [46].

The first synthesis of regioregular head-to-tail coupled PAT was reported by McCullough and Lowe early in 1992 (Figure 1-10) [47]. The PATs synthesized by this method contain ～100% HT-HT couplings. Molecular weights for HT-PTs are typically in the range of M_n = 2000 to 4000 (PDI≈1.4). The PDI was decreased into 1.07 via an improved method reported by Miyakoshi. R (Figure 1-11) [48].

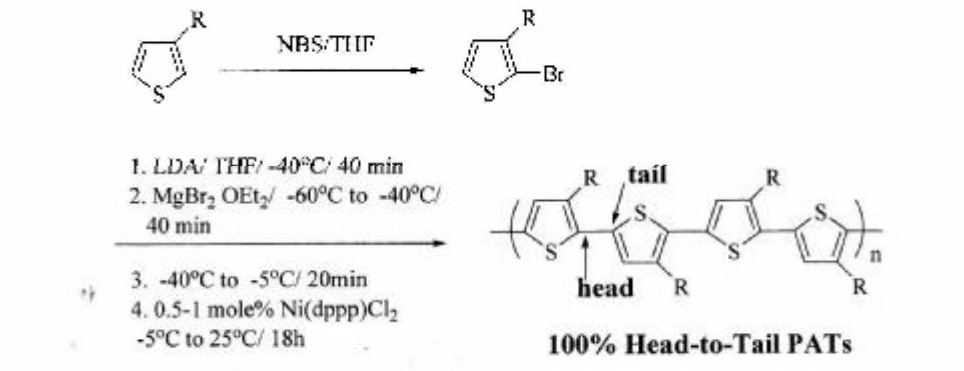

Figure 1-10. McCullongh method for the regioregular synthesis of poly(3-alkylthiophenes) (PATs) with 100% head-to-tail couplings.

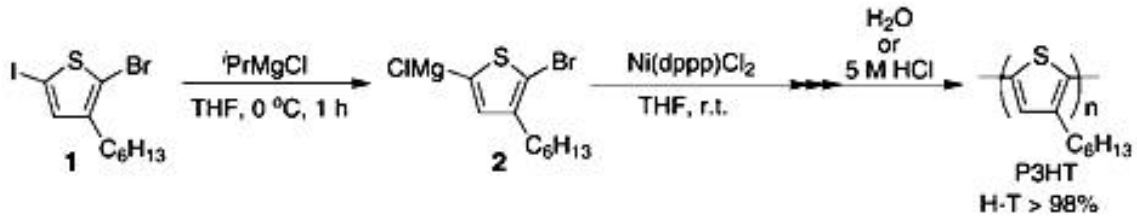

Figure 1-11. Synthesis of P3HT with high regioregularity.

1.3.3 Mechanism of polythiophene polymerization

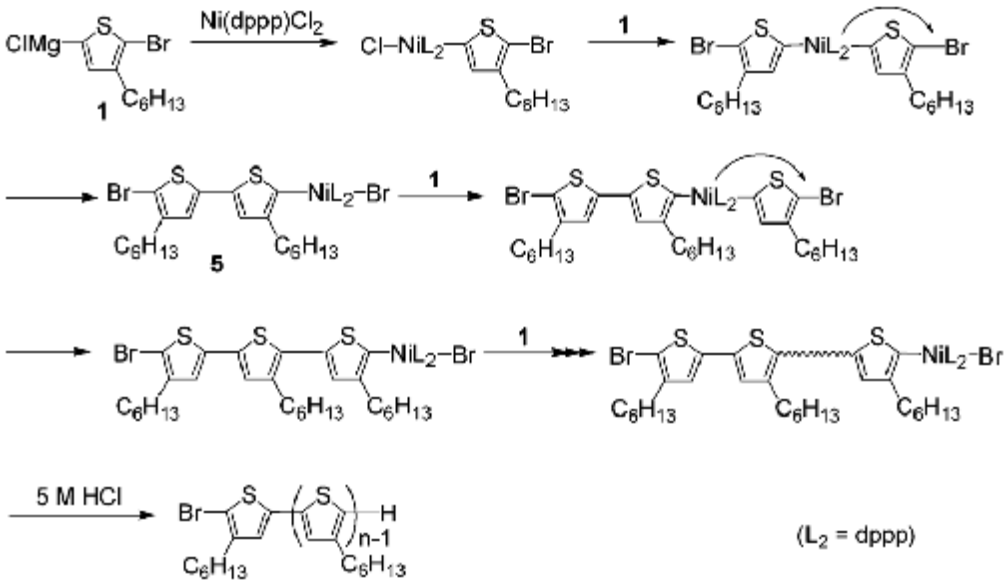

Figure 1-12. The formation of poly(3-hexylthiophene).

One of proposed mechanisms of chain-growth polymerization [49] was shown in Figure 1-12. The polymerization is initiated by formation of the nickel complex thiophene, and thiophene chain grows by the coupling reaction between the polymer end group and monomer 1 via the intermolecular transfer of the Ni (0) to the terminal C-Br bond which will yield the polymer with Br/H-ends. If the Ni (0) was inserted intermolecularly into the C-Br bond of the polymer end group, polymers with Br/Br and H/H end groups would be obtained, as well as the polymer with Br/H end groups. The molecular weight distribution would also become broader, because the coupling reaction would occur equally between all monomers and oligomers in a step-growth polymerization manner. However, these features are inconsistent.

1.4 PCBM

A fullerene derivative [6,6]-phenyl-C61-butyric acid methyl ester (PCBM) is being investigated in organic solar cell [50].

PCBM is a fullerene derivative of C60 buckyball that was first synthesized by the staff of Jan Hummelen and others [51] at the UC Santa Barbara. PCBM is an electron accepting material and is often

used in plastic solar cells or flexible electronics in combination with electron donating materials such as P3HT or other polymers. It is a more practical choice for an electron acceptor compared with fullerenes because of its high solubility in chlorobenzene. This allows solution processable donor/acceptor mixtures, which is a necessary property for the production of printable solar cells.

1.5 Phase separated morphology of thin film

In BHJ donor–acceptor based organic solar cells showing higher power conversion efficiencies, the microscale phase-separated morphology is formed inside composite films. Generally, although polymer/polymer or polymer/small molecule blends form phase-separated structures in a certain condition, there are thermodynamically unstable ones causing low device durability. In addition, fabricating such a structure also requires optimization of processing conditions. On the other hand, block copolymers can form various microphase-separated structures such as lamella and cylinder [52,53]. These structures are more thermodynamically stable than that created by polymer blends. Furthermore, the scale of these structure lies in the order of tens nanometer, which allows photo-generated excitons to reach the interface between *p*- and *n*-type semiconductors effectively. The annealing processes are also effective for controlling the morphology in photovoltaic devices based on BHJ. Two main annealing methods were reported as followed.

1.5.1 Block copolymer base on polythiophene

Block copolymers [54-56] are able t o form definite microphase-separated structure like sphere, cylinder, and lamella. Moreover it is also possible to control the domain size and assist the regular alignment of each domain in the block polymer/small molecule system. Diblock copolymer and triblock copolymer were the main two kinds of block copolymers.

Because the P3HT–nickel complex reacts with the vinyl-containing Grignard reagent selec-tively at the x-chain end to form the mono-functionalized P3HT which is used as a precursor, the AB diblock type were mainly obtained. Sommer. M.[57] synthesized poly(3-hexylthiophene)-*b*-poly(perylene bisimide acrylate), and found that the microphase-separated domain in bulk is formed. This strategy seems promising for photovoltaic applications (vide infra, Section 1-6) because the thermodynamically stable phase-separated structure in nanometer size is formed in the film spontaneously. Poly(3-hexylthiophene)-*b*-poly- (2-vinylpyridine) (P3HT-P2VP) showed nano-structures, of sphere,

cylinder, lamella, and nano fiber structures according to different P2VP volume fractions [58].

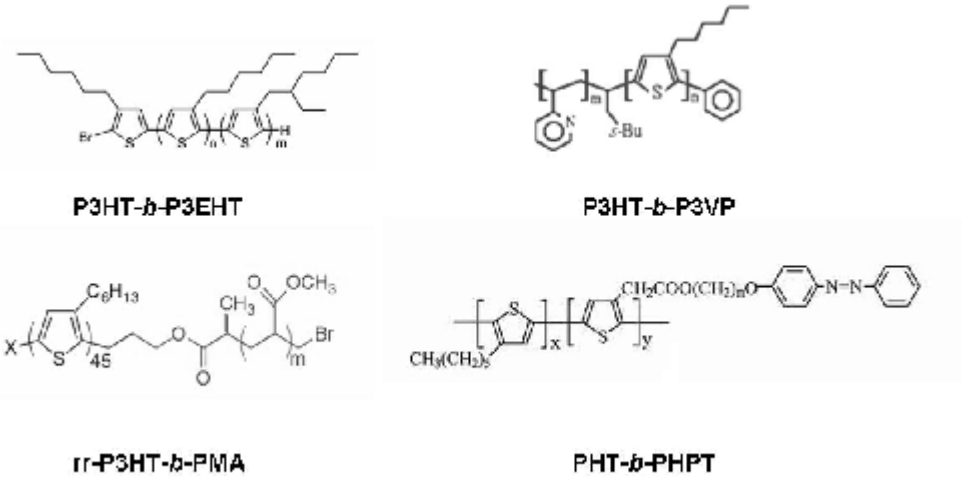

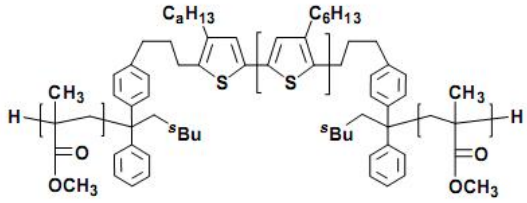

PMMA-P3HT-PMMA

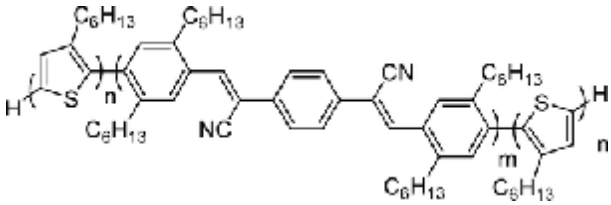

P3HT-HCNPPV-P3HT

Figure 1-13. The block copolymers based on poly(3-hexylthiophene).

In recent years, more complex multi-segmented blocks, such as ABA type, were synthesized. Prof. Mitsuru Ueda[59] reported a kind of triblock of PMMA-*b*-P3HT-*b*-PMMA, which showed continuous nanofibril structures with 12–15 nm widths in thin film prepared by drop casting from a toluene solution at room temperature, followed by annealing at 120 ^{o}C for 24 h. On the contrast, Prof. Ullrich Scherf [60] synthesized an BAB triblock, P3HT-HCNPPV-P3HT. In the surface of P3HT-HCNPPV-P3HT thin film, the

regular nano-sized mesostructure with a diameter of 60-90 nm can be observed by Atomic force microscopy, followed by annealing at 120 ^{o}C for 6 h, which is smaller than that of P3HT.

1.5.2 Thermal annealing

Device fabrication process has been also investigated to achieve high efficiency. Among the various manufacturing techniques, annealing treatment of the semiconducting polymer layer by heating or organic solvent vapor has shown excellent improvement in conversion efficiency. The power conversion efficiency (PCE) of photovoltaic devices was improved from 1.6 to 2.6% based on poly(3-hexylthiophene) (P3HT) and [6,6]-phenyl-C_{61}-butyric acid methyl ester (PCBM) after thermal annealing [61]. The PCE of photovoltaic devices significantly depends on the annealing temperature. Kim et al. investigated the effect of the annealing temperature on the performance of the photovoltaic devices based on P3HT/PCBM blend, found that the annealing temperature at around 140 °C was most effective to achieve high PCE [62-64]

1.5.3 Solvent annealing

Solvent annealing is another way to control the morphology in thin films prepared with block copolymer or polymer blend [65-67] for the device based on P3HT/PCBM, solvent annealing (including solvent aging) can also improve the efficiency of the device [68,69]. For example, Kim. S. H. reported the PEO-*b*-PS block thin film could support an ordered arrays of cylindrical micro domains with domain size of 42.8 nm via simple benzene vapor for 48h.

Shrotriya *et al*. [70] showed that the efficiency improvement was due to the enhancement of exciton generation rate and dissociation probability. Li. G reported that the structure of P3HT chain in P3HT/PCBM blend film after solvent annealing is similar to an ideal RR-P3HT structure, whereas that of P3HT chain showed a common region-random P3HT structure without annealing. After solvent annealing under 1,2-dichlorobenzene(DCB), the PCE increased into 3.7% from 0.8% before solvent annealing, and the optical absorption, J_{sc} increased too [71]. By solvent annealing, the fill factor of solar cell with P3HT and [6,6]-phenyl-C_{71}-butyric acid methyl esters ($PC_{71}BM$) increased to 73% and the power conversion efficiency to 3.80% [72].

1.6 Synthesis method

1.6.1 Atom transfer radical polymerization

As for the preparation of graft and block copolymers, it is important to control their formation including functionality, composition, size and molecular weight dispersity. The traditional living anionic polymerization yields products with very low polydispersities, however it has been carried out under very strict conditions to avoid impurities such as water and oxygen and the highly reactive carbanion prohibits the use of various functional groups. Recently, this has been overcome by the development of the controlled/“living” radical polymerization techniques, particularly atom transfer radical polymerization (ATRP) [73-76]. Figure 1-14 shows a application of ATRP for polymerization of polystyrene.

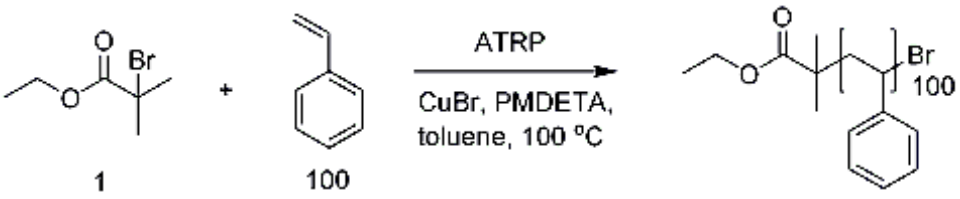

Figure 1-14. An example of ATRP polymerization for polystyrene.

The control of the polymerization afforded by ATRP is a result of the formation of radicals that can grow, but are reversibly deactivated to form dormant species.

Mechanistically, as shown in Figure 1-15, ATRP is based on an inner sphere electron transfer process，which involves a reversible (pseudo)halogen homolytic transfer between a dormant species, an added initiator or the propagating dormant chain end, (R-X) and a transition metal complex in the lower oxidation state (Mt^m/L_n) resulting in the formation of propagating radicals (R·) and the metal complex in the higher oxidation state with a coordinated halide ligand (e.g. X- Mt^{m+1}/L_n). The active radicals form at a rate of activation (k_{act}), subsequently propagate with a rate (k_p) and reversibly deactivate (k_{deact}), but also terminate (k_t). As the reaction progresses radical termination is diminished as a result of the persistent radical effect, (PRE), polymer chain length, and the equilibrium is strongly shifted towards the dormant species ($k_{act} < k_{deact}$). Such a process results in a polymer chain that slowly, but steadily, grows and has a well-defined end group (for ATRP that end group is usually an alkyl halide) [77-80].

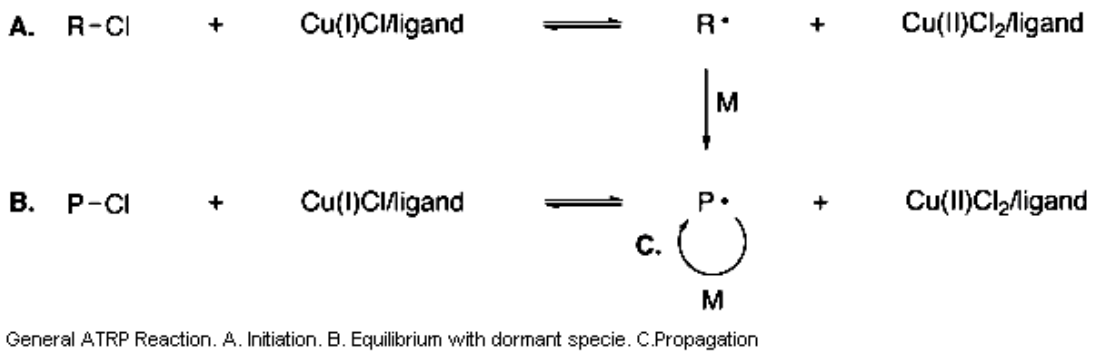

Figure 1-15. Mechanism of metal complex-mediated ATRP [82].

The initiator is generally a simple, commercially available, alkyl halide. The catalyst is a transition metal that is complexed by one or more ligands; the catalyst does not need to be used in a one-to-one ratio with the initiator, and it can be used in much smaller amounts. The deactivator can be formed in situ, or for better control, a small amount (relative to the catalyst) can be added. Additionally, the catalyst is tolerant of water and a trace amount of oxygen.

Although other controlled radical polymerization systems have been established, ATRP remains the most powerful, versatile, simple and inexpensive. Only ATRP has been able to polymerize a wide range of monomer including various styrenes, acrylates and methacrylates as well as other monomers such as acrylonitrile, vinyl pyridine and dienes.

1.6.2 Suzuki coupling reaction

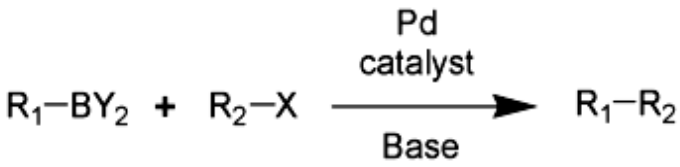

Figure 1-16. Scheme of Suzuki coupling reaction.

Suzuki reaction is cross coupling of an aryl- or vinyl-boronic acid with an aryl- or vinyl-halide catalyzed by a palladium(0) complex (Figure 1-16) [83,84]. It is widely used for the preparation of substitute biphenyls, and has been extended to incorporate alkyl bromide [85-87]. Suzuki reaction was awarded to the 2010 Nobel Prize in Chemistry.

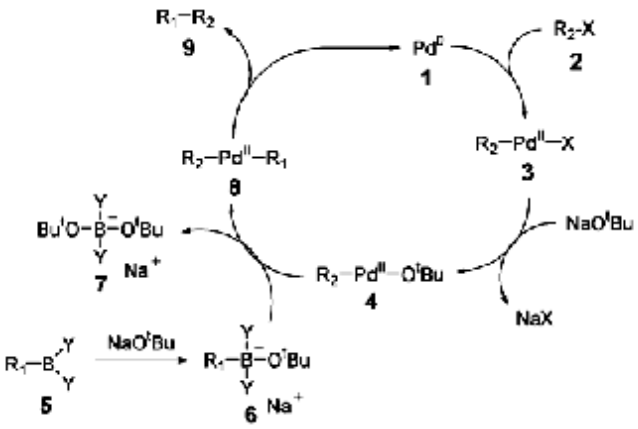

Figure 1-17. Mechanism of Suzuki coupling reaction.

The reaction also works with pseudohalides, such as triflates, instead of halides, and also with boron-esters instead of boronic acids.

The reaction relies on a palladium catalyst such as tetrakis(triphenylphosphine)palladium(0) to effect part of the transformation. The palladium catalyst (more strictly a pre-catalyst) is 4-coordinate, and usually involves phosphine supporting groups.

The mechanism of the Suzuki reaction is best viewed from the perspective of the palladium catalyst as shown in Figure 1-17. The first step is the oxidative addition of palladium to the halide 2 to form the organopalladium species 3. The reaction with base gives intermediate 4, which via transmetalation with the boronate complex 6 forms the organopalladium species 8. The reductive elimination of the desired product 9 restores the original palladium catalyst 1.

According to the report of Fujioka. M.[88], a novel triblock polymer of poly(ethylene oxide)-*b*-poly(4-butyltriphenylamine)-*b*-poly(ethylene oxide) consisting of PBTPA and inert PEO was synthesized via Suzuki coupling of end brominated PBTPA and PEO with pinacol borate moiety.

1.7 Concept for this work

The polymer solar cells based on P3HT/(fullerene derivatives) blends have widely been researched for their excellent charge conductive property. The high photovoltaic conversion efficiency is believed to be achieved by suitable phase separated morphology known as bulk heterojunction. It means that the morphology of polymer will be well controlled in order to achieve higher efficiency. Because polymer blends or co-orposites are thermal dynamically unstable, the author focused on block copolymers containing charge transporting segment such as P3HT to utilize advantages such as higher stability and ability to form regular phase-separated structure.

In this thesis, the author designs the block copolymers consisting of regioregular P3HT and an inert block. It is possible to control the morphology in the composite film consisting of *p*-type P3HT block copolymer and *n*-type small molecule (PCMB) during a formation of microphase separated structure. The author selected polystyrene (PS) and poly(ethyl oxide) (PEO) as the other segment to build up diblock copolymer. The former, which is hydrophobic, shows affinity with PCBM, while the latter, which is hydrophilic, showing little affinity with PCBM. The establishment of the relationship between precisely controlled morphology and the device performance is also aimed.

In Chapters **2** and **3**, the block copolymer of poly(3-hexylthiophesne)-*block*-polystyrene (P3HT-*b*-PS) was synthesized by Suzuki coupling reaction between polystyrene and highly regioregular P3HT. Since P3HT and polystyrene were separately prepared by Grignard metathesis and atom transfer radical polymerizations, respectively, the regioregularity and the polydispersity of polymers are precisely controlled. The phase-separated structure in the thin film of the composites of block copolymer with PCMB was investigated by UV and AFM analyses to clarify the relationship between morphologies constructed in the polymer layer and the device performance.

In order to control the phase-separated structure precisely, annealing by heating or immersing in solvent vapor atmosphere were carried out on the thin film prepared from P3HT and P3HT-*b*-PS, respectively. The annealing time and temperature were optimized for the block copolymer system.

Finally, the devices based on P3HT-*b*-PS and P3HT with PCBM were fabricated. The *I*-*V* curve was measured to evaluate conversion efficiency.

In Chapters **4** and **5**, another block copolymer, poly(3-hexylthiophene)-*block*-poly(ethylene oxide)

(P3HT-*b*-PEO) was synthesized by the Suzuki coupling reaction between polar and flexible PEO with the end group of boronic ester and highly regioregular P3HT. PEO was selected as the second block because some researchers reported that the block copolymers containing PEO segment afforded the microphase-separated structure which aligned vertical to a substrate as mentioned above. The microphase-separated structure in these thin films was investigated by UV and AFM analyses. Annealing by heating or immersing in solvent vapor atmosphere was carried out on the photovoltaic devices prepared from P3HT or P3HT-*b*-PEO blended with PCBM. The effect of spin-coating speed and the weight conception of PEO segment of block copolymer for active layer thickness were optimized for block copolymer system. The *I-V* characteristics were evaluated for the devices, and the correlation between the morphology and the device performance was discussed.

In Chapter **6**, general conclusions about the study are described.

1.8 Reference

[1]. Blom, P. W.; Mihailetchi, V. D.; Koster, L. J.; Markov, D. E. *Adv. Mater*. **2007**, 19, 1551.

[2]. Economopoulos, S. P.; Govaris, G. K.; Chochos, C. L. *Macromol. Symp*. **2004**, 205, 19.

[3]. Zhang, Y.; Tajima, K.; Hirota, K.; Hashimoto, K. *J. Am. Chem. Soc*. **2008**, 130, 7812.

[4]. Gupta, D.; Kabra, D.; Kolishetti, N; Ramakrishnan, S. *Adv. Funct. Mater*. **2007**, 17, 226.

[5]. Harald, H.; NiyaziSerdar, S. *J. Mater. Res*. **2004**, 19, 7.

[6]. Burroughes, J. H.; Bradley, D. D. C.; Brown, A. R.; Holmes, A. B. *Nature*. **1990**, 347, 539.

[7]. Braun, D.; Heeger, A. *J. Appl. Phys. Lett*. **1991**, 58, 1982.

[8]. Organic Light-Emitting Devices: *A Survey. Shinar*. New York. **2004**.

[9]. Roncail.; J. *Chem. Rev*. **1992**, 92, 711.

[10]. Roncail.; J. *Chem. Rev*. **1999**, 9, 1875.

[11]. Yamamoto, T.; Sanechika, K.; Yamamoto, A. *J. Polymer. Sci, polymer. Lett. Ed*. **1980**, 18, 9.

[12]. Lin, J. W.; Dudek, P. *J. Polym. Sci, Polym. Chem. Ed*. **1980**, 18, 2869.

[13]. Yamamoto, T.; Morita, A.; Miyazaki, Y.; Maruyama, T. *Macromolecules*. **1992**, 25, 1214.

[14]. Jen, K. Y.; Oboodi, R.; Elsenbaumer, R. L. *Polym. Mater. Sci. Eng*. **1985**, 53, 79.

[15]. Elsenbaumer, R. L.; Jen, K. Y.; Oboodi, R. *Synth. Met*. **1986**, 15, 169.

[16]. Miller, G. G.; Elsenbaumer, R. L. *J. Chem. Soc. Chem. Commun*. **1986**, 1346.

[17]. Sugimoto, R.; Takeda, S.; Gu. H. B.; Yoshino, K. *Chem. ExPress*. **1986**, 1, 635.

[18]. Sato, M.; Tanaka, S.; kaeriyama, K. J. Chem. Soc, *Chem. Commun*. **1986**, 873.

[19]. Hotta, S.; Rughuooputh, S. D. D. V. A.; Heeger, J.; Wudl, F. *Macromolecules*. **1987**, 20, 212.

[20]. Street, G. B.; Clarke, T. C. IBM, J. *Res. Dev*. **1981**, 25, 51.

[21]. Schopf, G.; Kobmehl, G. *Adv. Polym. Sci*. **1997**, 129, 1.

[22]. Reddinger, J. L.; Reynolds, J. R. *Adv. Polym. Sci*. **1999**, 145, 57.

[23]. McQuade, D.; Tyler. Pullen. Anthony. E. Swager. *Chemical Reviews*. **2000**, 100, 2537.

[24]. Yoshino, K.; Hayashi, S.; Sugimoto, R. *J. Appl. Phys*. **1984**, 23, 899.

[25]. Osterholm, J. E.; Laakso, J.; Nyholm, P.; Isotala, H.; Inganas, O. *Synth. Met*. **1989**, 28, 435.

[26]. Hoda, S.; Soga, M.; Sonata, N. *Synth. Met*. **1988**, 26, 267.

[27]. Yoshino, K.; Nakajima, S.; Suginoto, R. *J. Appl. Phys*. **1987**, 26, 1038.

[28]. Kulszewicz, B. I.; Pwlicka, A.; Olenkiewicz, J.; Lefrant, S. *Synth. Met*. **1989**, 30, 335.

[29]. Leclerc, M.; Diaz, F. M.; Wgner, G.; *Macromol. Chem.* **1989**, 190, 3105.

[30]. Pomerantz, M.; Tseng, J. J.; Zhu, G.; Sproull, S. J.; Rynolds, J. R. *Synth. Met*. **1991**, 41, 825

[31]. Abdou, M. S. A.; Lu, X.; Xie, Z. W.; Orfino, F.; Deen, M. J. *Chem. Mater*. **1995**, 7, 631.

[32]. Chen, F.; Mehta, O. G.; Takiff, L.; McCullough, R. D. *J. Mater. Chem*. **1996**, 6, 1763.

[33]. Niemi, V. M.; Knuuttila, O.; Isterholm, J. E.; Korvola. *J. Polymer*. **1992**, 33, 1559.

[34]. Laakso, J.; Jarvinen, H.; Sgerberg. B. *Synth. Met*. **1993**, 55, 1204.

[35]. Jarvinen, H.; Lathtine, L.; Nasma, J.; Hormi, O.; Tammi, A. L. *Synth. Met*. **1995**, 69, 299.

[36]. Taka, T.; Nyholm, P.; Laakso, J.; Loponen, M. T.; Osterholm, J. E. *Synth. Met*. **1995**, 69, 299.

[37]. Yoshino, K.; Nakajima, S.; Fuji, S.; Suginomo, R. *Polym. Commun*. **1987**, 28, 309.

[38]. Inganas, O.; Salaneck, W. R.; Osterholm, J.; Laasko, J. *Synth. Met*. **1988**, 22, 395.

[39]. Reynolds, J. R.; Ruiz, J. I.; Child. A. D.; Marynick, S. *Macromolecules*. **1991**, 24, 678.

[40]. Yoshino, K.; Nakajima, S.; Onada, M.; Sginoto, R. *Synth. Met*. **1989**, 28, 349.

[41]. Gatum, O. R.; Carlsen, O. H. J.; Samuelsen, E. j.; Mardalen, J. *Synth. Met*. **1993**, 58, 115.

[42]. Chen, F.; Mehta, O. G.; Takiff, L.; McCullough, R. D. *J. Mater. Chem*. **1996**, 6, 1763.

[43]. Sato, M.; Morii, H. *Polym. Commun*. **1991**, 32, 42.

[44]. Sato, M.; Morii, H. *Macromolecules*. **1991**, 24, 1196.

[45]. Perepichka, I. F.; OErepichka, D. F.; Meng, H.; Wudl, F. *Adv*. *Mater*. **2005**, 17, 2281.

[46]. McCullogh, R. D.; Lowe, R. D. J. Chem. Soc. *Chem. Commun*. **1992**, 70.

[47]. Miyakoshi, R.; Yokoyama, A.; Yokozawa, T. *Macromol. Rapid Commun*. **2004**, 25, 1663.

[48]. Miyakoshi, R.; Yokoyama, A.; Yokozawa, T. *J. Am. Chem. Soc*. **2005**, 127, 17545.

[49]. Cecilia, B.; Andrzej, B.; Jakub, B.; Mattias, S. *Journal of Physics: Condensed Matter*. **2005**, 17, 529.

[50]. Hummelen, J.; Knight, B, W.; LePeq, F.; Wudl, F.; Yao, J.; Wilkins, C. L. *J. Org. Chem.* **1995**, 60, 532.

[51]. Lindner, S. M.; Httner, S.; Chiche, A.; Thelakkat, M. *Angew. Chem. Int. Ed*. **2006**, 45, 3364.

[52]. Hauch, J. A.; Schilinsky, P.; Choulis, S. A. *Sol. Enrg. Mat. Sol. C*. **2008**, 92, 727.

[53]. Sauve, G.; McCullough, R. D. *Adv. Mater*. **2007**, 19, 1822.

[54]. Zhang, Y.; Tajima, K.; Hirota, K.; Hashimoto, K. *J. Am. Chem. Soc.* **2008**, 130, 7812.

[55]. Zhao, X. Y*. J. Mater. Sci.* **2005**. 40. 3423.

[56]. Sommer, M.; Lang, A.; Thelakkat, M. *Ange*. *Chem*. **2008**, 47, 7901.

[57]. Dai, C.; Yen, W.; Lee, Y.; Ho, C.; Su, F. *J. Ameri. Chem. Soc.* **2007**, 129, 11036.

[58]. Higashihara, T.; Ueda, M. *React Funct Polym*. **2009**, 69, 457.

[59]. Nakamura, M.; Yang, C.; Tajima, C.; Hashimoto, K. *Sol. Enrg. Mat. Sol. C.* **2009**, 93, 1681

[60]. Cook, S.; Tuladhar, S. M.; Choulis, S. A.;McCulloch, I.; Ha. C.; Ree, M. *Nat. Mater*. **2006**, 5, 197.

[61]. Li, G.; Shrotriya, V.; Yao, Y.; Huang, J.; Yang, Y. *J. Mater. Chem*. **2007**, 17, 3126.

[62]. Reyes, R. M.; Kim, K.; Carroll, D. L. *Appl. Phys. Lett*. **2005**, 87.

[63]. Elbs, H.; Drummer, C.; Abetz, V.; Krausch, G. *Macromolecules*. **2002**, 35, 5570.

[64]. Kim, S. H.; Misner, M. J.; Russell, T. P. *Adv. Mater*. **2004**, 16, 2119.

[65]. Cavicchi, K. A.; Russell, T. P. *Macromolecules*. **2007**, 40, 1181.

[66]. Guo, R.; Huang, H. Y.; Chen, Y. Z.; Gong, Y. M.; Du, B. Y. *Macromolecules* **2008**, 41, 890.

[67]. Huang, W. Y.; Huang, P. T.; Han, Y. K.; Lee, C. C. *Macromolecules* **2008**, 41, 7485.

[68]. Shrotriya, V.; Yao, Y.; Li, G.; Yang, Y. *Appl. Phys. Lett*. **2006**, 89, 63505.

[69]. zhao, Y.; Xie, Z.; Qu, Y. *Appl. Phys. lett*. **2007**, 90, 4354.

[70]. Chu, C. W.; Yang, H.; Hou, W. J.; LI, J. H.; Li, G.; Yang, Y. *Appl. Phys. Lett*. **2008**, 92, 103306.

[71]. Wang, J. S.; Matyjaszewski, K. *Macromolecules*. **1995**, 28, 7901.

[72]. Wang, J. S.; Matyjaszewski, K. *J. Am. Chem. Soc*. **1995**, 117, 5614.

[73]. Patten, T.; Xia, J.; Abenathy, T.; Matyjaszewski, K.; Sheiko, M. *Macromolecules*. **1998**, 31, 9413.

[74]. Beers, K.; Gaynor, S.; Matyjaszewski, K.; Sheiko, S.; Moller, M. *Macromolecules*. **2001**. 31, 9413.

[75]. Boerner, H.; Beers, K.; Matyjaszewski, K.; Sheiko, S.; Moller, M. *Macromolecules*. **2001**. 34, 4375.

[76]. Singleton, D. A.; Nowlan, D. T. I.; Jahe, N.; Matyjaszewski, K. *Macromolecules*. **2003**, 36, 8609.

[77]. Fisher, H. *Chem. Rev*. 2001, 101, 3581.

[78]. Vana, P.; Davis, T. P.; Barner-kowollik, C. *Macromolecular Rapid Commun*. **2002**, 23, 952.

[79]. Tang, W.; Tsarevsky, N. V.; MAtyjaszewski, K. *J. Am. Chem. Soc*. **2006**, 128, 1598.

[80]. Kaft, A.; Grimsdale, A. C.; Holmes, A. B. *Angew. Chem. Int. Ed*. **1998**, 37, 402.

[81]. Miyaura, N.; Yamada, K.; Suzuki, A.*Tetrahedron Letters*. **1979**, 20, 3437

[82]. Miyaura, N.; Suzuki, A. *Chem. Commun*. **1979**, 18, 866.

[83]. Suzuki, A. *Pure. Appl. Chem*. **1991**, 63, 419.

[84]. Singleton, D. A.; Nowlan, D. T. I.; Jahe, N.; Matyjaszewski, K. *Macromolecules*. **2003**, 36, 8609.

[85]. Reynolds, J. R.; Ruiz, J. I.; Child. A. D.; Marynick, S. *Macromolecules*. **1991**, 24, 678.

[86]. Suzuki, A. *J. Organomet Chem*. **1999**, 576, 147.

[87]. Matos, K.; Soderquist, J. A. *J. Org. Chem*. **1998**, 63, 461.

[88]. Fujioka, M.; Sato, H.; Tsuchiya, K.; Ogino, K. *Chem. lett*. **2008**, 37, 350.

Chapter 2 . Synthesis and Characterization of Poly(3-hexylthiophene)-*b*-polystyrene Block Copolymer

2.1 Introduction

Poly(3-hexylthiophene) (P3HT) and its derivatives are important members of conducting polymer family for promising a great number of potential applications such as photovoltaic device due to due to their high electric conductivity and thermal stability [1,2]. Organic solar cells based on P3HT in combination with a fullerene derivative have been intensively investigated to show highly conversion efficiency around 5% [3,4]. Highly device performance in such a blend system is assumed to be achieved by suitable phase-separated morphology known as bulk heterojunction. The scale of these structure lies in the order of tens nanometer, which allows photo-generated excitons to reach the interface between *p*- and *n*-type semiconductors effectively [5,6]. Therefore precise control of morphology of the active layer is a key to improve the conversion efficiency of polymer solar cells.

Various block copolymers consisting of charge transporting segments have been reported[7-11]. Block copolymers show self assembly to form various microphase-separated structures such as lamella and cylinder, and are expected to control the domain size and assist the regular alignment of each domain in the block polymer/small molecule system.

In this chapter, a new block copolymer, poly(3-hexylthiophene)-*b*-polystyrene (P3HT-*b*-PS) was synthesized via Suzuki coupling reaction. P3HT with high regioregularity and PS with well-defined structure were separately prepared by Grignard metathesis and atom transfer radical polymerizations, respectively. Figure 2-1 shows the synthetic scheme for P3HT-*b*-PS. The resulting polymers were characterized by NMR and GPC. The microphase-separated structure in the thin polymer films was examined by UV and AFM analyses.

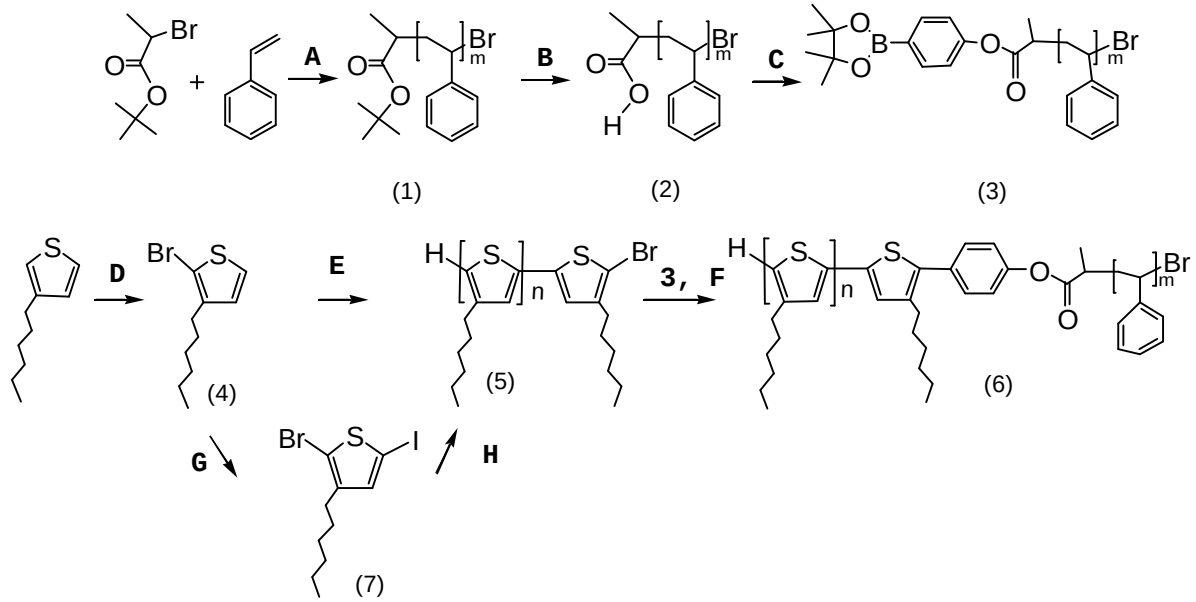

Conditions: (A) CuBr, $CuBr_2$, PMDETA; (B) *p*-toluene sulfonic acid, 1.4-dioxane; (C) DCC, DMAP, tetramethyl borolan phenol; (D)NBS; (E) isopropylamine, *n*-butyllithium, $ZnCl_2$, $Ni(dppp)Cl_2$; (F) $Pd(PPh_3)_4$; (G) $PhI(OAc)_2$, I_2; (H) $Ni(dppp)Cl_2$, isopropyl MgBr.

Figure 2-1. Synthesis of P3HT-*b*-PS via Suzuki coupling polymerization.

2.1 Experimental

2.1.1 Materials and instrumentation

Tetrahydrofunan (THF) was dried by distilling over calcium hydride, and stored under nitrogen atmosphere. Styrene was distilled under vacuum. The other reagents and solvents were obtained commercially and were used as received.

2.1.2 Preparation of homopolymer of PS (1) by ATRP

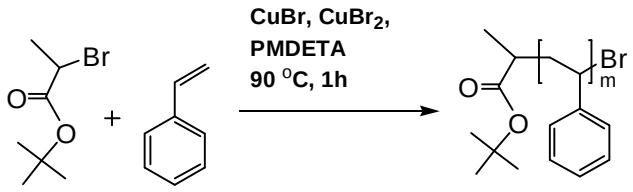

Figure 2-1. Preparation of homopolymer of PS (1) by ATRP.

2-Bromopropionic acid *tert*-butyl ester (0.146 ml, 0.875 mmol), styrene (20 ml, 0.175 mmol), anisole (4.7 ml, 0.0438 mol), CuBr (0.125 g, 0.875 mmol), $CuBr_2$ (0.01 g, 0.0438 mmol), and *N,N',N'',N'''*-pentamethyldiethylenetriamine (0.185 ml, 0.875 mmol) were added into a flask. The mixture was subject to freeze-and-thaw cycles to eliminate air, then was heated for 24 h at 90 °C. The reaction mixture was poured into methanol to precipitate the product. M_n: 1800; Yield: 4.06 g, 20%.

2.1.3 Preparation of PS with end group of carboxylic acid (2)

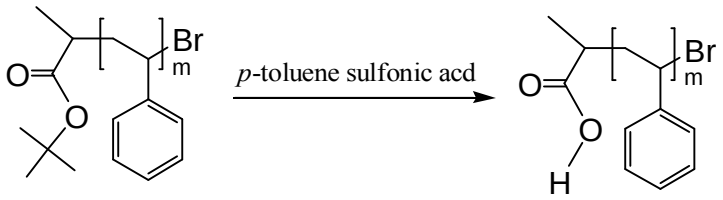

Figure 2-2. Preparation of PS with end group of carboxylic acid (2)

Polystyrene **1** (3.6 g, 2.0 mmol), *p*-toluenesulfonic acid (3.44 g, 20 mmol), dioxane (anhydrous, 9 ml, 10 mmol) were placed into a flask, and the mixture was stirred for 24 h at 95 °C. The product was precipitated in methanol. Yield: 2.1 g, 61.2%.

2.1.4 Preparation of PS with end group of boron ester (3)

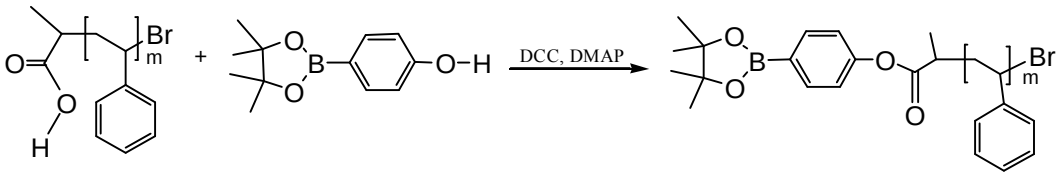

Figure 2-3. Preparation of PS with end group of boron ester (3)

Homopolymer **2** (0.36 g, 0.2 mmol), CH_2Cl_2 (5 ml), 4-(4,4,5,5-tetramethyl-1,3,2-dioxaborolan-2-yl)phenol (0.155 g, 0.7 mmol), DCC (0.076 g, 0.6 mmol), DMAP (0.123 g, 0.6 mmol) were placed into a flask, then the mixture was stirred for 24 h at r.t. The product was precipitated in methanol. Yield: 0.287 g, 71.8%.

2.1.5 Preparation of 2-bromo-3-hexylthiophene (4)

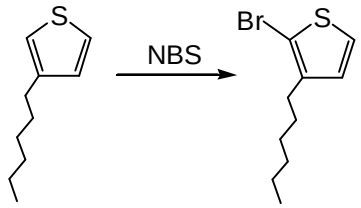

Figure 2-4. Preparation of 2-bromo-3-hexylthiophene (4)

3-Hexylthiophene (5.00 g, 29.7 mmol) and THF (50 ml) were placed to flask. NBS (5.43 g, 30.5 mmol) was separated into 5 parts, and each part was added every 3min at 0 ^{o}C. After two hours reaction at r.t, the product was extracted with chloroform, purified into 99% by the column chromatography (silica/hexane). Yield: 92%.

2.1.6 Preparation of 2-bromo-3-hexyl-5-iodothiophene (7)

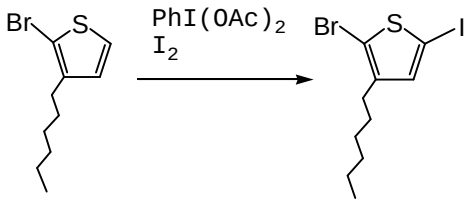

Figure 2-5. Preparation of 2-bromo-3-hexyl-5-iodothiophene (7)

Iodine (2.84 g, 11.2 mmol) and Iodobenzene diacetate (3.93 g, 12.2 mmol) were added successively to a stirred solution of 2-bromo-3-hexylthiophene (5.00 g, 29.7 mmol) in CH_2Cl_2 (50 ml) at 0 ^oC, and the reactive mixture was stirred for 4h at r.t. Then 10% aqueous NaS_2O_3 was added. The mixture was extracted with Et_2O. The product was purified by silica gel column chromatography (eluent: hexane). Yield: 2.86 g, 38%.

2.1.7 Polymerization of P3HT from 2-bromo-3-hexylthiophene (5)

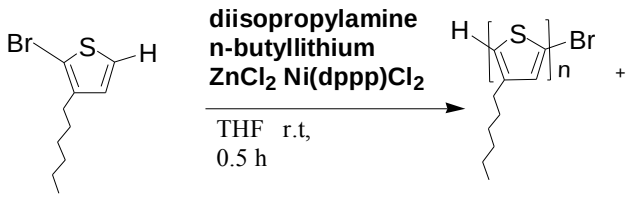

Figure 2-6. Preparation of P3HT from 2-bromo-3-hexylthiophene (5)

Distillated THF were placed into a flask and cooled down to -78 ^oC. Diisopropylamine (3.72 ml, 26.3 mmol)、*n*-butyllithium (2.6 mol/L solution, 9.61 ml, 25.0 mmol) was added, and then the temperature was increased up to rt. After stirring for 5 min. the temperature was returned to -78 ^oC, and then 2-bromo-3-hexylthiophene (6.50 g, 26.3 mmol) was added. After stirring for 5 min, $ZnCl_2$ (3.76 g, 27.6 mmol) was add. The reaction mixture was stirred for 2 h, and then the temperature rised up to ^oC. After the addition of bis(diphenylphosphino) propanedichloronickel(iiII) ($Ni(dppp)Cl_2$), the stirring was continued for 30 min. The resulting mixture was poured into methanol to precipitate the product which was extracted by Soxhlet with hexane, dichloromethane, and THF in turn. Yield: 0.0248 g, 0.130 g, 0.734 g and 0.57%, 3.0% and 17%, respectively.

2.1.8 Preparation of P3HT from 2-bromo-3-hexyl-5-iodothiophene

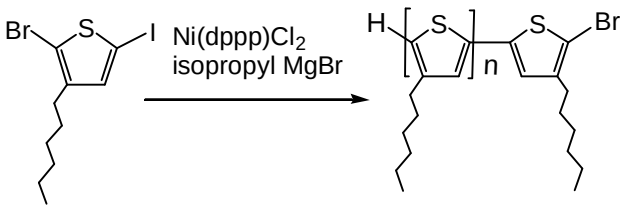

Figure 2-7. Preparation of P3HT from 2-bromo-3-hexyl-5-iodothiophene

2-Bromo-3-hexyl-5-iodothiophene (2.8g, 7.2 mmol), THF (30 ml), isopropylmagnesium chloride (3.5 ml, 2.0M in THF) were added into flask and reacted for 1h at 0 ^{o}C. Ni(dppp)Cl_2 (12 mg, 0.022 mmol) and dry THF 5 ml were added and reacted for 8h at r.t. The product was reprecipitated in methanol three times. Yield : 1.102g, 39.3%.

2.1.9 Preparation of block copolymer P3HT-*b*-PS (6)

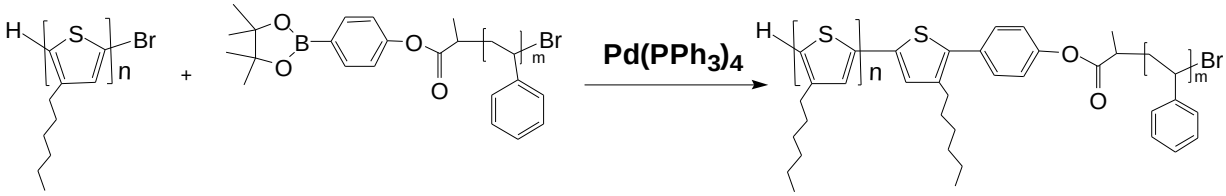

Figure 2-8. Preparation of P3HT-*b*-PS block copolymer (6)

$Pd(PPh_3)_4$ （0.023 g, 0.02 mmol）, 3 M K_2CO_3 (aqueous solution, 0.35 ml), homopolymer **3** (0.108 g，0.06 mmol) and homopolymer **5** (0.104 g, 0.02 mmol), toluene (6.7 ml) were placed into a flask, followed by freeze-and-thaw cycles to eliminate air in the mixture. Then the mixture was stirred for 24 h at 100 ^{o}C. The product was reprecipitated in methanol twice and in acetone twice. Yield: 0.084 g, 40%.

2.2 Measurements

Nuclear magnetic resonance (NMR) spectroscopy

^{1}H and ^{13}C NMR spectra were obtained on a JEOL ALPHA500 instrument at 500 and 125 MHz, respectively. Deutrated chloroform was used as a solvent with tetramethylsilane as an internal standard.

Gel permeation chromatography (GPC)

Number- and weight-average molecular weights (M_n and M_w) were determined by gel permeation chromatography (GPC) analysis with a JASCO RI-2031 detector eluted with chloroform at a flow rate of 1.0 ml/min and calibrated by standard polystyrene samples.

Differential scanning calorimetry (DSC)

Differential scanning calorimetry (DSC) analyses were performed on a Rigaku DSC-8230 under a nitrogen atmosphere at heating and cooling rates of 10 °C/min.

The second circle was used with heating speed of 10℃/min from 80 ℃ to 280 ℃

High Performance Liquid Chromatography (HPLC)

The purify of 2-bromo-3-hexylthiophene was checked by HPLC with system of LC-Net Ⅱ ADS (JASCO). Methanol: H_2O= 9:1 (in volume) was used as an eluent. The effluent was monitored with UV detector (JASCO) at 254 nm.

UV-vis absorption spectroscopy

UV-vis absorption spectra were obtained on a JASCO V-570 spectrophotometer for thin films fabricated with spin-coating on glass slides using 10 mg/ml of chloroform solution and 0.01 mg/ml solutions in THF or chlorobenzene.

Fluorescence (PL) spectroscopy

Fluorescence spectra were obtained with JASCO FP-777. The samples were the same as those for UV measurements.

Atomic force microscopy (AFM)

Atomic force microscopy (AFM) measurements were performed on a JEOL JSPM-4200 system in tapping mode (phase and topographic modes) with an MPP-11100-10 silicon probe (resonant frequency: 300 kHz, force constant: 40 N/m).

2.3 Results and Discussion

2.3.1 Synthesis of 2-bromo-3-hexylthiophene

2-Bromo-3-hexylthiophene was synthesized from 3-hexylthiophene and the product was always a mixture of raw 3-hexylthiophene (or 2-bromo-3-hexylthiophene) and 2,5-dibromo-3-hexylthiophene. In order to obtain P3HT with high regioregularity, it is necessary to use highly pure monomer. Therefore, the column chromatography was carried out. The ratio of monobromo thiophene in product increased into 99.3% after column chromatography from 89.8% before, which was checked by HPLC as shown in Figures 2-9.

^{1}H and ^{13}C-NMR spectrum were shown in Figures 2-10 and 2-11. High purity of the monomer was confirmed.

Table 2-1. Purify of 2-bromo-3-hexylthiophene before and after column checked by HPLC.

	ratio(%) (before column)	ratio(%) (after column)
monobromo	89.8	99.3
raw	4.14	0.462
dibromo	6.05	0.191

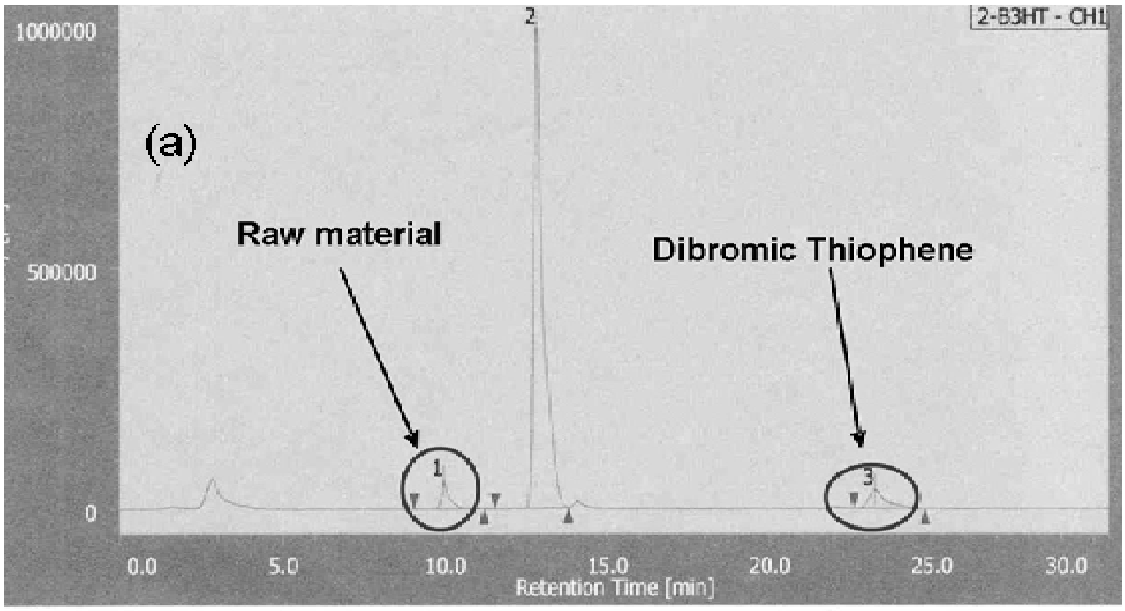

#	ピーク名	CH	tR [min]	面積 [μV*sec]	高さ [μV]	面積%	高さ%	定量値	NTP	分離度
1	Unknown	1	9.950	949698	58363	4.142	5.328	N/A	12818	7.215
2	Unknown	1	12.842	20595787	996426	89.806	91.144	N/A	13245	16.901
3	Unknown	1	23.233	1388002	36645	6.052	3.528	N/A	14127	N/A

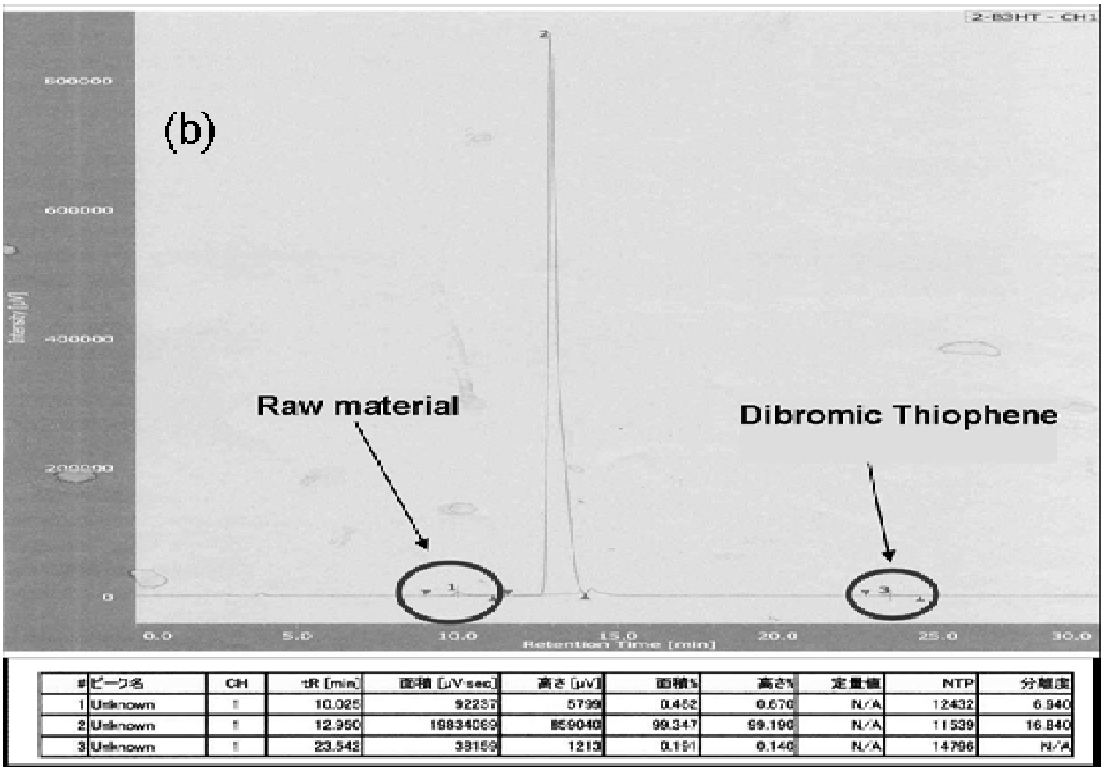

#	ピーク名	CH	tR [min]	面積 [μV*sec]	高さ [μV]	面積%	高さ%	定量値	NTP	分離度
1	Unknown	1	10.025	92237	5799	0.452	0.670	N/A	12432	6.940
2	Unknown	1	12.950	19934069	859049	99.347	99.199	N/A	11539	16.840
3	Unknown	1	23.542	38159	1213	0.191	0.140	N/A	14796	N/A

Figure 2-9. HPLC Chromato graphs of 2-bromo-3-hexylthiophene before (a) and after (b) column chromatography. Methanol: H_2O= 9:1 (in volume) was used as an eluent.

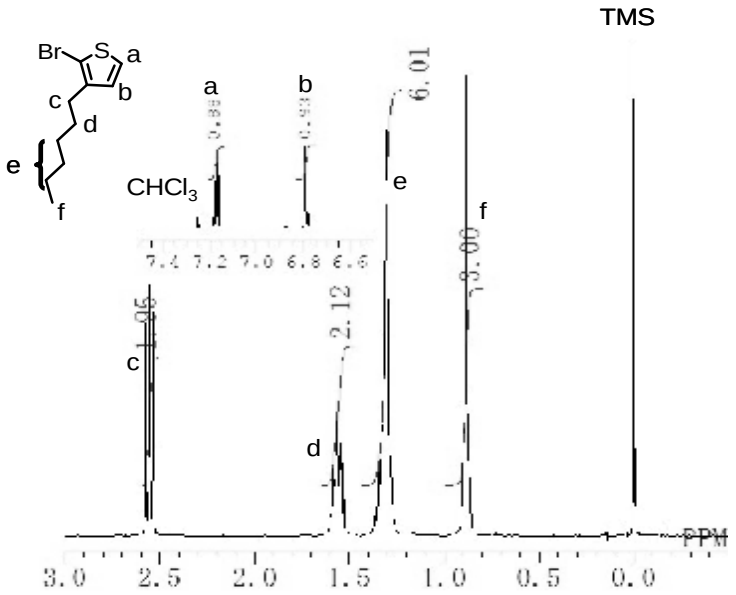

Figure 2-10. ^{1}H NMR spectrum of 2-bromo-3-hexylthiophene.

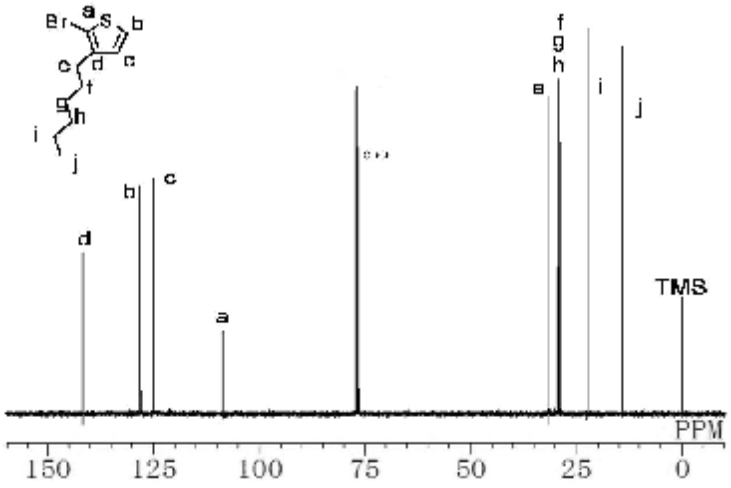

Figure 2-11. ^{13}C NMR spectrum of 2-bromo-3-hexylthiophene.

2.3.2 Synthesis of 2-bromo-3-hexyl-5-iodothiophene

2-Bromo-3-hexyl-5-iodothiophene was synthesized from 2-bromo-3-hexylthiophene. Figure 2-12 shows ^{1}H-NMR spectrum of monomer.

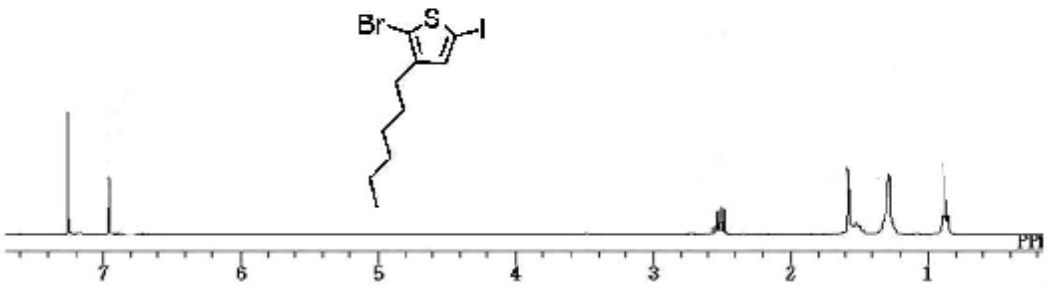

Figure 2-12. ^{1}H NMR spectrum of 2-bromo-3-hexyl-5-iodothiophene.

2.3.3 Synthesis of poly(3-hexylthiophene) from 2-bromo-3-hexylthiophene

Poly(3-hexylthiophene) with high regioregularity was obtained via coupling polymerization from 2-bromo-3-hexylthiophene by using nickel catalyst. ^{1}H and ^{13}C NMR spectrum were shown in Figures 2-13 and 2-14, respectively. The signals in 6.8~7.5 ppm were assigned to the aromatic protons and those in 0.5-3.0 ppm coming from aliphatic protons. The signal for the carbon attached with bromo atom at chain end appeared at 115 ppm in the ^{13}C NMR spectrum. The molecular weight and regioregularity of P3HT were also estimated by GPC and ^{1}H-NMR, as shown in Table 2-2, respectively. Five kinds of P3HT with different molecular weight were obtained, as shown in Table 2-2.

Table 2-2. Characteristics of P3HT.

	*M*n/10[4a)]	PDI[a)]	regioregularity[b)]
P1	0.52	1.47	99.0
P2	0.81	1.49	99.1
P3	1.64	2.02	99.4
P4	1.38	1.44	98.5
P5	1.92	1.42	98.9

a): determined by GPC, b): determined by ^{1}H-NMR.

P3HT (P1) was prepared from 2-bromo-3-hexyl-5-iodothiophene. The others were from 2-bromo-3-hexylthiophene.

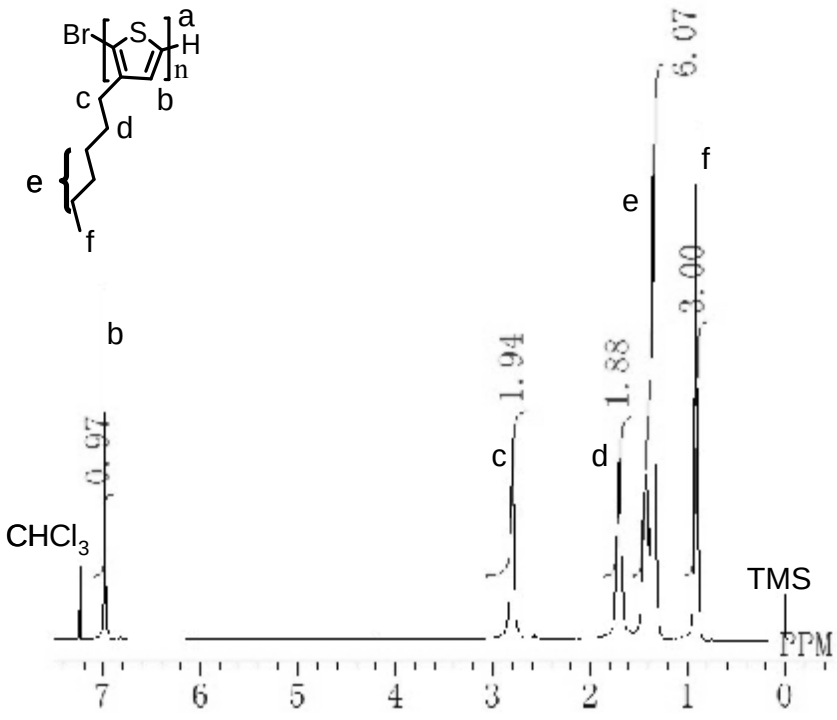

Figure 2-13. ^{1}H NMR spectra of P3HT(P2).

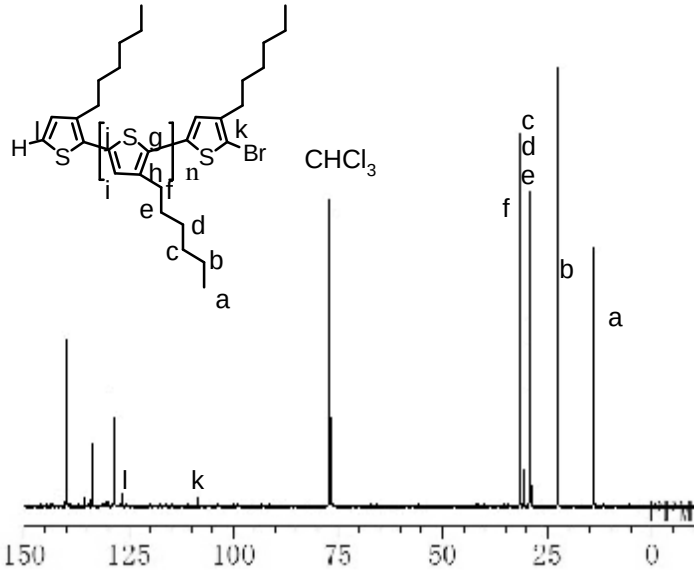

Figure 2-14. ^{13}C NMR spectra of P3HT(P2).

2.3.4 Synthesis of PS with tert-butyl ester at chain end

The homopolymer Polystyrene with *tert*-butyl ester as an end functional group (**1)** was obtained via ATRP as reported elsewhere [12].

^{1}H and IR spectrum were shown in Figures 2-15 and 2-16, respectively. The signals in 6.8~7.5 ppm were assigned to the aromatic protons and those in 0.5-3.0 ppm coming from aliphatic protons. Particularly, the signal at 1.35 ppm was assigned as the proton of *tert*-butyl ester end group.

As shown in Table 2-3, a series of polystyrene homopolymers were prepared via ATRP.

Table 2-3. Polymerization conditions and characteristics of polystyrene.

	M：I：CuBr：$CuBr_2$：L	Temp./^oC	Time /h	M_n[a)]	PDI[a)]	Yield(%)
S0	100:1:1:0.05:1	90	7	6100	1.35	65.9
S1	100:1:1:0.05:1	90	1	1800	1.33	26%
S2	50:1:1:0.05:1	90	3	2600	1.23	20
S3	50:1:1:0.05:1	90	7	3600	1.36	31.8
S4	25:1:1:0.05:1	90	7	2900	1.38	26.7
S5	25:1:1:0.05:1	90	1	2400	1.43	14
S6	25:1:1:0.1:1	90	1.5	2000	1.41	24.5
S7	25:1:1:0.1:1	90	0.5	508	2.26	10
S8	25:1:1:0.15:1	90	0.5	200	×	×
S9	25:1:1:0.15:1	90	1.2	1400	1.75	10.1

a): Determined by GPC.

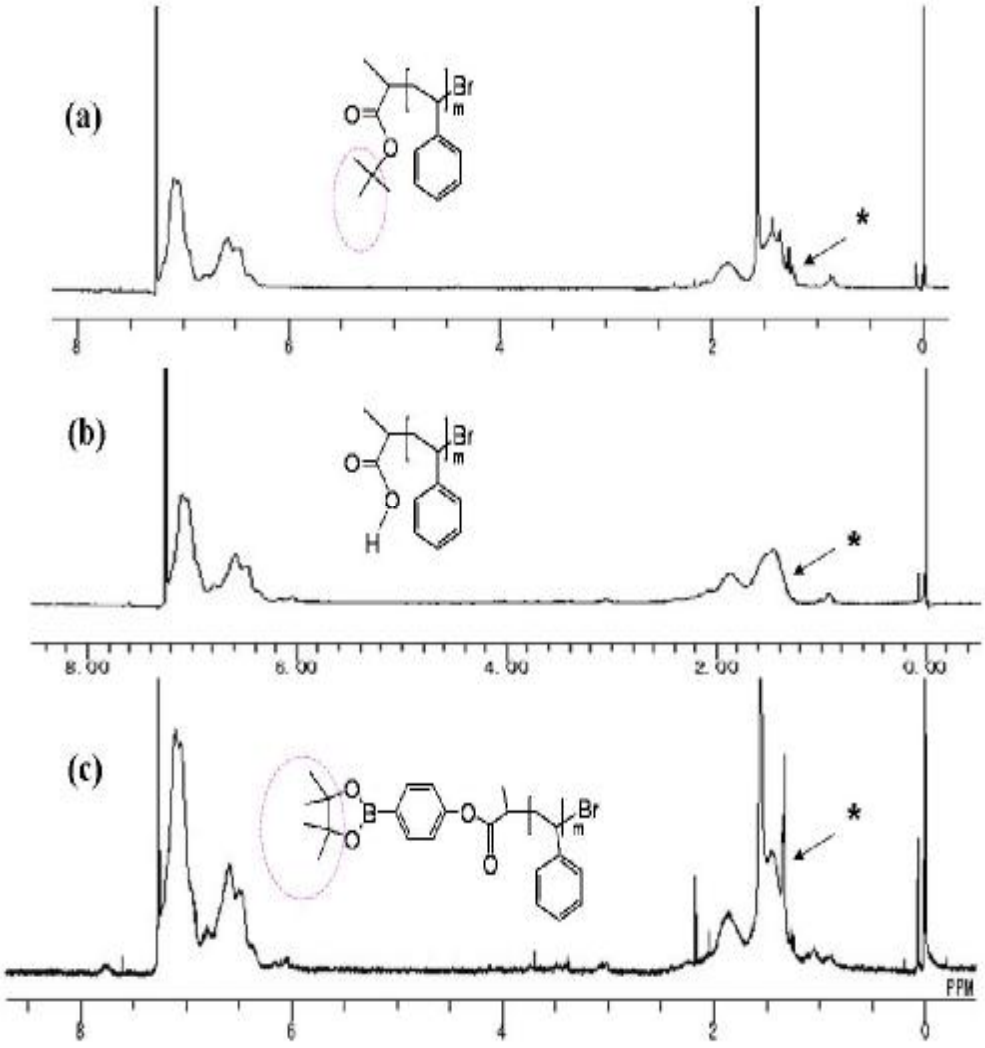

Figure 2-15. ^{1}H-NMR spectra of polystyrenes with end group of

(a) t-butyl ester, (b) carboxyl, and (c) boronic acid ester.

2.3.5 Synthesis of polystyrene with carboxyl end-group (2)

From Figure 2-16, the *t*-butyl group peak at 1360-1370 cm^{-1} (Figure 2-16a) decreased obviously after the hydrolysis reaction. Furthermore, the absorption peak of end ester end group at 1749 cm^{-1} (Figure 2-16a) disappeared and that of –COOH end group at 1709 cm^{-1} (Figure 2-16b) appeared confirming the successful hydrolysis reaction was confirmed. By the ^{1}H NMR spectrum of Figure 2-15b, the disappearance of signal at 1.35 ppm (Figure 2-15a) which represented the proton of *tert*-butyl ester end group also indicated this successively synthesis.

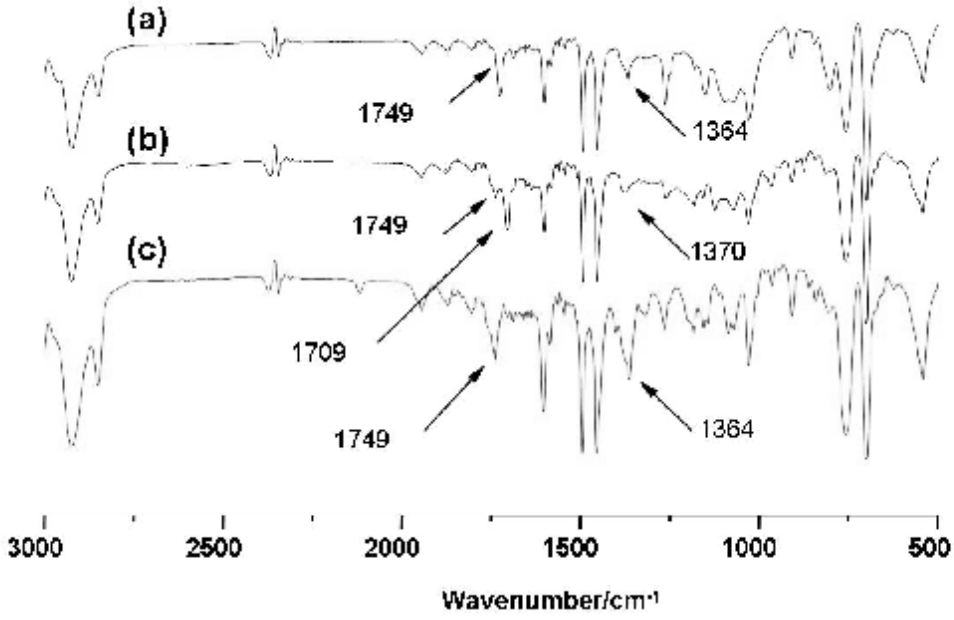

Figure 2-16. IR spectra for polystyrenes with end group of (a) t-butyl ester, (b) carboxyl; (c) boronic acid ester.

2.3.6 Synthesis of polystyrene with end-group of boronic acid ester

After the esterification reaction with benzoic acid containing phenol ester group, the absorption at 1360-1370 cm^{-1} (Figure 2-16c) for branched alkyl groups appeared again. Furthermore, the absorption peak of end ester end group appeared at 1749 cm^{-1} (Figure 2-16c).

^{1}H-NMR measurements also revealed the successful introduction of borate end group as shown in Figure 2-15c.

2.3.7 Synthesis of P3HT-*b*-PS

Finally, P3HT was coupled with PS via Suzuki coupling reaction to obtain diblock copolymer P3HT-*b*-PS. The molecular weights of polymers were measured by GPC and shown in Figure (1-17).

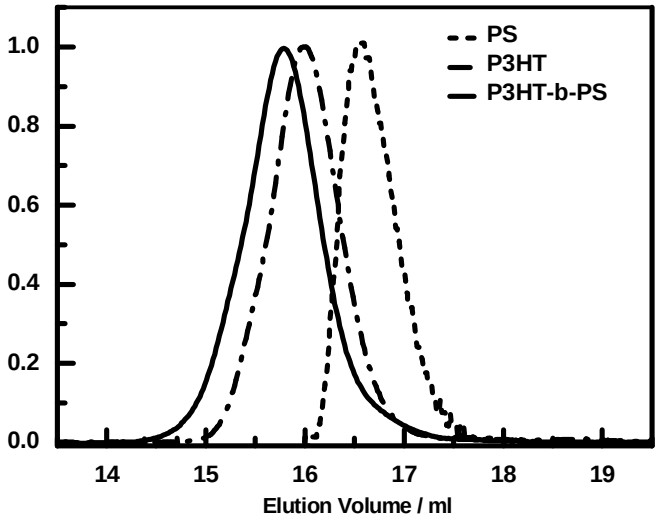

Figure 2-17. GPC chromatograms of PS (S2), P3HT (P2) and P3HT-*b*-PS (B3).

Table 2-5. Characteristics of block copolymers.

	P3HT		PS derivative		P3HT-*b*-PS			Ratio
	Mn(GPC)	PDI	Mn(GPC)	PDI	Mn(GPC)	PDI	yield	/mol (NMR)
B1	5200	1.47	1800	1.33	6500	1.21	60%	1:0.06
B2	5200	1.47	3600	1.36	8000	1.49	42%	1:0.20
B3	8100	1.49	2600	1.23	10000	1.99	92%	1:0.31
B4	8100	1.49	508	2.26	8800	1.63	70%	1:0.15

In ^{1}H NMR spectrum of **B3** (Figure 2-18c), the signals in aromatic region assignable to the protons on the phenyl ring of PS can be observed at 7.0 and 6.7 ppm. In addition, the disappearance of the small triplet signal at 2.56 ppm was observed, which is assigned as the signal of methylene proton on the first carbon of hexyl group substituted on the bromo-terminal unit as shown in Figure 2-14b[13]. These results indicated that PS block was successfully introduced at the end of **P3HT**. By comparing the integrations for alkyl protons of P3HT and aromatic protons of PS, the molar ratio of PS to P3HT segments was found to be 25:50, almost the same as the theoretical chemical composition. The increase in M_n of **B3** with a unimodal profile in the GPC chromatogram (M_n: 10000, PDI: 1.99) also indicated the formation of block copolymer without any trace of polystyrene homopolymer.

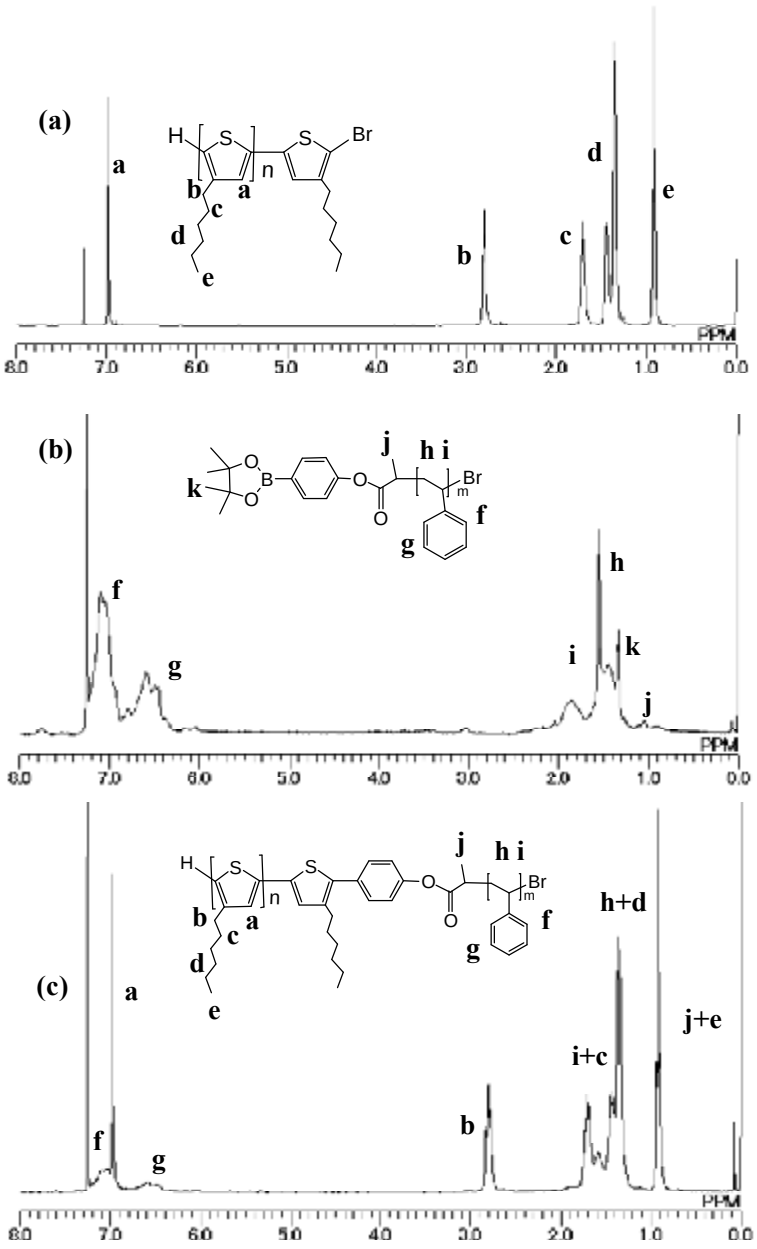

Figure 2-18. ^{1}H NMR spectrum of (a) P3HT(T2), (b)PS(S2), and (c) P3HT-*b*-PS (B3).

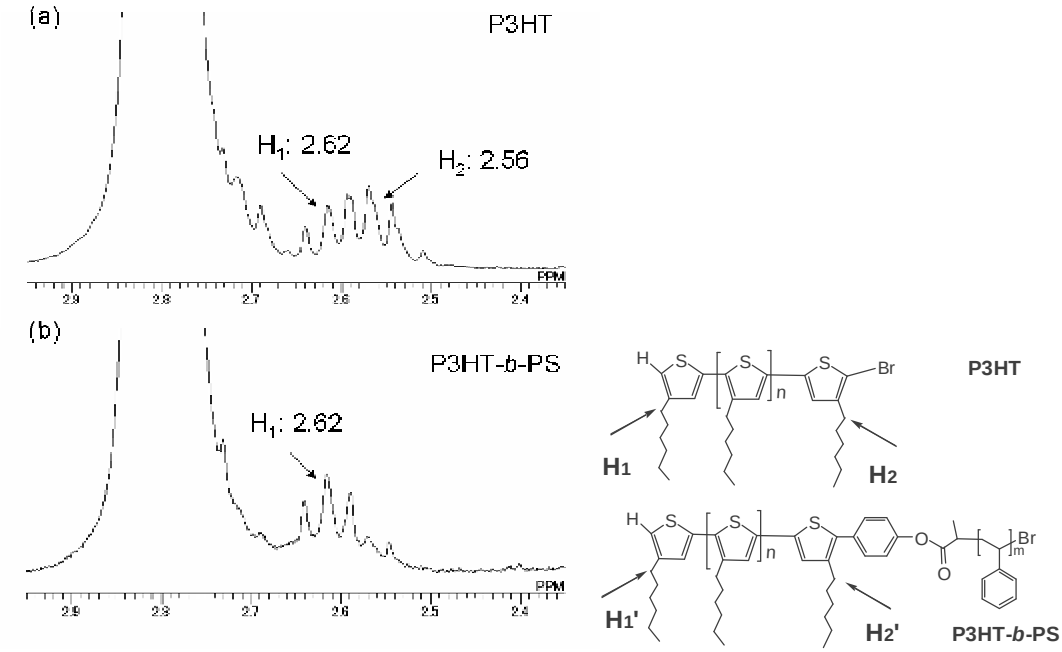

Figure 2-19. Expended ^{1}H NMR spectrum of (a) P3HT(P2) and (b) P3HT-*b*-PS (B3). Two small triplet at δ = 2.62 (H_1) and 2.56 (H_2) of the same intensity for (H/Br) terminated P3HT can be assigned to be the methylene protons on the first carbon substituted on the end unit. The H_2' of block copolymer disappeared at δ = 2.56 (H_2) because the bromine on the end unit of P3HT was metathesized by the end benzene unit of polystyrene derivative.

2.3.8 Thermal property of block copolymer (B3) (DSC)

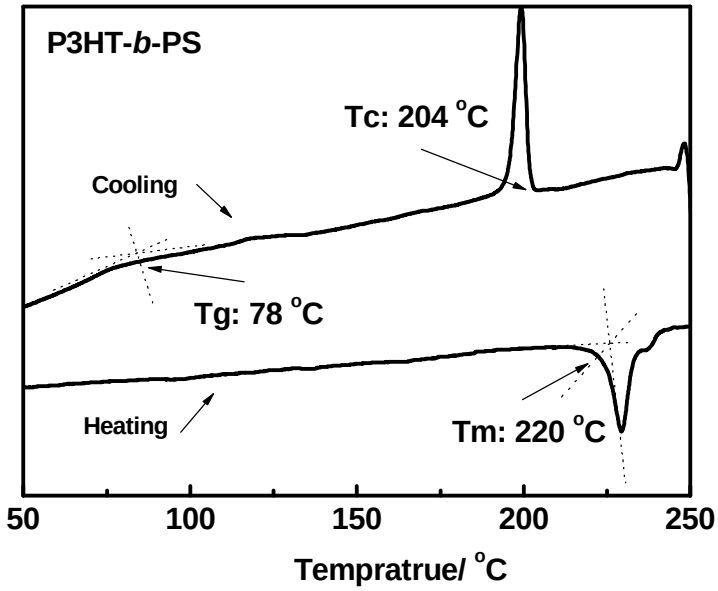

Figure 2-20. DSC thermograms of P3HT-*b*-PS (B3) obtained by heating and cooling rate of 5 °C/min.

DSC thermogram for **B3** (Figure 2-20) shows the glass transition of PS block and melting of P3HT block, and those transitions occur at almost the same temperatures as those of both homopolymers, indicating the microphase separation.

2.3.9 UV-vis spectroscopy of thin films

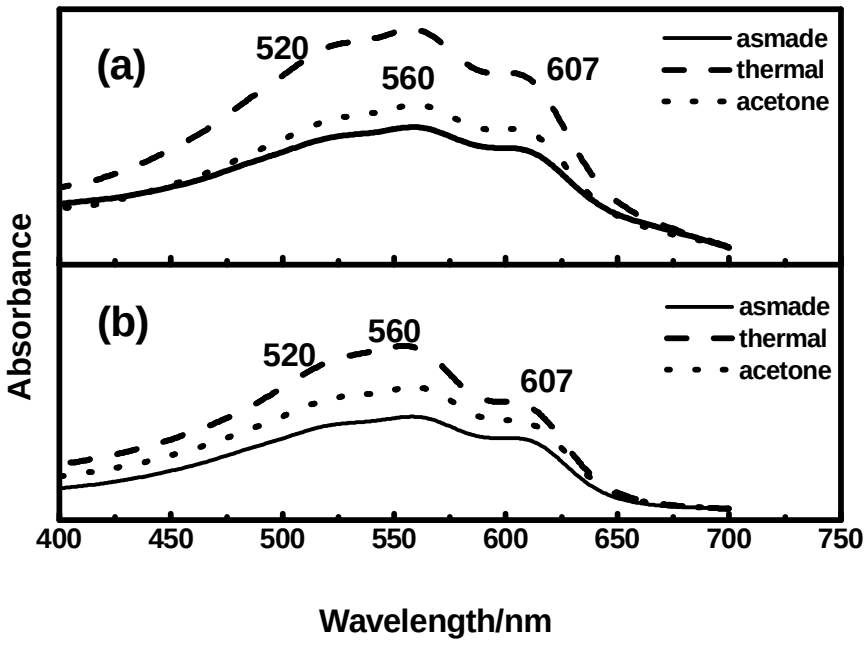

Figure 2-21. UV-vis spectra of (a) P3HT and (b) B3 in film before and after thermal or acetone annealing.

Aggregation state of P3HT chains can be evaluated by UV-vis spectroscopy (Figure 2-21). Thin films of **P3HT** and **B3** were prepared by spin coating from chloroform solution on glass substrates at room temperature. One set of films were thermally annealed at 150 °C for 20 min (thermal annealing), and the others were transferred into a jar filled with acetone vapor，exposed for 5 h (solvent annealing). All the spectra exhibit similar profile with maximum absorption wavelength at 560 nm. Both thermal and solvent annealing treatments provide a slight increase in absorbance at 607 nm which derived from the strong intermolecular interaction indicating the high crystallizability of the P3HT chains. Therefore, the author can conclude that the stacking of P3HT block is not interfered by the presence of PS block. Furthermore, it is considered that micro-phase separation makes P3HT block to form more densely stacked structure.

2.3.10 Surface morphology of polymers by Atomic force microscopy (AFM)

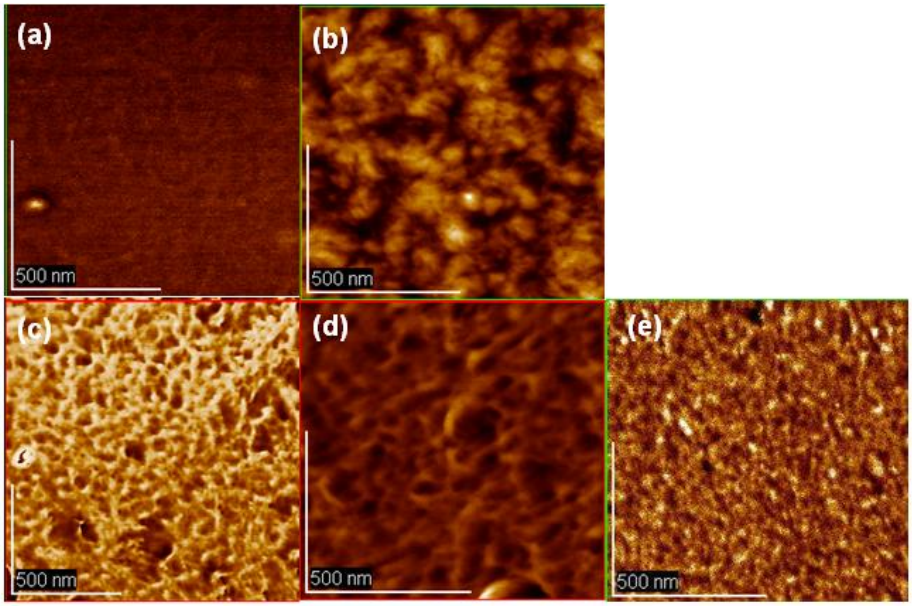

Figure 2-22. Atomic force microscopy (AFM) phase image (1 μm × 1 μm) of the thin films of **B3** before and after thermal annealing at 150 °C for 20 min or solvent annealing for 5 h. (a) as-made; (b) thermal annealed; (c) acetone annealed; (d) cyclohexane annealed; (e) toluene annealed.

Morphology of film surface was observed by atomic force microscopy (AFM). The phase images of the thin films of **B3** before and after annealing were shown in Figure 2-22. The thin films were also subjected to thermal annealing at 150 °C for 20 min or solvent annealing by acetone, cyclohexane, toluene for 5 h. Before annealing, a flat surface without any distinctive structure was observed (Figure 2-22 a). After thermal annealing, a phase-separated structure appeared with domain size of about 150 nm**.** On the contrast, the block polymer showed a clearer phase separation structure after solvent annealing. Since acetone is partially good solvent for PS, the PS chains can change the conformation by swelling with acetone. Therefore, the PS segment reconstructed a thermodynamically stable structure in the thin film under acetone vapor, which induced more densely stacked structure of P3HT. The other common solvents such as cyclohexane and toluene were also used for solvent annealing. However, no clear phase-separated morphology was observed for these thin films because the dewetting of the films probably occurred using these good solvents for both P3HT and PS segments.

2.4 Conclusion

The *p*-type conducting block copolymer poly(3-hexylthiophene)-*block*-polystyrene (P3HT-*b*-PS) was synthesized by Suzuki coupling between P3HT and PS homopolymers. The photo-physical properties were investigated by UV-vis absorption spectra, showing that the polystyrene block increased the relative intensity the band around 600nm, which indicated that microphase separation makes P3HT to form more densely stacked structure. By AFM measurement, a micro phase-separated structure appeared with domain size of about 100 nm in film of 5 and 150 nm in 6. the 6 showed a clearer phase separation structure than P3HT.

In the ongoing work, these copolymers will be utilized in the active materials for photovoltaic devices consisted of the P3HT/PCBM blend in order to investigate the correlation between morphology and device performance.

2.5 Reference

[1]. Soci, C.; Hwang, I. W.; Moses, D.; Zhu, Z.; Waller, D.; Gaudiana, R.; Brabec, C. J.; Heeger, A. J. *Adv.Funct.Mater*. **2007**, 17, 632.

[2]. Sugimoto, T.; Ebihara, Y.; Ogino,K.; Vacha,M. *Chem. Phys. Chem*. **2007**, 8, 1623.

[3]. Ma, W.; Yang, C.; Gong, X.; Lee, K.; Heeger, A. J. *Adv. Funct. Mater*. **2005**, 15, 1617.

[4]. Blom, P. W.; Mihailetchi, V. D.; Koster, L. J. A.; Markov, D. E. *Adv. Mater*. **2007**, 19, 1551.

[5]. Lindner, S. M.; Httner, S.; Chiche, A.; Thelakkat, M. *Angew. Chem. Int. Ed*. **2006**, 45, 3364.

[6]. Hauch, J. A.; Schilinsky, P.; Choulis, S. A. *Sol. Enrg. Mat. Sol. C*. **2008**, 92, 727.

[7]. Sauvéand, G.; McCullough, R. D. *Adv. Mater*. **2007**, 19, 1822.

[8]. Sommer, M.; Lang, A. S.; Thelakkat, M. *Angew. Chem. Int. Ed.* **2008**, 47, 7901.

[9]. Higashihara, T.; Ohshimizu, K.; Hirao, A.; Ueda, M. *Macromolecules*. **2008**, 41, 9505.

[10]. Higashihara, T.; Ueda, M. *Macromolecules.* **2009**, 42, 8794.

[11]. Wu, S.; Bu, L.; Huang, L.; Yu, X.; Han, Y.; Geng, Y.; Wang, F. *Polymer*. **2009**, 50, 6245.

[12]. Maeda, Y.; Shimoi, Y.; Ogino, K. *Polym. B*ull. **2005**. 53. 315.

[13]. Zhang, Y.; Tajima, K.; Hirota, K.; Hashimoto, K. *J. Am. Chem. Soc*. **2008**, 130, 7812.

Chapter 3 . Annealing Effect on Performance and Morphology of Photovoltaic Devices Based on Poly(3-hexylthiophene)-*b*-Poly(Styrene)

2.1 Introductions

As a method to improve the photovoltaic efficiency, the annealing processes are also effective for controlling the morphology in photovoltaic devices based on BHJ. For thermal annealing, the PCE of photovoltaic devices significantly depend on the annealing temperature. According to reports[1-3], the annealing temperature at around 140 °C was the most effective to achieve high PCE of the photovoltaic devices based on P3HT/PCBM blend. Solvent annealing is another way to control the morphology in thin films prepared with block copolymer or polymer blend [4-8]. For the device based on P3HT/PCBM, solvent annealing (including solvent aging) can also improve the efficiency of the device [9-11].

In this chapter, in order to utilize the microphase separation of block copolymers for controlling morphology in polymer photovoltaic devices, a novel block copolymer poly(3-hexylthiophene)-*block*-polystyrene (P3HT-*b*-PS) blended with PCBM was used as active layer of photovoltaic device. A series of annealing by heating or immersing in solvent vapor atmosphere were carried out on the photovoltaic devices prepared from P3HT or P3HT-*b*-PS blended with PCBM. UV-vis, AFM, *I-V* characteristics were evaluated for the devices, and the correlation between the morphology and the device performance was discussed.

3.1 Experiment

3.1.1 Materials

A series of poly(3-hexylthiophene)-*block*-polystyrene (P3HT-*b*-PS) diblock copolymers comprising of P3HT and PS segments were prepared by coupling reaction between each homopolymers as shown in Chapter 2 (designated as B3). Regioregular P3HT with a bromo terminal (P3HT-Br) was synthesized by Grignard metathesis polymerization. A tert-butyl ester terminal of PS was converted to boronic ester (PS-BE). P3HT-Br was coupled with large excess of PS-BE via Suzuki coupling reaction to give P3HT-*b*-PS without contamination of PS-BE which can be removed by reprecipitation in methanol. A series of P3HT-*b*-PS were synthesized with various PS segment weight ratios. Synthetic detail is described in Chapter 2.

3.1.2 Device Fabrication

All the devices were manufactured with a structure of ITO/PEDOT:PSS(30 nm)/active layer/LiF(0.5 nm)/Al(100 nm).

Spin-coating

The substrates were pre-cleaned in an ultrasonic bath of deionized water for 30 min.

Poly(3,4-ethylenedioxythiophene):polystyrene sulfonate (PEDOT:PSS) was spin-coated onto a glass slide coated by patterned indium tin oxide (ITO), and annealed at 200 °C for 1 h.

The active layer was spin coated on PEDOT:PSS coated substrate from the polymer/PCBM solution at speeds of 1000, 1500, 2000, 2500 and 3000 rpm for 30s respectively. Each of the substrates was transferred to a plastic container and exposed to vapor of the residual solvent.

Annealing treatment

The substrates were transferred inside a nitrogen-filled glove box under atmospheric pressure, annealed at 150 °C for 10 min, or under solvent vapor at r.t. by 5h.

Atomic force microscopy (AFM)

Atomic force microscopy (AFM) measurements were performed on a JEOL JSPM-4200 system in tapping mode (phase and topographic modes) with an MPP-11100-10 silicon probe (resonant frequency: 300 kHz, force constant: 40 N/m).

I-V characteristics

A 0.5 nm thick layer of lithium fluoride followed by a 100 nm thick top contact of aluminum was thermally evaporated onto the active layer in a vacuum chamber under 10^{-5} Pascal. The as-prepared cell performance was measured under AM 1.5 illumination using a Xenon lamp solar simulator in a nitrogen environment at room temperature, where the lamp intensity had been calibrated to 100 mW / cm^2. The photovoltaic characteristic of devices was measured by KEITHLEY 2400 Source Meter under 100 mW/cm^2. The structures of devices were shown in Figure 3-1.

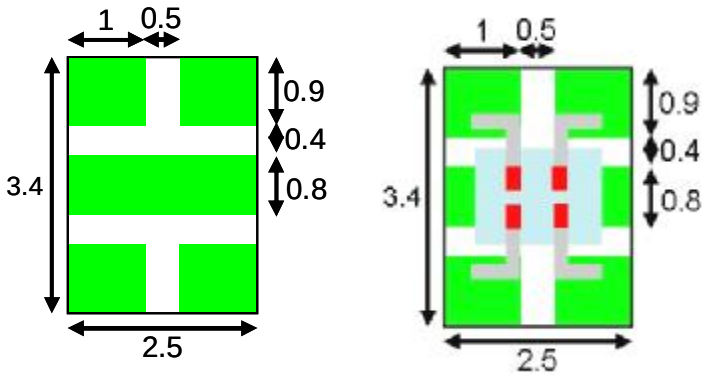

Figure 3-1. Structure of ITO substrates before (left) and after (right) diode the evaporation of aluminum electrode.

3.2 Results and Discussion

3.2.1 Morphology of film surface by Atomic force microscopy (AFM)

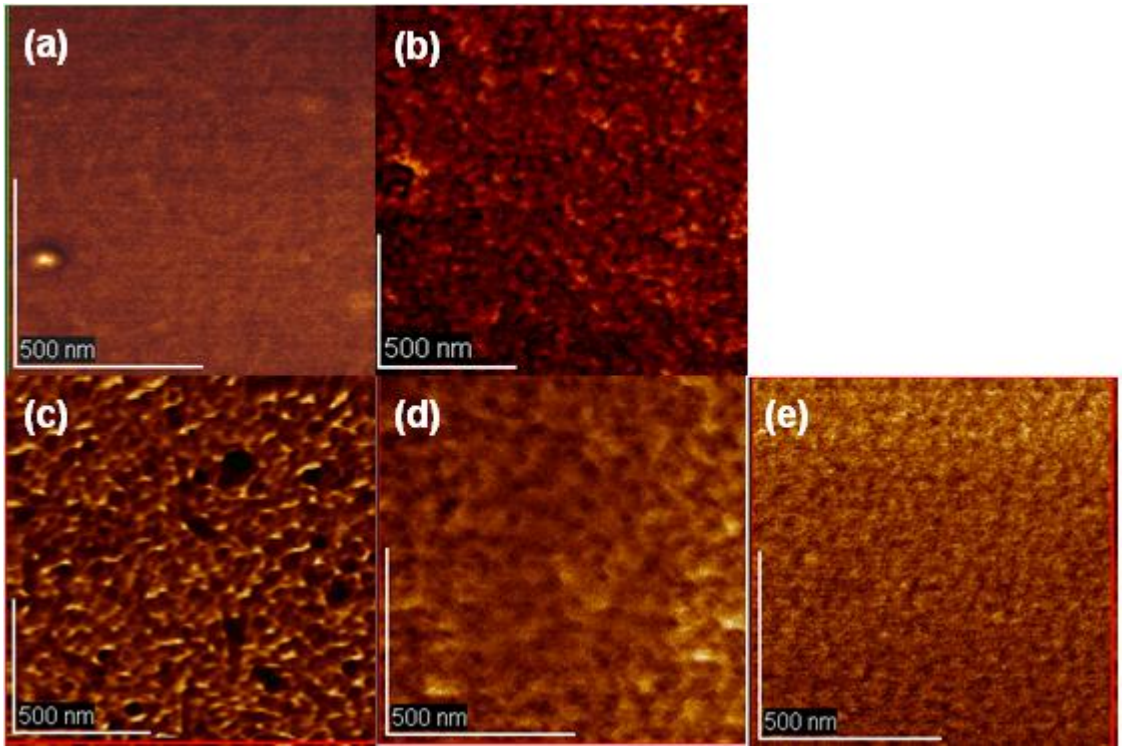

Figure 3-2. Atomic force microscopy (AFM) phase image (1 μm × 1 μm) of the thin films of **P3HT/PCBM** before and after thermal annealing at 150 °C for 20 min or solvent annealing for 5 h. (a) as-made; (b) thermal annealed; (c) acetone annealed; (d) cyclohexane annealed; (e) toluene annealed. Thin films were spin-coated from chlorobenzene solution (10 mg/ml) onto glass slides.

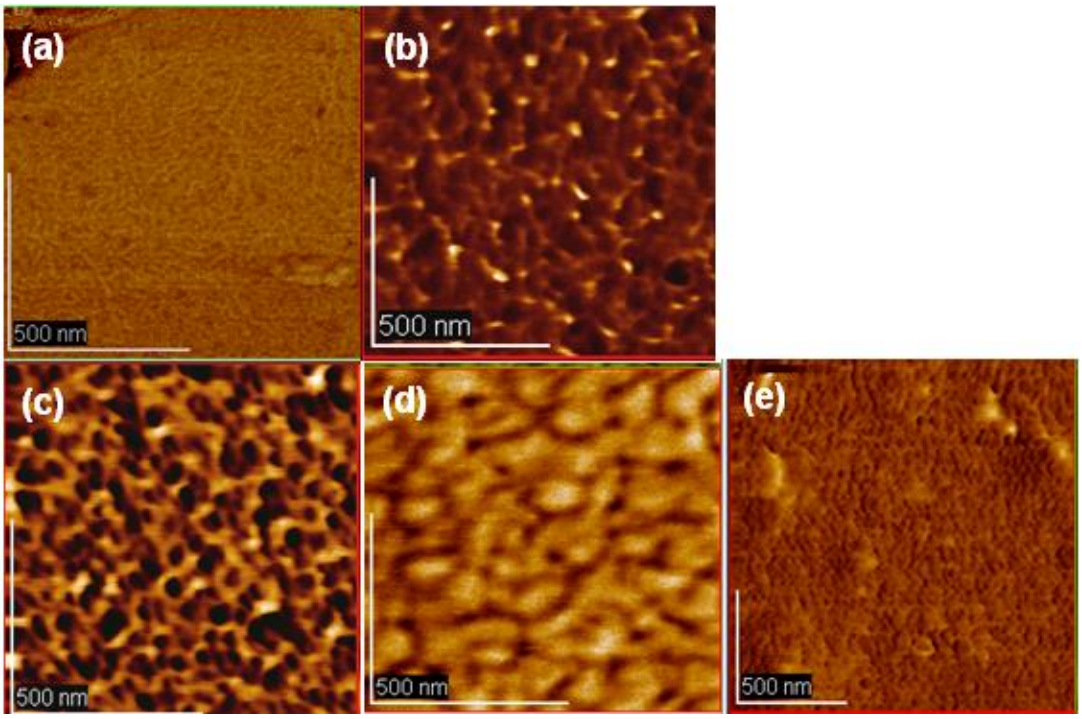

Figure 3-3. Atomic force microscopy (AFM) phase image (1 μm × 1 μm) of the thin films of **B3/PCBM** before and after thermal annealing at 150 °C for 20 min or solvent annealing for 5 h. (a) as-made; (b) thermal annealed; (c) acetone annealed; (d) cyclohexane annealed; (e) toluene annealed. Thin films were spin-coated from chlorobenzene solution (10 mg/ml) onto glass slides.

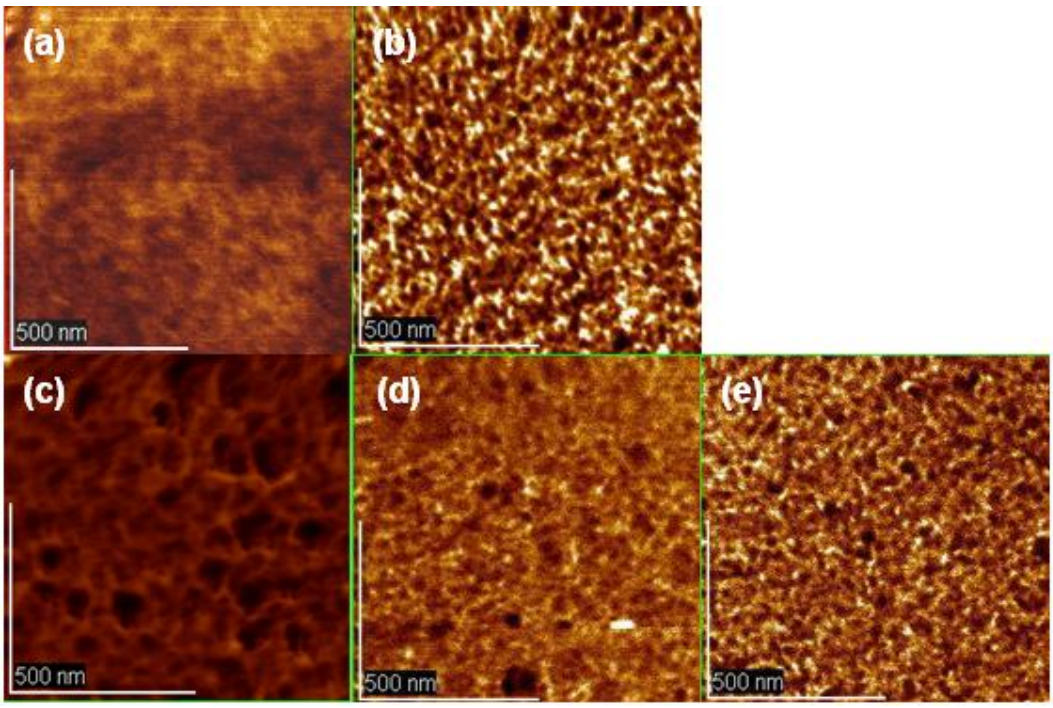

Figure 3-4. Atomic force microscopy (AFM) phase image (1 μm × 1 μm) of the thin films of **B4/PCBM** before and after thermal annealing at 150 °C for 20 min or solvent annealing under acetone vapor for 5 h.

(a) as-made; (b) thermal annealed; (c) acetone annealed; (d) cyclohexane annealed; (e) toluene annealed. Thin films were spin-coated from chlorobenzene solution (10 mg/ml) onto glass slides.

Morphology of film surface was observed by atomic force microscopy (AFM). The phase images of the thin films of **P3HT/PCBM, B3/PCBM** (1:1 weight ratio), **B4/PCBM** (1:1 weight ratio) were shown in Figure 3-2, Figure 3-3 and Figure 3-4. The films were subjected to thermal annealing at 150 °C for 20 min or solvent annealing for 5 h, respectively.

Before annealing, a flat surface without any distinct structure was observed in the AFM images for **B3/PCBM** (Figure 3-3a) and **B4/PCBM** (Figure 3-4a). Phase-separated structure appeared with domain size of about 30-40 nm in film of **B3/PCBM** and **B4/PCBM** after thermal annealing (Figure 3-2b), whereas the domain size observed in the film of **P3HT/PCBM** was less than 10 nm (Figure 3-2b). It is considered that the microphase separation of **B3 and B4** promoted the phase separation and aggregation of PCBM. The phase separation in the film of **B3/PCBM** after the acetone annealing became more distinct compared with the thermal annealing (Figure 3-2c). However, when the solvent was changed to cyclohexane or toluene, the microphase collapsed to the disordered structure, and domain sizes become larger, too. Since acetone is good solvent for **PCBM**, it accelerated the aggregation of **PCBM**. From UV-vis spectrum, both annealing processes induced more densely stacked structure of P3HT chain.

The blend films using different block copolymer B2 showed similar results with the microphase separation (Figure 3-4). AFM measurement revealed that, compared with the P3HT/PCBM blend, the clear microphase-separated morphologies is more likely to appear at block copolymer blend system by both thermal and solvent annealing.

I-V characteristics of the devices based polymers

Performance of photovoltaic cells based on **Polymer/PCBM** in 1:1 weight ratio was evaluated. The device structure is described as Al/LiF/composite/PEDOT:PSS/ITO. The *I-V* curves before and after annealing were shown in Figure 3-5 – Figure 3-8. For the as-made film, the conversion efficiency of the devices showed 0.42% for **B3** and 0.34 for **B4**. After thermal annealing process, the efficiencies of **B3** increased up to 1.93%, which is slightly higher than that observed in homopolymer-based device. This is probably due to the highly segregated structure of **B3/PCBM** as shown in Figure 3-3. The solvent annealing provided the efficiency for **B3** of 0.84% with acetone, 0.32% with cyclohexane and 0.96 with toluene, without obvious increasing compared with P3HT. It is considered that the domain size is too large for photo-generated excitons to reach the interface between *p*- and *n*-type phases in the solvent-annealed device.

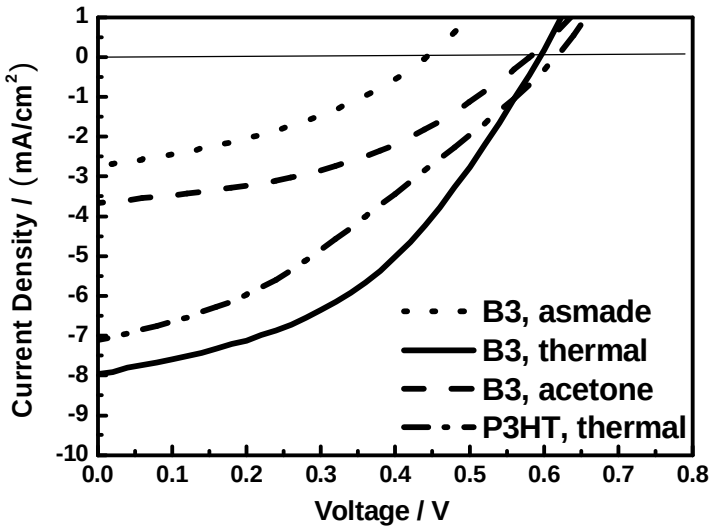

Figure 3-5. *I-V* characteristics on the devices based **P3HT** or **B3/PCBM** before and after thermal annealing at 150 °C for 20 min or solvent annealing under the vapor of acetone for 5 h.

Table 3-2. The performances of photovoltaic devices based on P3HT\PCBM

Polymer	Annealing	Time / min	V_{oc} / V	J_{sc} /(mA/cm^2)	Fill factor	Efficiency /%
P2	none	-	0.40	3.00	0.31	0.38
	thermal	10	0.60	7.04	0.33	1.38
	acetone	300	0.48	4.47	0.42	0.89
	cyclohexane	300	0.46	4.1	0.35	0.67
	tolune	300	0.5	3.83	0.38	0.74

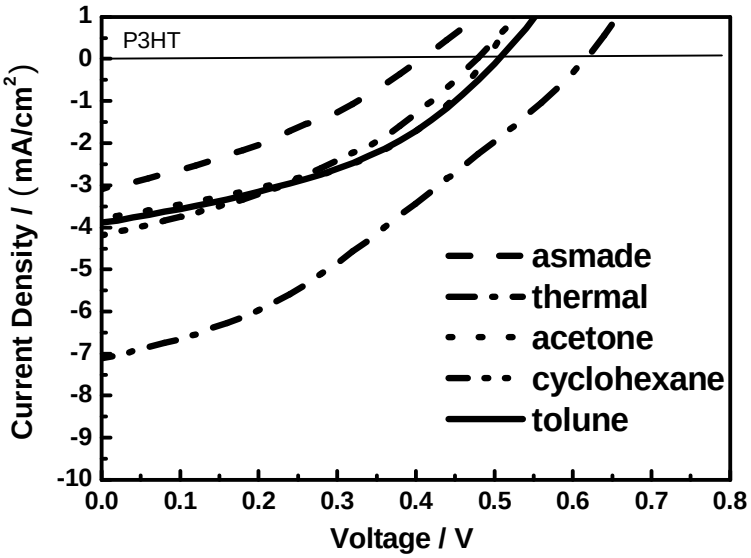

Figure 3-6. *I-V* characteristics on the devices based **P3HT/PCBM** before and after thermal annealing at 150 °C for 20 min or solvent annealing for 5 h.

Table 3-2. The performances of photovoltaic devices based on P3HT-*b*-PS\PCBM

Polymer	Annealing	Time / min	V_{oc} / V	J_{sc} / (mA/cm^2)	Fill factor	Efficiency /%
B3	none		0.44	2.68	0.35	0.42
	thermal	10	0.58	7.90	0.42	1.93
	acetone	300	0.58	3.61	0.40	0.86
	cyclohexane	300	0.34	2.7	0.36	0.32
	tolune	300	0.5	5.0	0.38	0.96
B4	None		0.4	2.60	0.33	0.34
	thermal	10	0.5	4.9	0.36	0.90
	acetone	300	0.4	3.58	0.41	0.59
	cyclohexane	300	0.46	2.3	0.35	0.37
	tolune	300	0.36	3.5	0.37	0.47

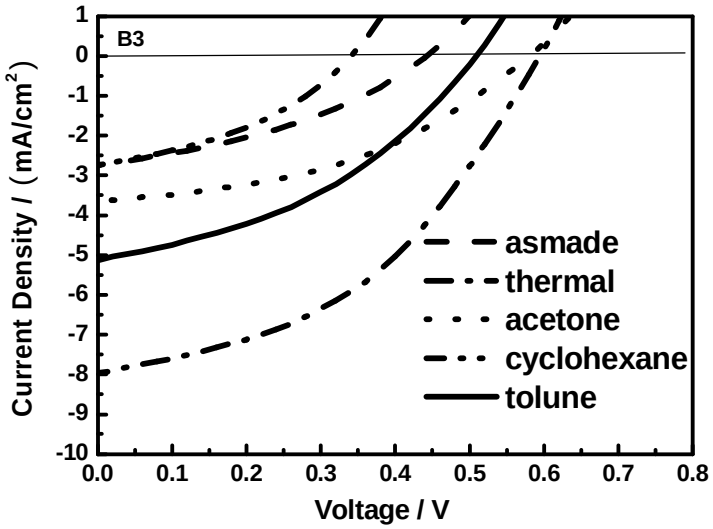

Figure 3-7. *I-V* characteristics on the devices based **B3/PCBM** before and after thermal annealing at 150 °C for 20 min or solvent annealing for 5 h.

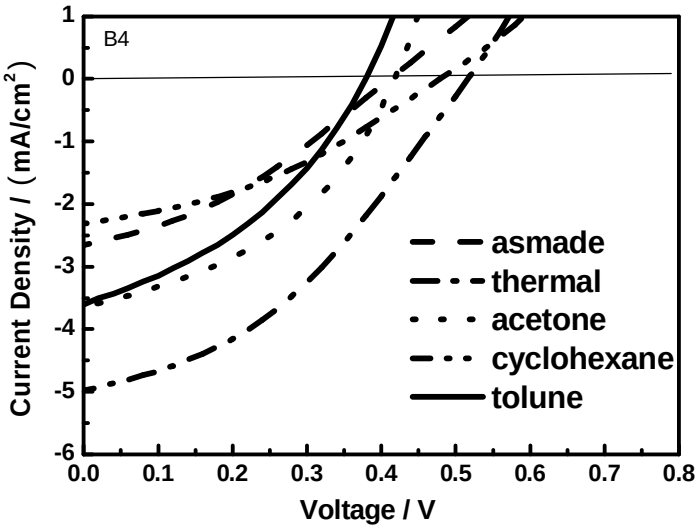

Figure 3-8. *I-V* characteristics on the devices based **B4/PCBM** before and after thermal annealing at 150 °C for 20 min or solvent annealing for 5 h.

3.3 Conclusion

In conclusion, the *p*-type conducting block copolymer poly(3-hexylthiophene)-block-polystyrene (P3HT-*b*-PS) was synthesized by Suzuki coupling reaction between P3HT and PS homopolymers. During thermal and solvent annealing processes, block copolymer assisted the segregation of PCBM through microphase separation. Photovoltaic cell was fabricated using P3HT-*b*-PS and PCBM, and the device provided conversion efficiency of 1.93% for **B3** after thermal annealing which is higher than that of P3HT. It is possible to control the morphologies in the *n*-type/*p*-type blend films by the utilization of the block copolymer.

Further investigation on the relationship between photovoltaic performance and morphologies of active layer is ongoing.

3.4 Reference

[1]. Kim, Y.; Cook, S.; Uladhar, S. M.; Choulis, S. A.; Nelson, J.; Durrant, J. R.; Bradley, D. D. C.; Giles, M.; McCulloch, I.; Ha, C.; Ree, M. *Nat*. *Mater*. **2006**, 5, 197.

[2]. Li, G.; Shrotriya, V.; Yao, Y.; Huang, J.; Yang, Y. *J. Mater*. *Chem*. **2007**, 17, 3126.

[3]. Reyes, R. M.; Kim, K.; Carroll, D. L. *Appl*. *Phys*. *Lett*. **2005**, 87.

[4]. Elbs, H.; Drummer, C.; Abetz, V.; Krausch, G. *Macromolecules*. **2002**, 35, 5570.

[5]. Kim, S. H.; Misner, M. J.; Russell, T. P. *Adv*. *Mater*. **2004**, 16, 2119.

[6]. Cavicchi, K. A.; Russell, T. P. *Macromolecules*. **2007**, 40, 1181.

[7]. Bang, J.; Kim, B. J.; Stein, G. E.; Russell, T. P.; Li, X.; Wang, J.; Kramer, E. J.; Hawker, C. J. *Macromolecules*. **2007**, 40, 7019.

[8]. Guo, R.; Huang, H. Y.; Chen, Y. Z.; Gong, Y. M.; Du, B. Y.; He, T. B. *Macromolecules*. **2008**, 41, 890.

[9]. Shrotriya, V.; Yao, Y.; Li, G.; Yang, Y. *Appl*. *Phys*. *Lett*. **2006**, 89, 63505.

[10]. Li, G.; Yao, Y.; Yang, H.; Shrotriya, V.; Yang, G; Yang, Y. *Adv*. *Funct*. *Mater*. **2007**, 17, 1636.

[11]. Huang, W. Y.; Huang, P. T.; Han, Y. K.; Lee, C. C.; Hsieh, T. L.; Chang, M. Y. *Macromolecules.* **2008**, 41, 7485.

Chapter 4 . Chapter 4. Synthesis and Characterization of Poly(3-hexylthiophene)-*b*-Poly(ethylene oxide) block copolymer

4.1 Introduction

Block copolymers are able to form definite microphase-separated structure such as a lamella and a cylinder. These structures are more thermodynamically stable than those created by polymer blends. Furthermore, the scale of these structures lies in the order of tens nanometer, which allows photo-generated excitons to reach the interface between *p*- and *n*-type semiconductors effectively. Therefore, some researchers have synthesized block copolymers consisting of charge transporting segments, and utilized these block copolymers as a component in polymer photovoltaic devices in order to construct suitable phase-separated structures[1-5]. For this reason, the block copolymer consisting of regioregular poly(3-hexylthiophene) (P3HT) and polystyrene was prepared in order to exploit these features for controlling the morphology in photovoltaic devices in Chapter 2.

In this chapter, in order to utilize the microphase separation of block copolymers for controlling morphology in polymer photovoltaic devices, a novel block copolymer poly(3-hexylthiophene)-*block*-poly(ethylene oxide) (P3HT-*b*-PEO) was synthesized by Suzuki coupling reaction between polar and flexible PEO with the end group of boronic ester and highly regioregular P3HT. In contrast to polystyrene, the hydrophilic PEO was selected as the second block because some researchers reported that block copolymers containing PEO segment afforded the microphase-separated structure which aligned vertical to a substrate[6,7]. The block copolymers were characterized by NMR, GPC, and DSC measurements. The thin films of block copolymers were prepared and annealing by heating or immersing in solvent vapor atmosphere was carried out. The microphase-separated structures in these thin films were investigated by UV-vis and AFM analyses.

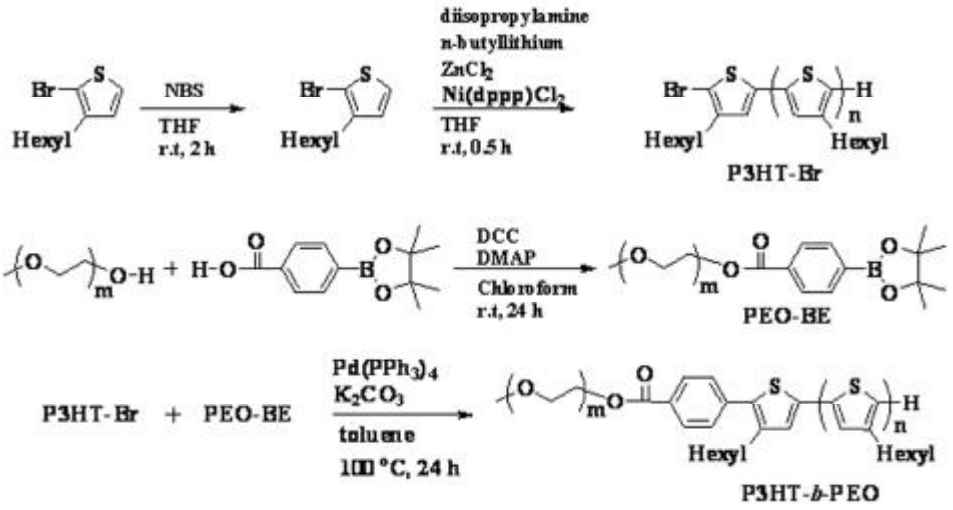

Figure 4-1. The synthetic route of P3HT-*b*-PEO via Suzuki coupling reaction.

4.2 Experimental

4.2.1 Materials

Regioregular P3HT with a bromo terminal (P3HT-Br) was synthesized by Grignard metathesis polymerization as shown in Chapter 2. All the other chemicals and solvents were used as received.

4.2.2 Synthesis of poly(ethylene oxide) with boronic acid pinacol ester(PEO-BE)

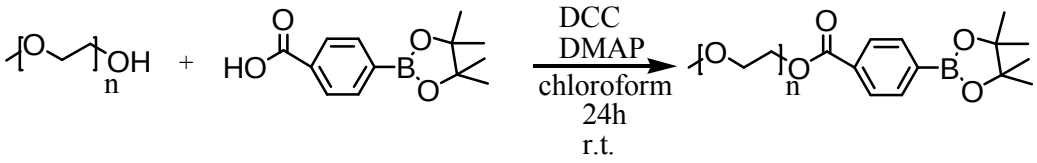

Figure 4-2. Preparation of PEO-BE.

After PEO (Mw: 5000, 5.00 g, 1 mmol) was added into a dried 100 ml two-necked flask, 4-(4,4,5,5-tetramethyl-1,3,2-dioxaborola*n*-2-yl)benzoic acid 0.870 g (3.50 mmol) and dichloromethane (40 ml) were added, and stirred for 10 min at r.t, then DCC (0.625 g, 3.00 mmol) was added. After 1 h, DMAP (0.367 g, 3.00 mmol) was added, and the mixture was stirred for 24 h at r.t. The product was precipitated in diethyl ether. Yield: 4.44g, 84%

By changing the M_w of PEO to 1000 or 2000, three kinds of poly(ethylene oxide) with boronic acid pinacol ester were obtained.

4.2.3 Synthesis of P3HT-*b*-PEO by Suzuki coupling reaction

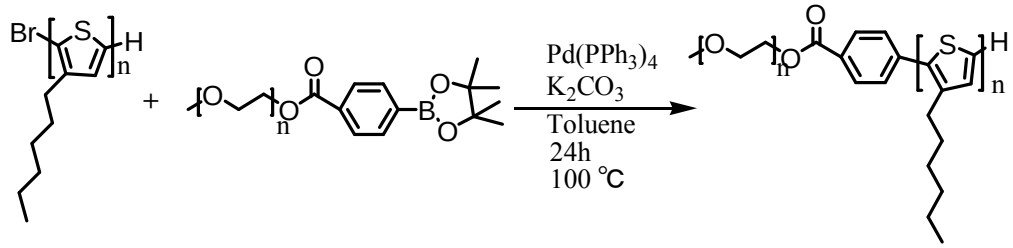

Figure 4-3. Preparation of P3HT-*b*-PEO.

To a two-necked flask equipped with a stopcock, P3HT-Br (0.221 g, 0.01 mmol), PEO-BE (0.201 g, 0.0402 mmol), tetrakis(triphenylphosphine)palladium(0) ($Pd(PPh_3)_4$) (4.97 mg, 0.00430 mmol), and dry

toluene (13 ml) were added under nitrogen. After 3 mol/L potassium carbonate (K_2CO_3) aq. (3 ml) was added, the mixture was stirred at 100 °C for 24 h. The mixture was extracted by chloroform, then the organic layer was dried by $MgSO_4$. The solution was concentrated and poured into methanol to obtain the polymer. Yield: 0.239 g, 84%

By changing the M_w of P3HT-Br or PEO-BE, P3HT-*b*-PEO block copolymers with different P3HT/PEO ratios were obtained.

4.2.4 Measurements

Nuclear magnetic resonance (NMR)

^1H and ^{13}C NMR spectrum were obtained on a JEOL ALPHA500 instrument at 500 and 125 MHz, respectively. Deutrated chloroform was used as a solvent with tetramethylsilane as an internal standard.

Gel permeation chromatography (GPC)

Number- and weight-average molecular weights (M_n and M_w) were determined by gel permeation chromatography (GPC) analysis with a JASCO RI-2031 detector eluted with chloroform at a flow rate of 0.5 ml/min and calibrated by standard polystyrene samples.

Differential scanning calorimetry (DSC)

Thermal analyses were performed on a Rigaku DSC-8230 under a nitrogen atmosphere at the heating and cooling rates of 10 °C/min.

High Performance Liquid Chromatography (HPLC)

The purification of 2-bromo-3-hexylthiophene was measured by HPLC made by JASCO, with system of LC-Net II ADS. Methanol:H_2O=9:1 was used as eluent and was treated by ultrasonic for 5 min before measurement.

UV-vis absorption analysis

UV-vis analysis was conducted on a JASCO V-570 spectrophotometer for the solution of 0.01 mg/ml in THF or chlorobenzene, or for the films prepared by spin coating from a solution of 10 mg/ml in chlorobenzene.

Photoluminescence (PL) analysis

Fluorescence of polymers was conducted by JASCO FP-777 for the solution of 0.01 mg/ml in THF or chlorobenzene, or for the films prepared by spin coating from a solution of 10 mg/ml in chlorobenzene.

Atomic force microscopy (AFM)

Surface morphology measurements were performed on a JEOL JSPM-4200 system in tapping mode (phase and topographic modes) with an MPP-11100-10 silicon probe (resonant frequency: 300 kHz, force constant: 40 N/m).

4.3 Results and Discussion

4.3.1 Characterization of poly(ethylene oxide) with boronic acid pinacol ester (PEO-BE)

PEO-BEs with M_w of 1000, 2000, and 5000 were obtained by the condensation between PEO and benzoic acid with boronic acid pinacol ester. ^{1}H NMR spectrum of the product was shown in Figure 4-4.

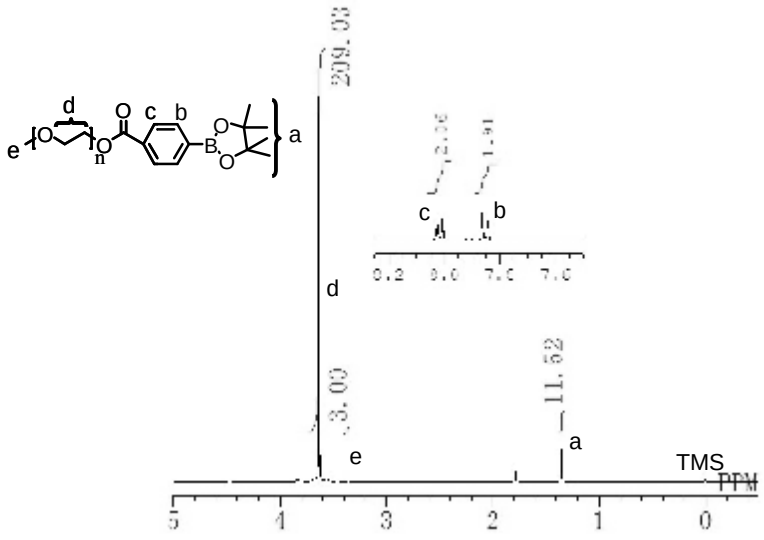

Figure 4-4. ^{1}H NMR spectrum of poly(ethylene oxide) (1000) with boronic acid pinacol ester.

4.3.2 Characteristic of poly(3-hexylthiophene)-*b*-poly(ethylene oxide) (P3HT-*b*-PEO)

The diblock copolymer comprising P3HT and PEO segments were prepared by coupling reaction between each homopolymers, the structures were confirmed by ^{1}H and ^{13}C NMR spectrum as shown in Figure 4-5 and 4-6. The signal assignable to PEO was observed at 3.6 ppm in ^{1}H NMR spectrum of P3HT-*b*-PEO. Compared with the spectrum of PEO-BE, the shift of signals (*) in aromatic region assignable to the protons on the phenyl ring at the junction point indicated that the terminal thiophene unit was completely substituted by PEO segment in Suzuki coupling. The weight ratios of P3HT and PEO segments were estimated from integral ratio of the signals. As shown in Table 4-1, five kinds of block copolymers with different PEO weight ratios were prepared.

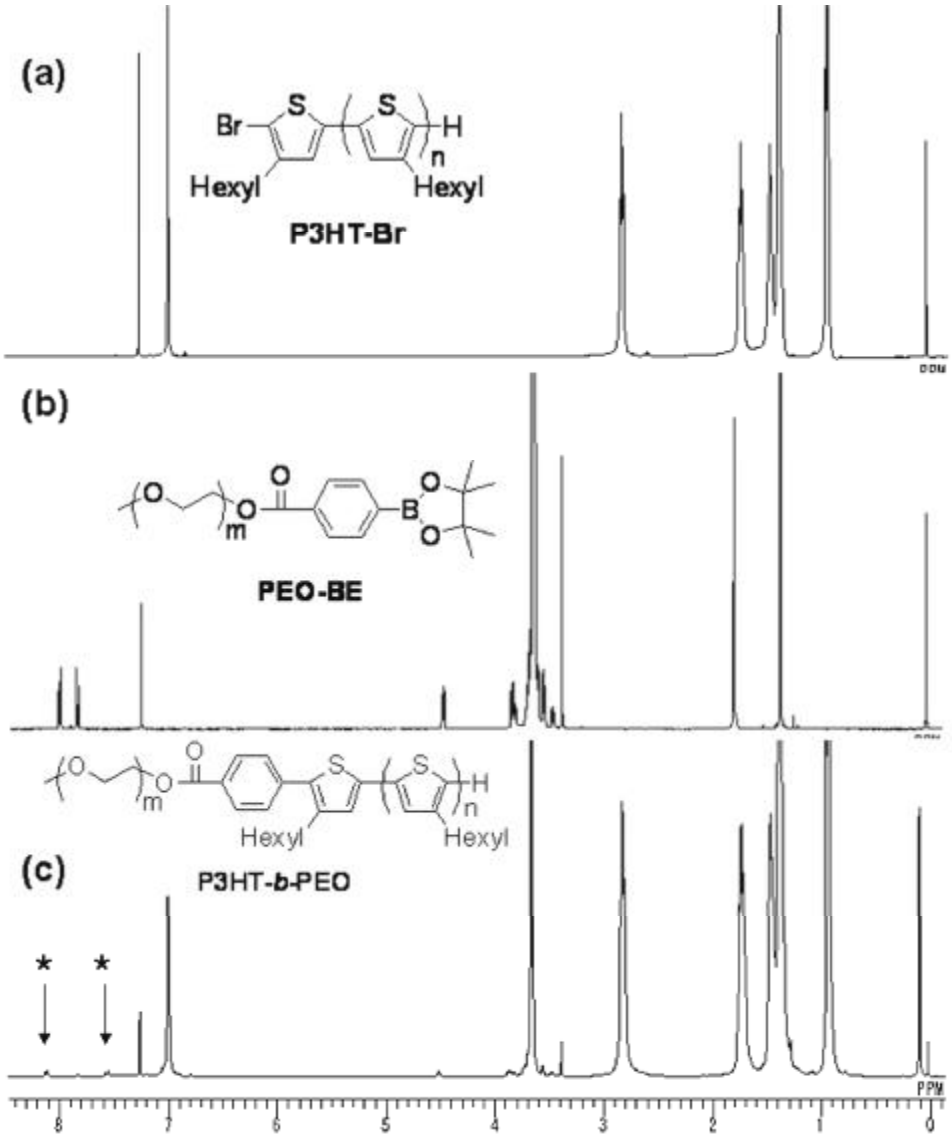

Figure 4-6. ^{1}H NMR spectra of (a) P3HT-Br, (b) PEO-BE, and (c) B2. Asterisks indicate signals of aromatic protons.

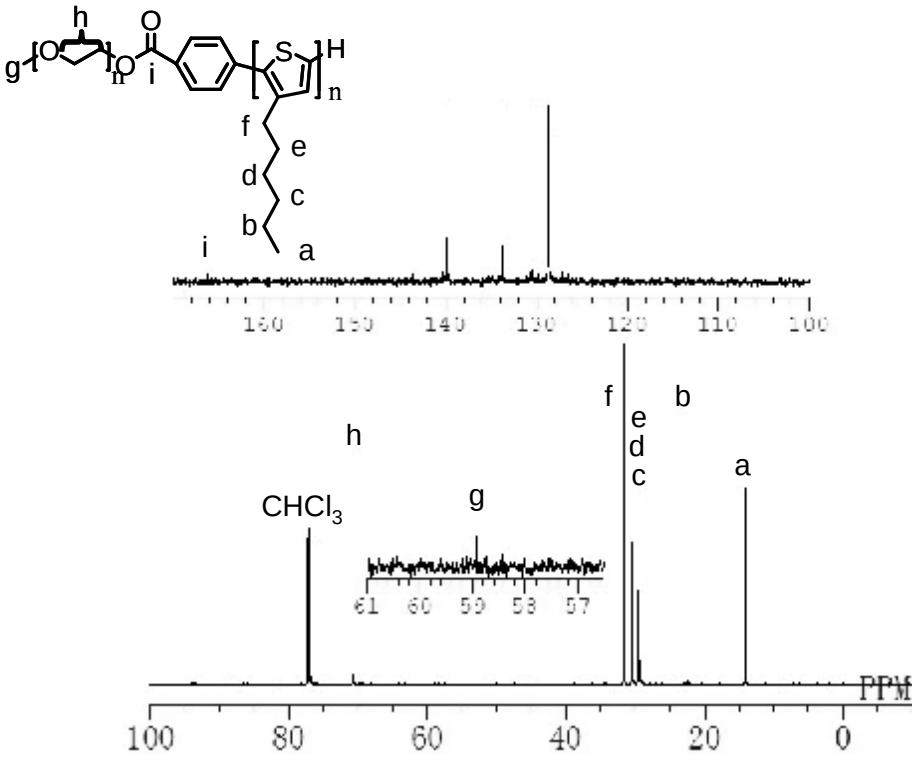

Figure 4-5. ^{13}C NMR spectrum of block copolymers (B2) .

Table 4-1. Molecular weight and component ratio of PEO in block copolymers.

Polymer	M_n of P3HT-Br[a]	PDI of P3HT-Br[a]	M_n of PEO-BE[a]	M_n[a]	PDI[a]	PEO weight ratio[b]
B1	19200	1.42	1000	22200	2.22	2.9%
B2	13800	1.44	1000	14400	1.71	6.9%
B3	16400	2.02	2000	22800	1.86	9.3%
B4	13800	1.44	2000	15700	1.97	15%
B5	19200	1.42	5000	21800	1.60	21%

[a] Determined by GPC with polystyrene standards.

[b] Determined by ^{1}H NMR.

4.3.3 Thermal property of block copolymer

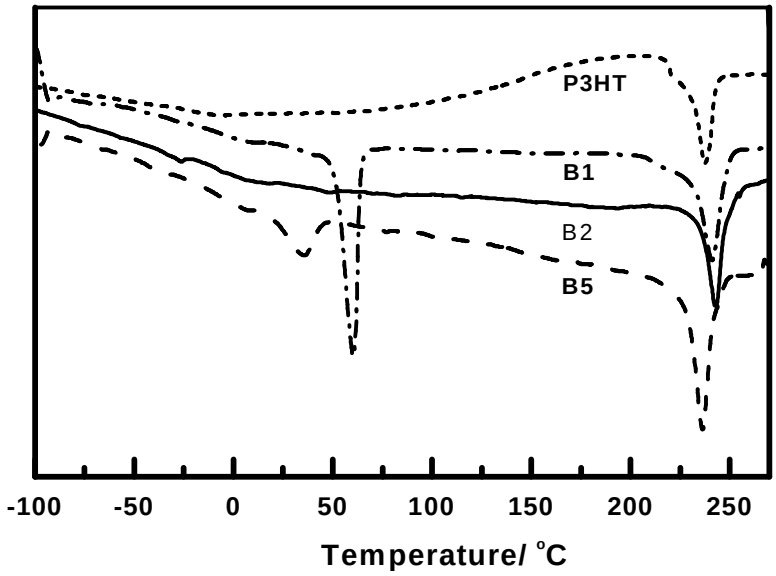

Figure 4-7. DSC profiles of P3HT and P3HT-*b*-PEO in the second heating.

The thermal properties of P3HT-*b*-PEO were measured by differential scanning calorimeter (DSC). The DSC thermograms of P3HT and P3HT-*b*-PEO (B1, B2, B5) were shown in Figure 4-7. The melting temperature (T_m) of P3HT appears at 220 °C, whereas the block copolymer exhibits T_ms at around 25-45 °C and 220 °C, which correspond to those of PEO and P3HT segments, respectively. The results from DSC measurement indicated that both the PEO and P3HT segments indeed exist.

4.3.4 Optical properties of polymers

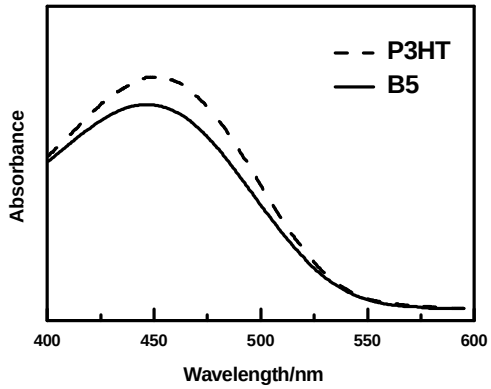

Fig. 4-8. UV-vis spectra of P3HT and P3HT-*b*-PEO (B5) solutions in chloroform (0.01 mg/ml).

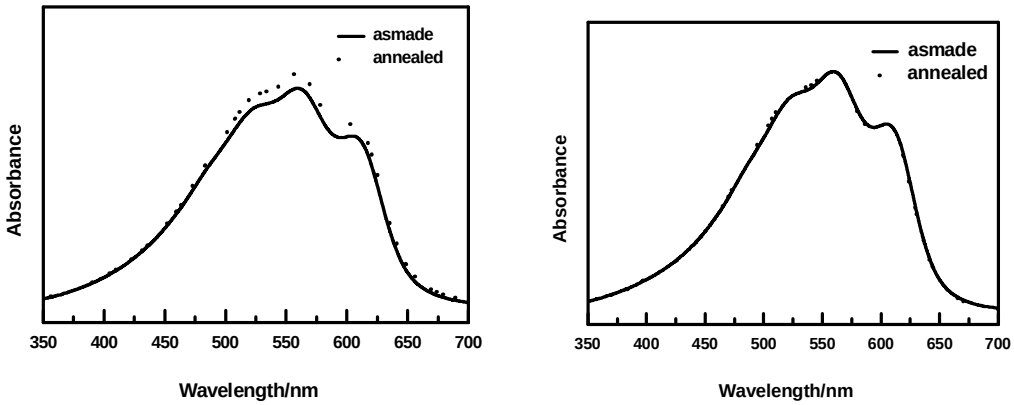

Figure 4-9. UV-vis spectra of P3HT (left) and P3HT-*b*-PEO (B5) (right) films before and after thermal annealing at 150 °C for 10 min.

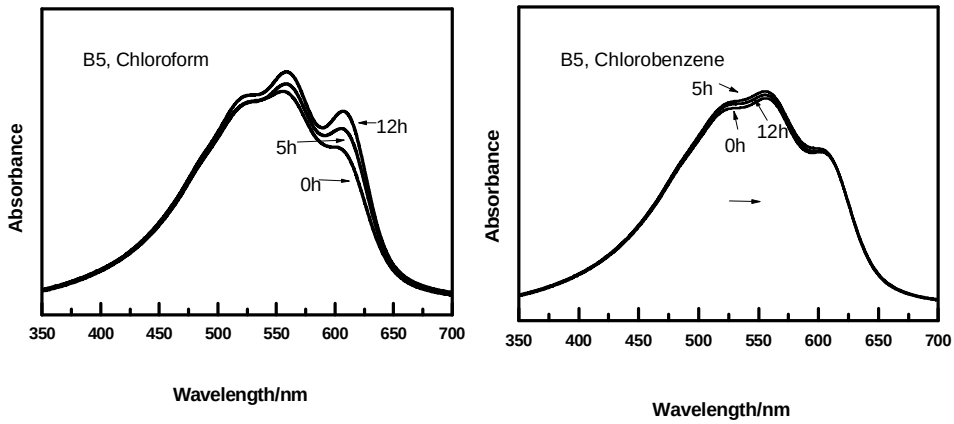

Figure 4-10. UV-vis spectrum of P3HT-*b*-PEO (B5) films before and after solvent annealing by chloroform (left) and chlorobenzene (right).

UV-vis absorption spectrum were measured for the thin films of P3HT and P3HT-*b*-PEO (B5) before and after thermal or solvent annealing process as shown in Figure 4-9 and Figure 4-10. Compared with the spectrum of P3HT or P3HT-*b*-PEO solution in chloroform (Figure 4-8), all the λ_{max} values of films showed a bathochromic shift. The absorption wavelengths of all the block films appeared at approximately 520, 560, and 610 nm, which are similar with those of the P3HT film, which reveals that the intermolecular π-π stacking of P3HT is not affected by the presence of PEO segment.

4.3.5 Surface morphology of P3HT-*b*-PEO block

The surface morphology of the P3HT-*b*-PEO (B5) films was observed by AFM. The films were subjected to the thermal annealing at 150 °C for 10 min or solvent annealing by chloroform or chlorobenzene. Figure 4-11 show AFM phase images of the surface of P3HT-*b*-PEO (B5) films.

A rough microphase separation with a domain size of around 100 nm can be observed at the surface of P3HT-*b*-PEO (B5) film before annealing (Figure 4-11a), which is not observed in the surface of the P3HT film (Figure 2-14a). After thermal annealing, the clear microphase-separated structure appeared with a domain size of about 30 nm (Figure 4-11b).

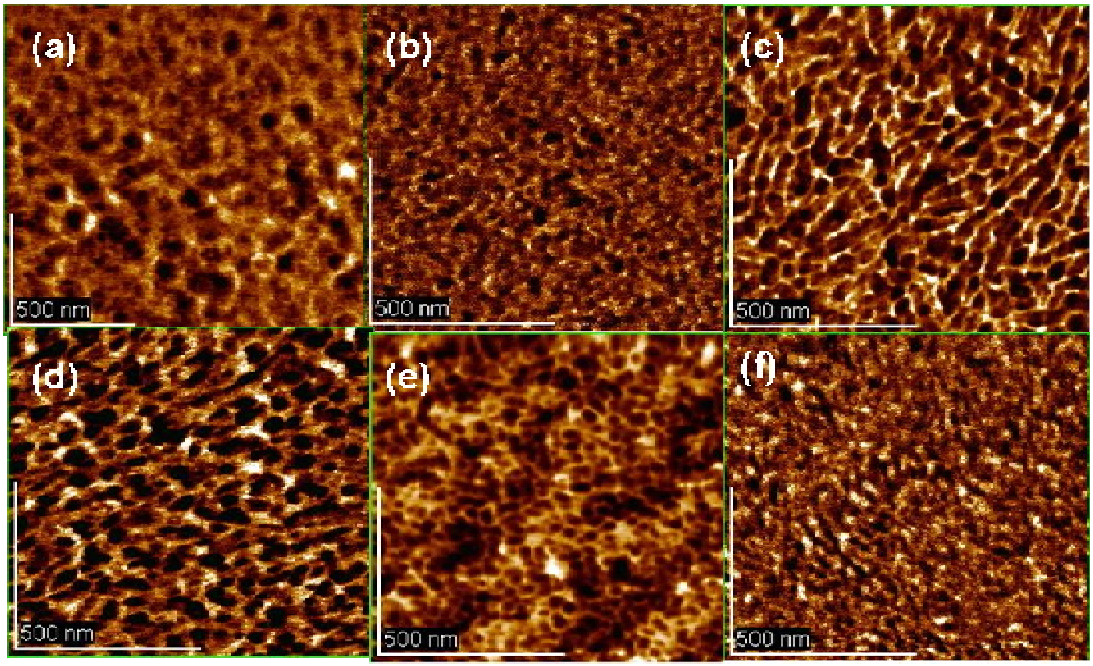

Figure 4-11. AFM images of P3HT-*b*-PEO (B5) thin film (a) before and (b) after thermal annealing at

150 °C for 10 min, and solvent annealing by (c) chloroform for 5 h, (d) chloroform for 12 h, (e) chlorobenzene for 5 h, and (f) chlorobenzene for 12 h.

After solvent annealing with chloroform, a clearer microphase-separated structure appeared, but the domain size enlarged up to 100nm. When the annealing solvent was changed to chlorobenzene, the film showed microphase-separated morphology with a smaller domain size of 20 nm. AFM measurement revealed that the block copolymer consisting of P3HT and PEO shows clear microphase-separated morphologies which can be utilized for the morphological control in photovoltaic devices.

4.4 Conclusion

The *p*-type conducting block copolymer poly(3-hexylthiophene)-*block*-poly(ethylene oxide) (P3HT-*b*-PEO) was synthesized by Suzuki coupling reaction between P3HT and PEO homopolymers. The photophysical properties investigated by UV-vis absorption spectrum showed that the polystyrene block increased the relative intensity the band around 600 nm, which indicated that microphase separation makes P3HT to form more densely stacked structure. In the AFM image, the microphase-separated structure appeared with a domain size of about 50 nm (Figure 4-13b) was observed at the surface of P3HT-*b*-PEO thin film, which is more uniform, smaller domain size than that observed in the P3HT blend film. Block copolymer is more likely to form clear microphase-separated morphologies by both thermal and solvent annealing.

4.5 Reference

[1]. Sommer, M.; Lang, A. S.; Thelakkat, M. *Angew. Chem. Int. ed*. **2008**, 47, 7901.

[2]. Zhang, Q. L.; Cirpan, A.; Russell, T. P.; Emrick, T. *Macromolecules*. **2009**, 42, 1079.

[3]. Chueh. C.; Higashihara. T.; Tsai. J.; Ueda. M.; Chen. W. *Org. Electron*. **2009**, 10, 1541.

[4]. Sary, N.; Richard, F.; Brochon, C.; Leclerc, N.; Lévêque, P.; Audinot, J.; Berson, S.; Heiser, T.; Hadziioannou, G.; Mezzenga, R. *Adv. Mater*. **2010**, 22, 763.

[5]. Heiser, T.; Adamopoulos, G.; Brinkmann, M.; Giovanella, U.; Ouldsaad, S.; Brochon, C.; Vandewetering, K.; Hadziioannou, G. *Thin Solid Films*. **2006**, 511, 219.

[6]. Lin, Z.; Kim, D. H.; Wu, X.; Boosahda, L.; Stone, D.; LaRose, L.; Russell, T. P. *Adv. Mater*. **2002**, 14, 1373.

[7]. Morikawa, Y.; Nagano, S.; Watanabe, K.; Kamata, K.; Iyoda, T.; Seki, T. *Adv. Mater*. **2006**, 18, 883.

Chapter 5 . Annealing Effect on Performance and Morphology of Photovoltaic Devices Based on Poly(3-hexylthiophene)-*b*-Poly(ethylene oxide)

5.1 Introduction

In order to overcome the limitations of the photo-voltaic conversion efficiency, controlling morphologies in the active layer is a key issue for the photovoltaic devices based on bulk heterojunction (BHJ) structure. The BHJ organic photovoltaic materials are represented by a combination of regioregular poly(3-hexyl thiophene) (P3HT) as a donor and [6,6]-phenyl-C_{61}-butyric acid methyl ester (PCBM) as an acceptor [1-5]. In this chapter, in order to utilize the microphase separation of block copolymers for controlling morphology in polymer photovoltaic devices, a novel block copolymer poly(3-hexylthiophene)-*block*-poly(ethylene oxide) (P3HT-*b*-PEO) blended with PCBM was used as active layer of photovoltaic device. A series of annealing by heating or immersing in solvent vapor atmosphere ware carried out on the photovoltaic devices prepared using P3HT or P3HT-*b*-PEO blended with PCBM. The UV-vis, AFM, and *I*-*V* characteristics were evaluated, and the relationship between the morphology and the device performance was discussed.

5.2 Experiment

5.2.1 Materials

The poly(3-hexylthiophene)-*block*-poly(ethylene oxide) (P3HT-*b*-PEO) diblock copolymers comprising P3HT and PEO segments were prepared by coupling reaction between each homopolymers as shown in Chapter 4. Regioregular P3HT with a bromo terminal (P3HT-Br) was synthesized by Grignard metathesis polymerization. A hydroxyl-terminal of PEO was converted to boronic ester (PEO-BE). P3HT-Br was coupled with large excess of PEO-BE via Suzuki coupling reaction to give P3HT-*b*-PEO without contamination of PEO-BE which can be removed by reprecipitation in methanol. A series of P3HT-*b*-PEO were synthesized with various PEO segment weight ratios.

The weight ratios of P3HT and PEO segments were estimated from ^{1}H NMR. As shown in Table 5-1, three kinds of block copolymers with different PEO weight ratios were used.

Table 5-1. Characteristics of P3HT-*b*-PEOs.

Polymer	M_n of P3HT-Br[a]	PDI of P3HT-Br[a]	M_n of PEO-BE[a]	M_n[a]	PDI[a]	PEO weight ratio[b]
B1	19200	1.42	1000	22200	2.22	2.9%
B2	13800	1.44	1000	14400	1.71	6.9%
B3	16400	2.02	2000	22800	1.86	9.3%

[a] Determined by GPC with polystyrene standards.
[b] Determined by ^{1}H NMR.

5.2.2 Characteristic Measurements

UV-vis absorption analysis

UV-vis analysis was conducted on a JASCO V-570 spectrophotometer for the solution of 0.01 mg/ml in THF or chlorobenzene, or for the films prepared by spin coating from a solution of 10 mg/ml in chlorobenzene.

Atomic force microscopy (AFM)

Atomic force microscopy (AFM) measurements were performed on a JEOL JSPM-4200 system in tapping mode (phase and topographic modes) with an MPP-11100-10 silicon probe (resonant frequency: 300 kHz, force constant: 40 N/m).

5.2.3 Device Fabrication

All the devices were manufactured with a structure of ITO/PEDOT:PSS(30 nm)/active layer/LiF(0.5 nm)/Al(100 nm).

Spin-coating

The substrates were pre-cleaned in an ultrasonic bath of deionized water for 30 min.

Poly(3,4-ethylenedioxythiophene):polystyrene sulfonate (PEDOT:PSS) was spin-coated onto a glass slide coated by patterned indium tin oxide(ITO), and annealed at 200 °C for 1 h.

The active layer was spin coated on PEDOT:PSS coated substrate from the polymer/PCBM solution at speeds of 1000, 1500, 2000, 2500 and 3000 rpm for 30s respectively. Each of the substrates was transferred to a plastic container and exposed to vapor of the residual solvent.

Annealing treatment

The substrates were transferred inside a nitrogen-filled glove box under atmospheric pressure , annealed at 150 °C for 10 min, or under solvent vapor at r.t. by 5h.

Atomic force microscopy (AFM)

Atomic force microscopy (AFM) measurements were performed on a JEOL JSPM-4200 system in tapping mode (phase and topographic modes) with an MPP-11100-10 silicon probe (resonant frequency: 300 kHz, force constant: 40 N/m).

I-V characteristics

A 0.5 nm thick layer of lithium fluoride followed by a 100 nm thick top contact of aluminum was

thermally evaporated onto the active layer in a vacuum chamber under 10^{-5} Pascal. The as-prepared cell performance was measured under AM 1.5 illumination using a Xenon lamp solar simulator in a nitrogen environment at room temperature, where the lamp intensity had been calibrated to 100 mW / cm^2. The photovoltaic characteristic of devices was measured by KEITHLEY 2400 Source Meter under 100 mW/cm^2 shown in Figure 3-1.

5.3 Result and discussion

5.3.1 The photophysical property of polymer/PCBM blend thin films

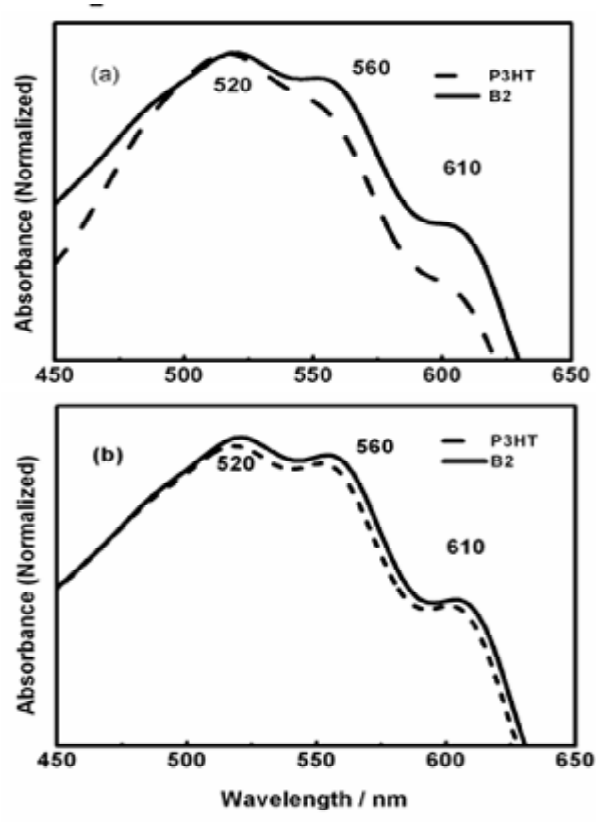

Figure 5-1. UV-vis spectra of the thin films based on P3HT/PCBM and P3HT-*b*-PEO (B2)/PCBM after (a) thermal annealing at 150 °C for 10 min and (b) chloroform annealing for 5 h.

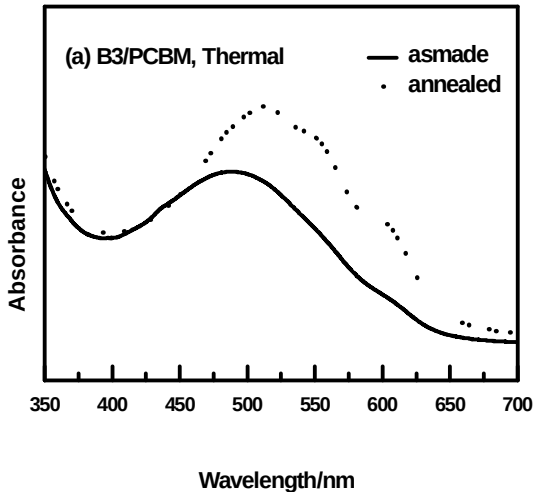

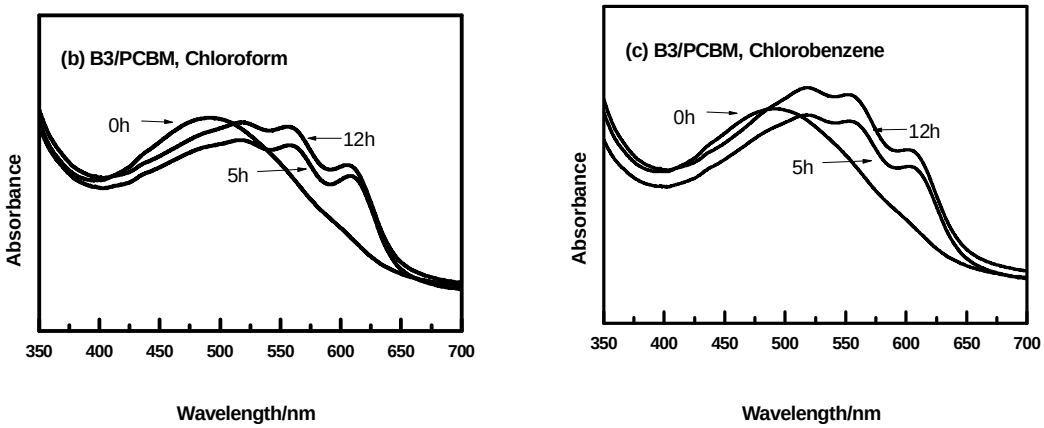

Figure 5-2. UV-vis spectra of the thin films based on P3HT-*b*-PEO (B3)/PCBM. (a) thermal-annealed at 150 °C for 10 min; (b) annealed by chloroform; (c) annealed by chlorobenzene;

UV-vis absorption spectra were measured for the blend films of P3HT/PCBM and P3HT-*b*-PEO/PCBM after thermal or solvent annealing process as shown in Figure 5-1 and Figure 5-2. As demonstrated in Chapter 4, all the blend films showed the absorption band from 400 to 650 nm derived from the P3HT segment. In the case of the blend films, the absorption peak derived from PCBM also appeared at 340 nm. It is found that not only the PEO segment but also PCBM do not influence the intermolecular π-π stacking of P3HT.

Furthermore, the intensity at 610 nm is higher in P3HT-*b*-PEO/PCBM blend films than that in P3HT/PCBM blend films. According to the reported work [8], this peak derived from a strong intermolecular interaction of π-π stacking and hence the high crystallizability of the P3HT main chains. Thus it can be assumed that PEO segment makes P3HT to form more densely stacked structure.

5.3.2 AFM images of thin films of the polymer blends with PCBM

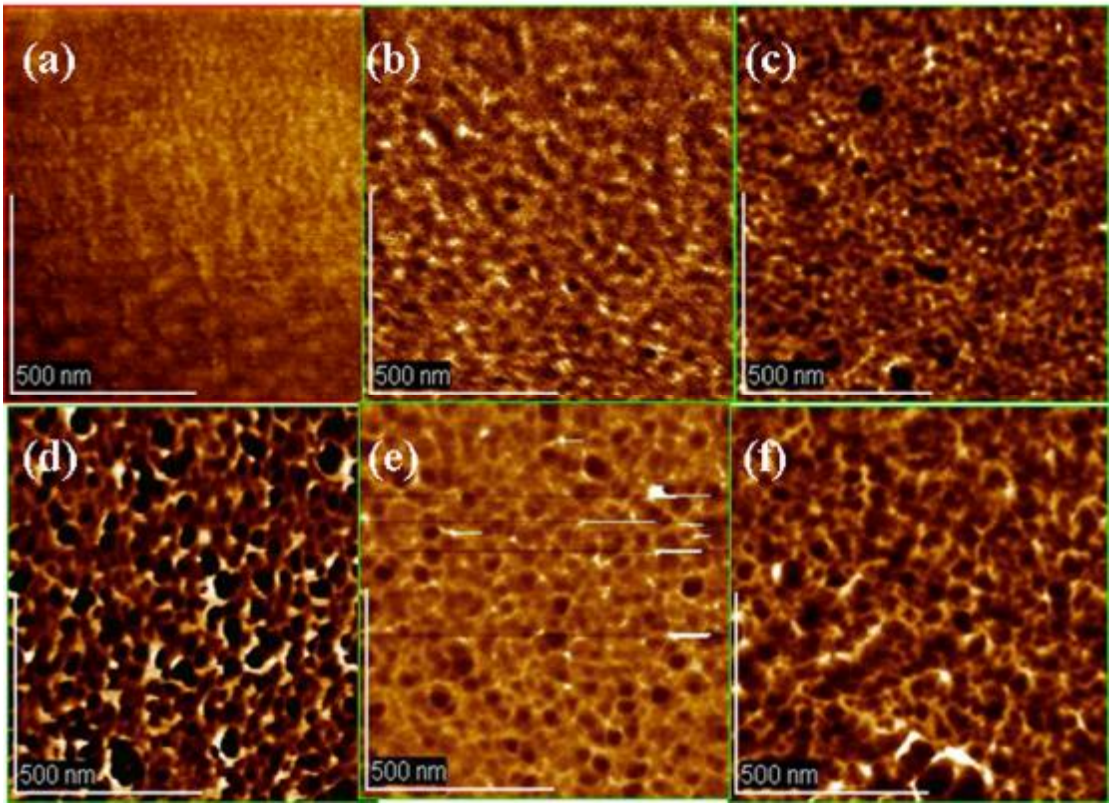

Figure 5-3. AFM images of P3HT/PCBM blend films (a) before and (b) after thermal annealing at 150 °C for 10 min, and solvent annealing by (c) chloroform for 5 h, (d) chloroform for 12 h, (e) chlorobenzene for 5 h, and (f) chlorobenzene for 12 h.

The surface morphology of the P3HT/PCBM or P3HT-*b*-PEO (B3)/PCBM blend films was observed by AFM. The films were subjected to the thermal annealing at 150 °C for 10 min or solvent annealing by chloroform or chlorobenzene. Figure 5-3 shows AFM phase images of the surface of P3HT/PCBM blend films. The large domains with a size of around 100 nm can be observed before annealing, which is assumed to be the aggregation of PCBM (Figure 5-3a). After thermal annealing, the microphase-separated structure appeared with a domain size of about 50 nm (Figure 5-3b). For solvent annealing using chlorobenzene for 5 h, the film surface showed smaller microphase-separated structure with a domain size less than 40 nm (Figure 5-3e). Annealing for longer time made the size of domains larger and more disordered because of the instability of phase-separated structure created by the polymer blend (Figure 5-3d and 5-3f).

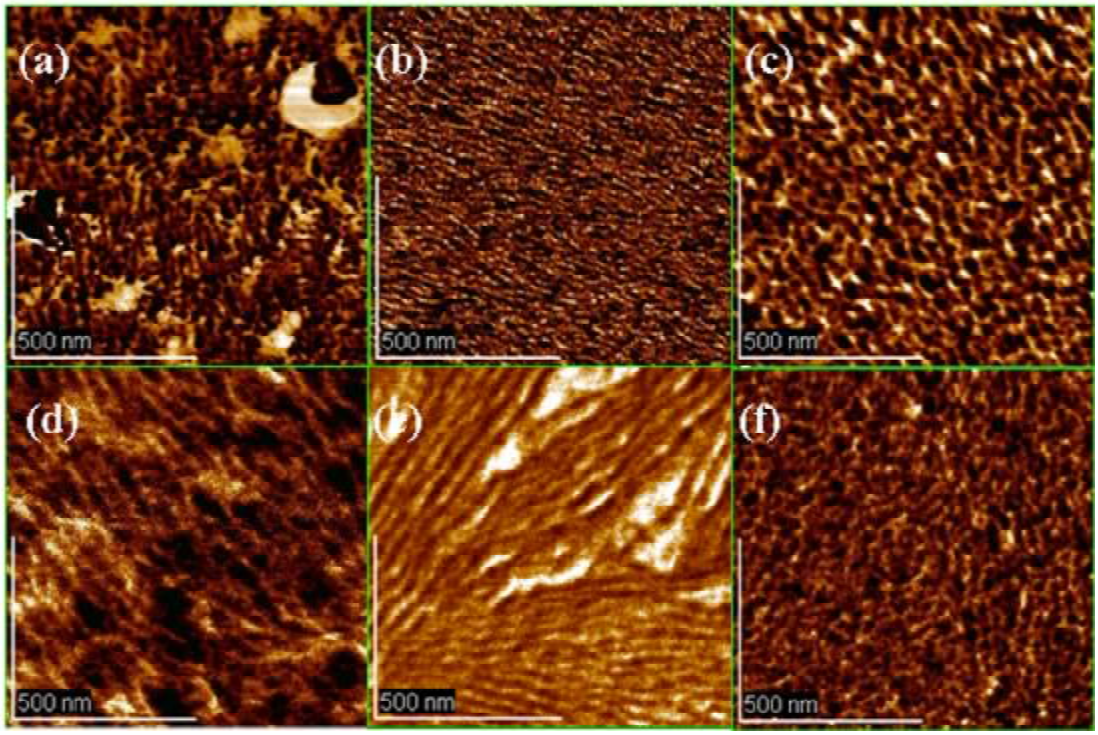

Figure 5-4. AFM images of P3HT-*b*-PEO (B3)/PCBM blend films (a) before and (b) after thermal annealing at 150 °C for 10 min, and after solvent annealing via (c) chloroform for 5 h, (d) chloroform for 12 h, (e) chlorobenzene for 5 h, (f) chlorobenzene for 12 h.

The AFM phase images of the P3HT-*b*-PEO/PCBM blend films were shown in Figure 5-4. For the P3HT-*b*-PEO blend film, thermal annealing provided more uniform, smaller domain size less than 20 nm than that observed in the P3HT blend film (Figure 5-4b). The microphase-separated structure was an ordered lamella with a domain size smaller than 20 nm, indicating that the introduction of PEO segment is useful for controlling the morphology.

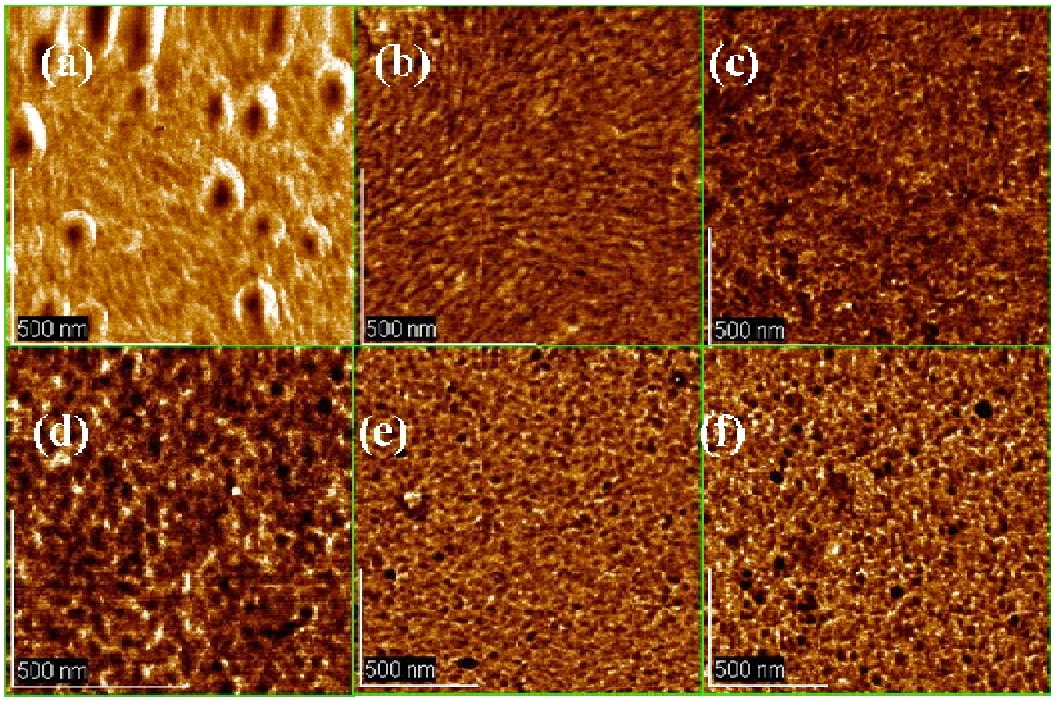

Figure 5-5. AFM images of P3HT-*b*-PEO(B2)/PCBM blend films (a) before and (b) after thermal annealing at 150 °C for 10 min, and after solvent annealing by (c) chloroform for 5 h, (d) chloroform for 12 h, (e) chlorobenzene for 5 h, and (f) chlorobenzene for 12 h.

After solvent annealing with chloroform, the lamellar structure was also build up, but the domain size slightly became larger compared with thermally annealed one (Figure 5-4c and 5-4d). When the solvent was changed to chlorobenzene, the film showed lamellar morphology after annealing for 5 h (Figure 5-4e). Keeping annealing for 12 h, the lamella collapsed to the disordered structure, but still maintained the small domain size (Figure 5-4f). The blend films using different block copolymer B2 showed similar results with the microphase separation (Figure 5-5). AFM measurement revealed that, compared with the P3HT/PCBM blend, block copolymer blend system is more likely to create clear microphase-separated morphologies by both thermal and solvent annealing.

5.3.3 Evaluation of photovoltaic devices based on P3HT-*b*-PEO

In order to investigate the photovoltaic performance of the devices based on block copolymers, a series of devices using P3HT-*b*-PEOs with different PEO contents blended with PCBM in 1:1 weight ratio were fabricated. All the devices were annealed at 150 °C for 10 min in glove box filled with argon or solvent-annealed by chloroform or chlorobenzene vapor atmosphere. Solvent annealing was performed by settling the devices in a desiccator filled with each solvent vapor. The *I-V* curves for the photovoltaic devices were obtained under simulated AM 1.5 (100 mW/cm^2) illumination.

5.3.4 The active layer thickness of polymer/PCBM blend thin films

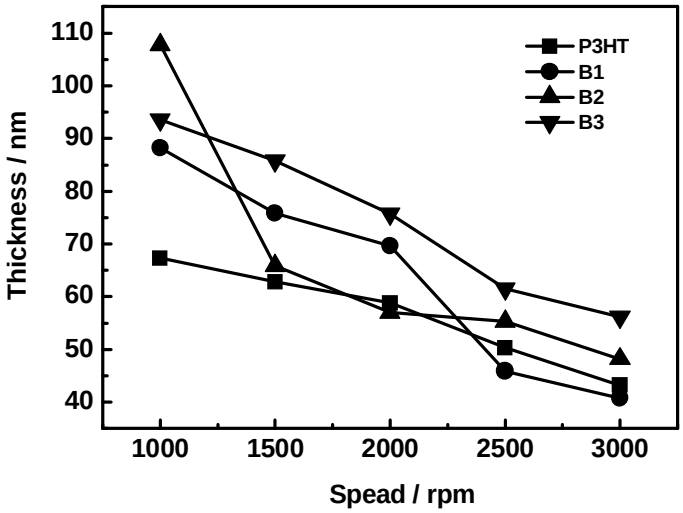

Figure 5-6. Active layer thicknesses of P3HT/PCBM and P3HT-*b*-PEO/PCBM bulk heterojunction thin films under various spin-coating speeds with the concentration of 20 mg/ml in chloroform.

At first, the effect of spin-coating speed for the active layer thickness was investigated. As shown in Figure 5-6, with the increasing of spin-coating speed from 1000 to 3000 rpm, the thickness of all polymers decreased continuously from 70-110 nm to approximately 50 nm.

5.3.5 The effect of active layer thickness for photovoltaic device

In order to investigate the photovoltaic characteristics of polymers, the devices with a series of active

layer thickness were fabricated. The J_{sc}-V_{oc} curves of P3HT/PCBM photovoltaic cells with the active layer thicknesses from 54.9 to 87.3 nm were shown in Figure 5-7.

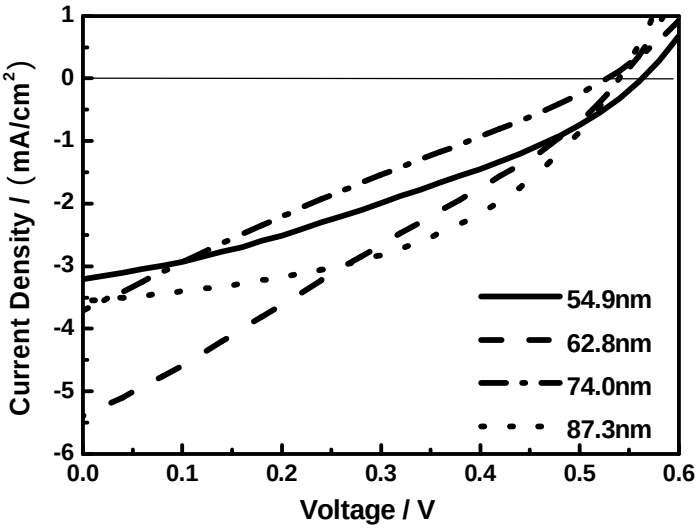

Figure 5-7. Current-voltage characteristics of the P3HT/PCBM photovoltaic device with different active layer thickness.

The device with the active layer thickness of 74 nm exhibited the highest photovoltaic performances (J_{sc} = 7.04 mA/cm^2 ; η = 1.38%; V_{oc} = 0.60 V; *FF* = 0.33) than those with other active layer thicknesses. The dependences of the device performances on the active layer thickness were summarized in Figure 5-8 for the devices using P3HT/PCBM or P3HT-*b*-PEO/PCBM. All of the devices showed the optimum photovoltaic performances with a thickness of active layer at approximately 70 nm. The thicker the thickness of the active layer became, the higher conversion efficiency was obtained below 70 nm, whereas the opposite case above 70 nm. When the thickness was less than 70 nm, the photon absorption was not enough to obtain the high photocurrent. However, when the thickness increased over 70 nm, the recombination of charges occurred during charge transportation, resulting in low efficiency even with high photon absorption. Therefore, the thickness of the active layer was set at 70 to 80 nm for the following evaluation.

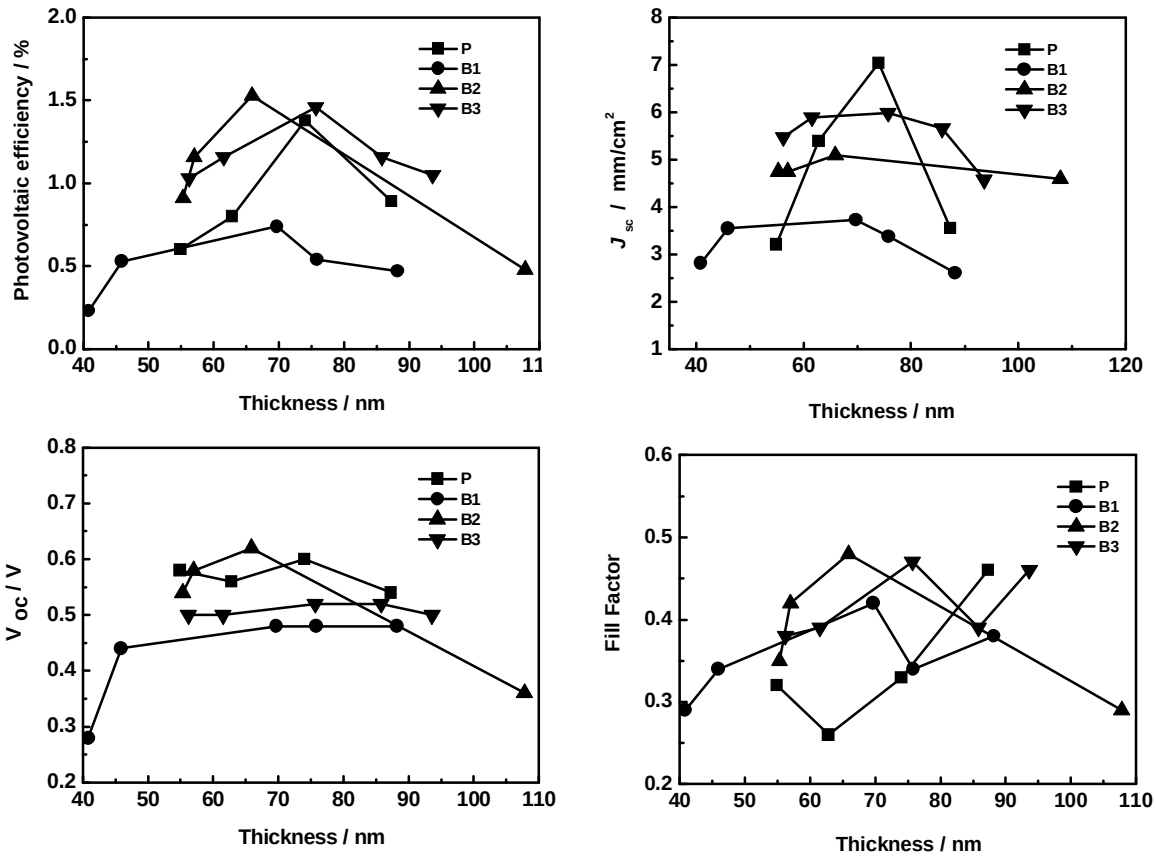

Figure 5-8. Photovoltaic device characteristics at various thicknesses. (a) efficiency; (b) J_{sc}; (c) V_{oc}; (d) fill factor.

The device based on P3HT-*b*-PEO/PCBM exhibited higher performances than that of the device based on P3HT/PCBM. The short circuit current (J_{sc}) also showed a maximum around 70 nm of active layer thickness. On the other hand, the open circuit voltage (V_{oc}) and the fill factor are independent of the active layer thickness.

The performances of the devices based on P3HT-*b*-PEO/PCBM with different PEO contents are evaluated at the almost same thickness of the active layer. The characteristics are summarized in Table 5-2. The efficiency increased with an increase in PEO contents, and reached maximum of 1.05% at the PEO weight ratio of 9.3% (B3). Higher PEO content over 10% made the efficiency extremely decreased, and no photovoltaic characteristic behavior was observed for B5 with the PEO content of 21%. Excessive introduction of PEO segment may create an insulating domain between P3HT and PBCM domains, which impedes the charge dissociation at the interface and the charge transportation.

Table 5-2. Performances of photovoltaic devices based on P3HT-*b*-PEO blends with different PEO weight ratios.

Polymer	PEO content / wt%	V_{oc} / V	J_{sc} / (mA/cm^2)	Fill factor	Efficiency /%
B1	2.9	0.48	3.61	0.38	0.47
B2	6.9	0.36	4.6	0.29	0.48
B3	9.3	0.5	4.58	0.46	1.05
B4	15	0.12	1.23	0.26	0.04
B5	21	—	—	—	—

Table 5-3. Annealing effect on the performance of the devices based on P3HT/PCBM.

Annealing	Annealing time / min	V_{oc} / V	J_{sc} / (mA/cm^2)	Fill factor	Efficiency /%
none	-	0.56	2.9	0.31	0.5
thermal	10	0.6	7.04	0.33	1.38
chloroform	300	0.48	4.32	0.39	0.82
	720	0.46	5.01	0.47	1.07
chlorobenzene	300	0.5	7.23	0.47	1.71
	720	0.32	4.61	0.28	0.42

Table 5-4. The Annealing effect on the performance of the devices based on P3HT-*b*-PEO/PCBM.

Polymer	Annealing	Time / min	V_{oc} / V	J_{sc} / (mA/cm^2)	Fill factor	Efficiency /%
B2	none	-	0.54	2.46	0.28	0.37
	thermal	10	0.62	5.1	0.48	1.53
	Chloroform	300	0.6	1.37	0.13	0.1
		720	0.58	3.05	0.39	0.7
	Chlorobenzene	300	0.6	2.42	0.35	0.5
		720	0.58	2.86	0.34	0.56
B3	none		0.40	1.75	0.30	0.21
	thermal	10	0.52	5.99	0.47	1.46
	Chloroform	300	0.46	4.21	0.45	0.86
		720	0.44	4.04	0.41	0.72
	Chlorobenzene	300	0.44	2.24	0.35	0.35
		720	0.26	2.04	0.27	0.14

In order to improve the efficiency by controlling the inner structure of the active layer, thermal or solvent annealing was employed for the devices. The performance of devices was summarized in Table 5-3 for P3HT/PCBM and in Table 5-4 for P3HT-*b*-PEO/PCBM. The *I*-*V* curves for the devices giving high efficiencies are shown in Figure 5-9 by thermal annealing and Figure 5-10 to 5-13 by solvent annealing. For thermal annealing, both of P3HT and P3HT-*b*-PEO systems showed higher efficiencies compared with those before annealing. The device using B2 exhibited the highest efficiency of 1.53% among all of the thermal-annealed devices. Introducing PEO improved the efficiency of the device of blend system probably because of morphological change inside the active layer.

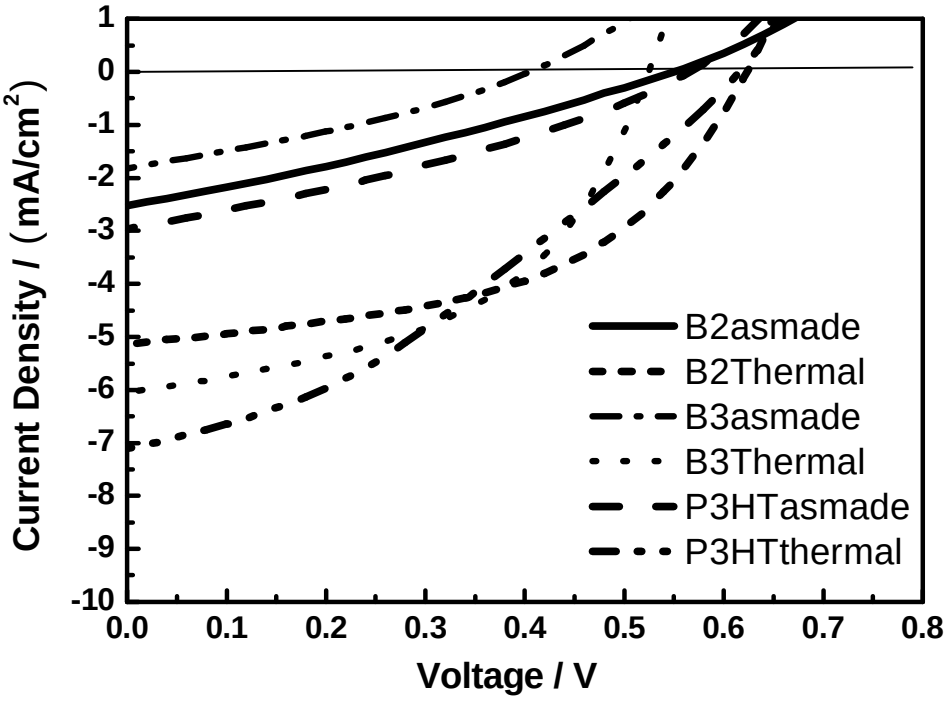

Figure 5-9. *I*-*V* curves for the devices based on P3HT/PCBM and P3HT-*b*-PEO (B2, B3)/PCBM after thermal annealing.

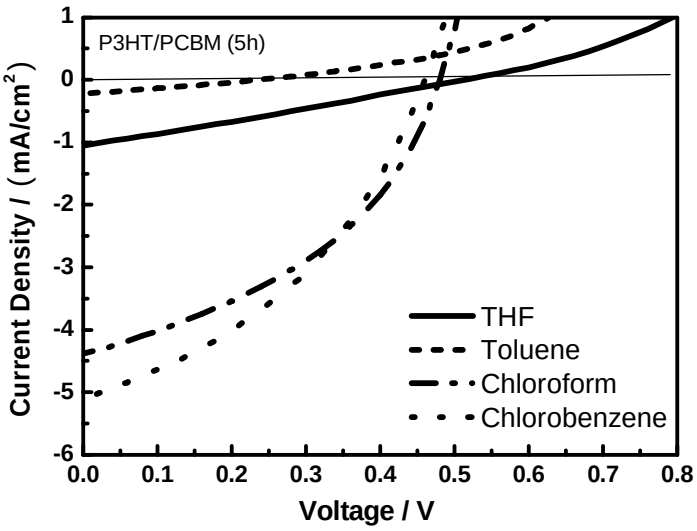

Figure 5-10. *I-V* curves for the devices based on P3HT/PCBM after solvent annealing by various solvents for 5h.

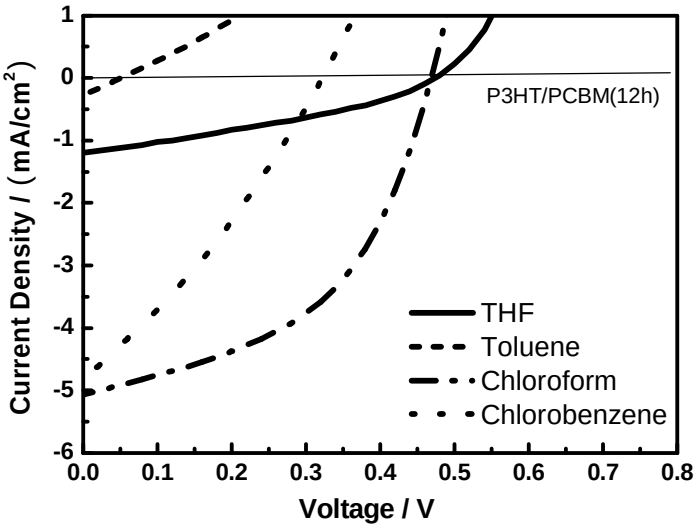

Figure 5-11. *I-V* curves for the devices based on P3HT/PCBM after solvent annealing by various solvents for 12h.

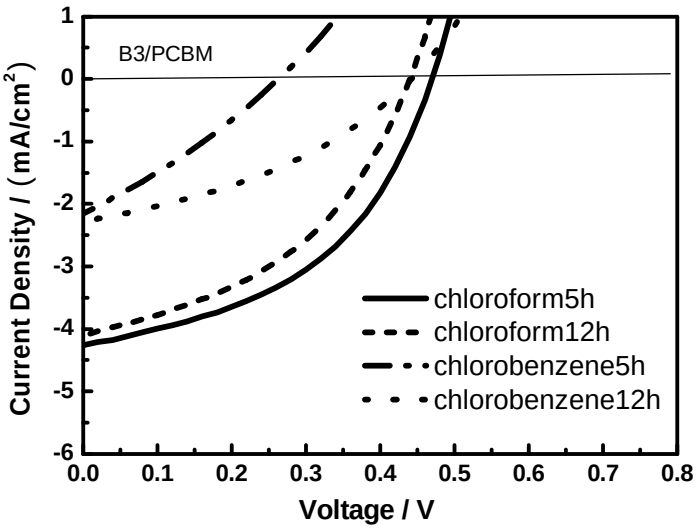

Figure 5-12. *I-V* curves for the devices based on P3HT-*b*-PEO(B3)/PCBM after solvent annealing by various solvents.

Solvent annealing with good solvents is more likely to induce ordered morphologies in block copolymer thin films compared with poor solvents.[18] Therefore, the good solvents for P3HT (chloroform and chlorobenzene) were selected for solvent annealing of the devices. In contrast with thermal annealing, the P3HT/PCBM devices showed higher efficiency than that of P3HT-*b*-PEO/PCBM devices after solvent annealing. Device of P3HT annealed by chlorobenzene for 5h with PCE as 1.71% was most effective to improve the performance for both devices based on P3HT and P3HT-*b*-PEO.

The AFM results reasonably correlate with the fact that the performance of the device based on P3HT-*b*-PEO/PCBM prevails over that of the P3HT/PCBM device after thermal annealing. However, the conversion efficiency after solvent annealing is not always better than that of thermal annealing, even with more ordered morphology. These results are assumed to be due to the heterogeneous morphology as shown in the AFM images of P3HT-*b*-PEO/PCBM films. Another explanation may be that dewetting of the surface occurred especially after longer annealing, which makes problems at the interface between the active layer and the electrode.

5.4 Conclusions

The novel block copolymers P3HT-*b*-PEO with different PEO contents were prepared via Suzuki coupling between P3HT and PEO homopolymers. AFM measurement of thin film based on P3HT-*b*-PEO/PCBM revealed that the introduction of PEO segment contributed to generate ordered lamellar morphology with the smaller size compared with the P3HT/PCBM blend. The devices were fabricated based on P3HT or P3HT-*b*-PEO blended with PCBM in 1:1 weight ratio, and the performance was evaluated after thermal or solvent annealing. For the devices based on P3HT-*b*-PEO/PCBM, the favorable PEO content to obtain the high efficiency was found to be 7 to 9%, where the active layer thickness was optimized at approximately 70 nm. After thermal annealing, the P3HT-*b*-PEO/PCBM device showed higher performance than that of the P3HT/PCBM device.

5.5 References

[1]. Blom, P. W. M.; Mihailetchi, V. D.; Koster, L. J. A.; Markov, D. E. *Adv. Mater*. **2007**, 19, 1551.

[2]. Li, G.; Yao, Y.; Yang, H.; Shrotriya, V.; Yang, G.; Yang, Y. *Adv. Funct. Mater*. **2007**, 17, 1636.

[3]. Thompson, B. C.; Frechet, J. M. J. *Angew. Chem. Int. ed*. **2008**, 47, 58.

[4]. Li, G.; Shrotriya, V.; Huang, J. S.; Yao, Y.; Moriarty. T.; Emery, K.; Yang, Y. *Nat. Mater*. 20**0**5, 4, 864.

[5]. Ma, W. L.; Yang, C. Y.; Gong, X.; Lee, K.; Heeger, A. J. *Adv. Funct. Mater*. **2005**, 15, 1617.

[6]. Zhang, Q. L.; Cirpan, A.; Russell, T. P.; Emrick, T. *Macromolecules.* **2009**, 42, 1079.

[7]. Lin, Z.; Kim, D. H.; Wu, X.; Boosahda, L.; Stone, D.; LaRose, L.; Russell, T. P. *Adv. Mater*. **2002**, 14, 1373.

[8]. Zhang, Y.; Tajima, K.; Hirota, K.; Hashimoto, K. *J. Am. Chem. Soc*. **2008,** 130, 7812.

Chapter 6 . Concluding remarks

As described in Chapter 1, organic solar cells have many advantages such as low cost, light weight, high flexibility and so on, except for the low solar efficiency. The conversion efficiency strongly depends on the morphology of the composites, like *p*-type conjugated polymer, poly(3-hexylthiophene) (P3HT) doped with *n*-type fullerene derivative, [6,6]-phenyl-C_{61}-butyric acid methyl ester (PCBM). In addition to post treatments such as thermal or solvent annealing, the author proposes the novel strategy for the control of the morphology, i.e., the utilization of block consisting of P3HT and electrically inert polymer, such as polystyrene (PS) and poly(ethylene glycol) (PEO).

Chapter 2 deals with the synthesis of *p*-type conducting block copolymer, poly(3-hexylthiophene)-*block*-polystyrene (P3HT-*b*-PS) by Suzuki coupling between P3HT and PS homopolymers. PS shows nonpolar nature, and high compatibility with PCBM. PS with an end group of boronic acid ester moiety was synthesized with atom transfer radical polymerization followed by esterification. Suzuki coupling of end functionalized PS and bromo terminated P3HT worked well for the preparation of block copolymers. ^{1}H-NMR analysis elucidated no contamination with homo-P3HT. In DSC thermogram for the block copolymer, melting of P3HT and glass transition of PS were observed indicating the microphase separation.

In Chapter 3, the thin films of composite consisting of P3HT-*b*-PS and PCBM were characterized, and photovoltaic devices based on the composite were evaluated. Relatively distinct phase separated structure was observed in the composite based on the block copolymer compared with that of homo-P3HT after thermal annealing. It is considered that PS chains promoted the aggregation of PCBM. Solvent annealing with acetone increased the domain size. Solar cells, ITO/PEDOT:PSS(30 nm)/active layer/LiF(0.5 nm)/Al(100 nm), were fabricate, and their photovoltaic properties were investigated. The conversion effciency of thermally annealed device based on P3HT-*b*-PS was higher than that based on P3HT. Solvent annealing with acetone made the domain size larger compared with thermal anneal.

Chapter 4 describes the synthesis of P3HT-*b*-PEO. PEO shows hydrophilic, or high polar nature, and little compatibility with PCBM. Hydroxy group of methyl terminated PEOs with different molecular weight

was converted to boronic ester moiety via esterification. Resulting PEOs were coupled with bromo terminated P3HT via Suzuki reaction. UV spectra of thin films of P3HT-*b*-PEO revealed that P3HT chains were stacked each other like homo-P3HT, indicating that PEO component had little effect on the crystallization of P3HT chain. DSC measurements showed melting points of PEO and P3HT chains, suggesting the microphase separation.

In Chapter 5, morphology and photovoltaic property of the composite films of P3HT-*b*-PEO with PCBM were investigated. AFM measurement of thin film based on P3HT-*b*-PEO/PCBM revealed that the introduction of PEO segment contributed to generate ordered lamellar morphology with the smaller size compared with the P3HT/PCBM blend. The devices were fabricated based on P3HT or P3HT-*b*-PEO blended with PCBM in 1:1 weight ratio, and the performance was evaluated after thermal or solvent annealing. For the devices based on P3HT-*b*-PEO/PCBM, the favorable PEO content to obtain the high efficiency was found to be 7 to 9%, where the active layer thickness was optimized at approximately 70 nm. After thermal annealing, the P3HT-*b*-PEO/PCBM device showed higher performance than that of the P3HT/PCBM device.

In conclusion, the film morphology if the composites with PCBM was strongly dependent on the nature of inert block. P3HT-*b*-PS composite showed distinct and larger domain compared with P3HT/PCBM. On the other hand, P3HT-*b*-PEO showed smaller size of regular phase separated structure. In some cases (e.g. solvent annealed films), each lamellar domain aligned perpendicular to the substrate. Although this well-defined structure seems favorable for photovoltaic performance, no significant increase of the efficiency was observed. This is probably due to the existence of defects in the film and/or insufficient control of domain size.